Fate and transport of viruses and colloids in saturated and unsaturated porous media

Saeed Torkzaban

Fate and transport of viruses and colloids in saturated and
unsaturated porous media

Lot en transport van virussen en colloïden in verzadigde en
onverzadigde poreuze media

Proefschrift

ter verkrijging van de graad van doctor
aan de Universiteit Utrecht
op gezag van de rector magnificus prof.dr. J.C. Stoof
ingevolge het besluit van het college voor Promoties
in het openbaar te verdedigen op maandag 15 oktober 2007 des morgens te 10.30 uur

door

Saeed Torkzaban

geboren op 11 september 1975 te Malayer, Iran

Promotor: Prof. Dr. S.M. Hassanizadeh

Abstract

The fundamental mechanisms involved in fate and transport of colloidal particles (viruses and latex microspheres) in saturated and unsaturated porous media were systematically examined. Two different bacteriophages were used as surrogate for pathogenic viruses to investigate the effects of various water contents and solution chemistries in terms of pH and ionic strength (IS) on virus transport. The experiments were complimented by utilizing a transport model that accounts for virus interaction with the solid-water interfaces (SWI) and air-water interfaces (AWI). It was found that under saturated conditions virus retention enhanced with decreasing the pH and increasing the IS. Under unsaturated conditions, viruses exhibited a high affinity to the AWI only when the pH was lower than 7. In contrast with the saturated experiments that a one-site kinetic model was sufficient to fit the breakthrough curves, a two-site kinetic model was needed to produce a good fit to the breakthrough curves obtained from unsaturated columns.

To complement the previous work, packed column and mathematical modeling studies were conducted to explore the influence of water saturation, IS, and grain size on the transport of larger colloids (latex microspheres; 1.1 μm) in porous media. Experiments were carried out under chemically unfavorable conditions for colloid attachment to both SWI and AWI. The breakthrough curve and final deposition profile in each experiment indicated that colloid retention was highly dependent on IS, water content, and sand grain size. Experimental and modeling results suggested that straining – the retention of colloids in low velocity regions of porous media such as grain junctions – was the primary mechanism of colloid retention under both saturated and unsaturated conditions. Increasing the solution ionic strength is believed to increase the depth of secondary minimum in the DLVO interaction energy profile and as a result, increase the adhesive force between colloids and the SWI by increasing. These weakly associated colloids can be funneled to small regions of the pore space formed adjacent to grain-grain junctions. For select systems, the IS of the influent was decreased to a low solution IS following the obtaining of the effluent concentration data. In this case, only a small portion of the deposited colloids was recovered in the effluent and the majority was still retained in the

sand. These observations suggest that the extent of colloid removal by straining is strongly coupled to solution chemistry.

This research established that colloid retention in porous media is a coupled process that strongly depends on solution chemistry, pore structure, and system hydrodynamics. Therefore, modeling colloid transport through porous media will require nontraditional approaches which account for the abovementioned factors.

To my parents, my wife Shiva, and my son Arman.

Acknowledgment

Working on my Ph.D. has been a wonderful and remarkable experience. It has been the real learning experience of how to approach a research problem, write papers and proposals, give talks, work in a group, and stay focus, etc.

I am indebted to many people for their support and advice during the preparation of this thesis.

First of all, I am deeply grateful to my advisor, Prof. Majid Hassanizadeh, for being an outstanding advisor. He has been a steady influence throughout my Ph.D. He has oriented and supported me with promptness and care, and has always been patient with my questions and encouraging in times of new ideas. He has listened to my ideas and discussions with patience and providing me his key insights. His ability to select and to approach compelling research problems, his high scientific standards, and his hard work set an example. I admire his ability to balance research interests and personal life. In general, he has been everything that one could want in an advisor.

I am also very grateful to Dr. Jack Schijven from RIVM for his support in my virus transport experiments, for his insightful comments on my work, and for many motivating discussions. It was a great privilege working with him for about two years. I also wish to acknowledge the helpful feedback and comments of Dr. Ana Maria de Roda Husman. H.A.M. de Bruin, Ronald Italiaander, and Harold van den Berg are also greatly acknowledged for their help in processing the microbiological samples. I would like to thank the Laboratory of Environmental Microbiology of RIVM for hosting me in the Lab and in the guesthouse for some months.

I have been very privileged to get to know Prof. Rien van Genuchten from USDA, Salinity Lab. He is a wonderful, kind, friendly, and humble man. I am especially grateful to him for supporting and arranging my visit to University of California, Riverside (UCR) where I was so lucky to get to work with Dr. Scott Bradford. Scott is a true researcher and a wonderful and generous man. I owe a huge debt of gratitude to him for helping me to understand the basis of colloid transport, for his scientific advice and instrumental suggestions. I hope one day I will be able to repay his generosity. I am also grateful to Dr. Sharon Walker who has been a great help and support during my research at UCR. I have greatly enjoyed my time working in her group over the last two years. I would also like to thank her PhD students: Gexin , Berat, Nick, Amy. Their help and support have been invaluable since I arrived in Riverside. Special thanks also to Hugo Galdamez for providing support and help for setting up my column experiments.

Back to Utrecht University, all my colleagues of our research- group (in particular, Henk, Abhishek, Sam, Phil, Bert-Rik, Marian, Simona, Cas, Twan) are thanked for their support and providing a pleasant and productive working atmosphere. I am deeply grateful to Prof. Ruud Schotting who supported me and my wife, Shiva, in numerous ways during our study. Many thanks go to our secretary, Ms. Margreet Evertman, who is so kind and helped me a lot during various stages of my PhD.

Table of Contents

Chapter 5   **Coupling of physical and chemical mechanisms of colloid straining in saturated porous media**

Chapter 6   **Summary and Conclusions and Recommendations**

Chapter 2

Chapter 3

Chapter 4

switched to low IS solution of 6 mM for the final 2-3 pore volumes.

Chapter 1

INTRODUCTION

Motivation and Background

In small communities and developing countries, microbiological contamination of groundwater has profound and severe implications for public health (EPA, 2000). Although waterborne diseases have largely been controlled in the USA, outbreaks continue to occur. As an example, in the period from 1971-1996, 643 outbreaks and over 570000 cases of illness were reported for all public surface water and groundwater systems (Craun and Calderon, 1996; EPA, 2000). Groundwater may become contaminated with viral, bacteria and protozoan pathogens from fecally contaminated water, e.g. from septic tanks or leaking sewage pipes. Surface water is contaminated with pathogenic microorganisms, mainly due to discharge of wastewater and by manure run-off from agricultural land. These pathogens can cause a range of gastrointestinal and other severe illnesses. Waterborne diseases may cause asymptomatic infections with a few days of mild diarrhea, to sever disease requiring hospitalization, and may possibly lead to death. However, acute gastroenteric illness is most common outcome of waterborne diseases (Gerba, 1984).

Groundwater can be protected from contamination with pathogenic microorganisms through engineering solutions such as applying adequate setback distances between sources of contamination and production wells, with the soil serving as a natural filter. Surface water can also be treated effectively to remove pathogens by means of passage through the subsurface such as riverbank filtration (e.g. Schijven and Rietveld, 1996). These strategies rely on knowledge of potential microbial transport processes and conditions that are needed to achieve safe drinking water. In this regard, considerable research has been carried out for quantifying and modeling processes that govern the removal of pathogenic microorganisms by soil passage (see e.g. the review by Schijven and Hassanizadeh, 2000). Once the fate and transport of pathogens in porous media is understood, a better and accurate estimate of the setback distances required for production of safe drinking water from groundwater is plausible. However, due to some limitations, like limited sensitivity of virus and pathogenic bacteria assay methods, it is common for surrogates to be used. Specifically, bacteriophages are used as surrogates for pathogenic viruses, and non-pathogenic bacteria or latex microspheres as representative of pathogenic bacteria. It is believed that the processes that determine removal of these surrogate colloidal particles (bactriophages and latex microspheres) during soil passage are

representative of the pathogenic microorganisms (Gerba, 1984)

In addition to the need for understanding the colloid transport and fate as an surrogate for pathogenic microorganisms, an accurate knowledge of colloid transport is vital to develop efficient bioremediation strategies (e.g. Rittman et al., 1992; Wilson and Jones, 1993; Kalogerakis et al., 2005), and to understand soil formation (McDowell-Boyer et al., 1986). Colloid movement in porous media is also of concern due to colloid-facilitated transport of a wide variety of inorganic (heavy metals and radionuclides) and organic (pesticides, aromatic hydrocarbons, and pharmaceuticals) contaminants that adsorb onto these particles and travel significant distances [de Jonge et al., 1998; Ryan et al., 1998; McGechan and Lewis, 2002]. Hence, comprehensive knowledge of the transport of colloids in general, and of biocolloids in particular (e.g. viruses, bacteria), in subsurface environments is essential for predicting the fate of pathogenic and chemical contaminants.

Colloid transport in porous media is affected by various physical and chemical processes including advection, diffusion, dispersion, interphase mass transfer, and biogeochemical reactions. Biological processes such as growth, death, inactivation, parasitism can result in the increase or removal of microorganisms in porous media (e.g. Dowd and Pillai, 1997; Gordon and Toze, 2003). Many of these biological processes are also influenced by physical and chemicals conditions (Nasser et al., 1993). Although biological processes are extremely important, they are outside the scope of this thesis. *Notably, the focus of this research is on the transport of colloidal particles (bactriophages and latex microsphere) through both saturated and unsaturated porous media.*

Colloidal properties of viruses

Viruses are the smallest intracellular parasites known. They are colloidal in size and generally range from 20 to 200 nm (Pollard, 1953; Bitton, 1975). Since their nucleic acid is encased in a pertinacious capsid, they behave as amphoteric colloids in which the surface charge is established by ionization of chemical functional group. The surface chemical characteristics of viruses and their charge behavior are very important in determining their transport in subsurface environment.

The surface charge of viruses is established by the protonation and deprotonation of functional groups of amino acids in the polypeptides comprising the virus capsid. The

majority of the functional groups are of the carboxyl and amino type (Taylor, 1981). Surface charge of viruses develops by the following acid-base reaction (Taylor, 1981).

$$COOH \Leftrightarrow COO^- + H^+$$
$$NR_2H^+ \Leftrightarrow NR_2 + H^+$$
$$Ph - OH \Leftrightarrow Ph - O^- + H^+$$
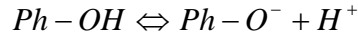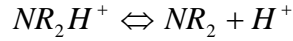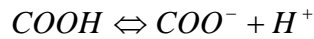
The total charge at any pH depends on the surface concentration of the ionizable groups and their dissociation constants. The pH at which a virus has no net charge, the iosoelectric point, varies with capsid composition. At lower pH, net protonation of ionizable groups produces positive charge, whereas at high pH deprotonation dominates to give a net negative charge.

Transport and fate of colloidal particles in porous media

The colloidal size range is about 10 nm to 10 μm, with the smallest colloids being those that are just larger than dissolved macromolecules (DeNovio et al. 2004; Stumn, 1977). Advection is the movement of colloidal particles with the bulk fluid flow. Imposing a moderate pressure gradient across a porous medium generates a laminar and stable flow field with defined streamlines. Colloids and solutes undergo advective transport moving with the pore water, whose velocity is governed by the hydraulic pressure gradient, porosity, and permeability distribution (Ginn et al., 2002). Solution of the Navier-Stokes equations at the pore scale indicates that even for fairly complex pore geometries, the local velocity profile is nearly parabolic with the faster streamlines in the center of the pore throats, and slower streamlines along the solid-water (SWI) and/or air-water (AWI) interfaces (de Marsily, 1986; Baumann and Werth, 2004). Thus, solutes and colloids that begin their transport near the central streamlines and in larger pores are advected at a considerably higher rate than those along the SWI and AWI and other low velocity regions (e.g. dead-end pores). This phenomenon creates dispersion of the colloids because of variations in the fluid velocity field and the tortuosity of the paths through the porous media (Auset and Keller, 2004). In addition, random interactions among molecules and/or particles can result in Brownian movements (Schwarzenbach et al., 1993) that can lead to diffusion of the colloids to the interfaces. Since diffusion due to Brownian motion is inversely proportional to the mass of the molecule or particle, solutes and small colloids

like viruses have a much higher probability of transferring among streamlines than larger colloids. However, larger colloids may come in contact with the interfaces by either virtue of their own sizes (this transport process is called interception) or due to influence of the gravitational force (this transport process is called sedimentation) (Yao et al., 1971).

Attachment of colloids to the SWI and AWI in a porous medium involves two processes: mass transport of colloids to interface (as discussed above) and colloid-surface interactions. Therefore the attachment rate coefficient depends on microscale flow and diffusion characteristics as well as surface properties of colloids and soil grains (Elimelech and O'Melia, 1990). Because the solution chemistry influences the property of colloids and grain surfaces, it also affects attachment and detachment rates. Colloid removal is expected to increase for the lower flow rates and small pore sizes available for flow (e.g. under unsaturated conditions) as mass transport to the interfaces becomes more dominant than advection.

Colloid filtration theory has been proposed to predict the colloid attachment to the SWI as an irreversible first-order process and the spatial distribution of concentration of retained colloids is hence predicted to have an exponential shape (Yao et al., 1971). The attachment rate coefficient is related to single collector efficiency η and the collision efficiency α as follows (Yao et al., 1971):

$$K_{att} = \frac{3}{2} \frac{(1-n)}{d_c} \alpha \eta v$$

Here, d_c is the average diameter of collector, [L], and n is the porosity of the porous medium [-]. The fraction of particles that collide with the collector is given by η. According to the filtration theory, a colloidal particle may come into contact with a particle of porous medium, the collector, either by diffusion controlling the transport of smaller particles, sedimentation or interception controlling the transport of larger colloids (larger than 1 μm) (Logan et al., 1995).

Observed effluent concentration curves and spatial distributions of retained colloids concentration in porous media have not always been in agreement with filtration theory (Bolster et al., 1999; Redman et al., 2001; Bradford et al., 2002; Tufenkji et al., 2003). Some of these discrepancies have been attributed to soil surface roughness (Redman et al., 2001) and charge variability (Johnson and Elimelech, 1995), heterogeneity in colloid

characteristics (Bolster et al., 1999), colloid detachment (Tufenkji et al., 2003), and straining (Bradford et al., 2002 and 2003). Other reasons have been reported for the observed discrepancies with filtration theory such as kinetic release of retained colloids from porous media (Johnson et al., 2001; Schijven and Simunek, 2001) and time dependent attachment coefficient (Johnson and Elimelech, 1995).

Straining is another mechanism for colloid retention which involves the entrapment of colloids in small pores where the water velocity is small. The critical pore size for straining will depend on the size of the colloid and the pore size distribution of the medium (McDowell-Boyer et al., 1986; Bradford et al., 2002 and 2003). Straining has been shown to be pronounced at the soil surface or at the boundary of two different soil textures where the colloids are encountering a new pore network (Bradford et al., 2003). Solution of the Navier-Stokes equations at the pore scale indicates that a higher average pore water velocity occurs in larger pores than in smaller pores. In the complex geometries of natural porous media, there are many regions which are almost stagnant such as small pores formed in the vicinity of grain-grain contact points and dead-end pores. Therefore, these regions are prone to colloid straining (Cushing and Lawler, 1998).

Considerable research has been devoted to the transport and fate of bacteriophages and colloids in saturated porous media [reviews are given by Schijven and Hassanizadeh, 2000; Harvey and Harms, 2002; de Jonge et al., 2004]. However, colloid transport in the unsaturated (vadose) zone has received little systematic research and the governing mechanisms are poorly understood (Wan and Wilson, 1994b; Wan and Tokunago, 1997; Schafer et al., 1998; Saiers and Lenhart, 2003). One of the key features of the vadose zone that plays a critical role in colloid movement is the presence of air–water interfaces in the system (Nicole et al. 2003). An improved understanding of colloid transport in the unsaturated zone is essential for protecting water resources from contamination, because the vadose zone acts as a first natural barrier against the pollution of groundwater.

Investigations have shown that water saturation of porous media plays a key role in the fate and transport of colloids in the vadose zone (e.g. Powelson et al., 1990; Chu et al., 2001; Torkzaban et al. 2006 *a or b*). Based on the pioneering work of Wan and Wilson (1994a), the interaction of colloids with the AWI has been invoked as a dominant process in colloid retention. It has been generally assumed, based on visualization studies using

etched-glass micromodels (Wan and Wilson, 1994a), that retention at the AWI is relevant to a wide variety of colloids, including hydrophilic and hydrophobic latex microspheres, clay particles, and bacteria. New findings, however, do not support this hypothesis. For example, Wan and Tokunaga (2002) demonstrated in bubble column experiments that only positively charged particles attached to the negatively charged AWI, suggesting that immobilization at the AWI would be limited to a smaller subset of environmental colloids. Christ et al. (2005 and 2006) using a novel pore-scale visualization technique, demonstrated that hydrophilic colloids do not attach to the AWI. Some recent column experiments also indicate that the enhanced retention of colloids under unsaturated conditions is unlikely to be due to attachment to the AWI (Chu et al. 2002; Chen and Flury 2005; Torkzaban et al. 2006a and b). It has been suggested that, as with attachment to the SWI, colloid attachment to the AWI is a function of ionic strength, pH, and the surface properties of the colloid, such as hydrophobicity and surface charge (Wan and Wilson, 1994a; Wan and Tokunaga, 2002; Torkzaban et al., 2006b). Increases in ionic strength will reduce the magnitude of the repulsive energy barrier between the negatively charged AWI and colloids, leading to progressively more favorable conditions for attachment and faster rates of the AWI capture.

Wan and Tokunaga (1997) introduced an additional mechanism of colloid immobilization in partially saturated porous media. They introduced the concept of film straining to suggest that the transport of suspended colloids could be retarded due to physical restrictions imposed when the thickness of water films is smaller than the diameter of the colloids. Wan and Tokunaga (1997) estimated that these films should be on the order of 20-40 nm, which is considerably thinner than a 1 µm *Escherichia coli*, but may not completely immobilize a 25 nm virus.

Scope and Objectives

The objective of this work was to gain a fundamental understanding of the mechanisms controlling the fate and transport of colloidal particles (bactriophages and latex microspheres) in subsurface porous media. Specifically, this research has focused on the interactions occurring between colloids and the SWI and AWI under various physicochemical conditions. The overall objective was to relate the kinetics of colloid

adsorption to the physical and chemical properties of the system.

Specific Objectives

1. To examine the effect of water content on the fate and transport of bactriophages in porous media, in particular their adsorption (attachment and detachment) behavior. The chemical conditions of the experiments were selected to allow for the investigation of the effect of water content on the SWI attachment.

2. To investigate the extent of attachment of bactriophages to the AWI and the factors controlling it. To this end, several column experiments were conducted using two different bacteriophages and solutions of various pH. In an attempt to minimize the influence of the SWI, phosphate buffer was chosen because the phosphate ions tend to block positively-charged sites on soil surfaces. The following issues were specifically investigated in this study: (i) attachment to the AWI; (ii) detachment from the AWI; and (iii) viability of viruses attached to the AWI.

3. To explore the effects of water content and solution ionic strength on colloid transport and deposition. Highly unfavorable attachment conditions were employed to ensure the existence of a repulsive energy barrier against attachment. Therefore, the retention mechanisms involved were not simply due to chemical interactions, but also to straining. To minimize colloid attachment to both the SWI and AWI, the experiments were conducted using hydrophilic, negatively charged microspheres in a buffered solution such that the quartz sand and the AWI were negatively charged. Unfavorable attachment conditions were confirmed to exist through complementary batch experiments and DLVO calculations (discussed in details in chapter 4).

4. To investigate the role of solution chemistry and hydrodynamics on colloid attachment and removal by straining. Negatively charged latex microspheres and quartz sands were used in packed column studies that encompassed a range of solution ionic strength (6-106mM) and Darcy water velocity (0.1-0.45 cm min-1). All experiments were conducted using electrolyte solution buffered to a pH of 10 to ensure highly unfavorable attachment conditions. Data analysis and

interpretation was aided through DLVO calculations of the total interaction energy between the colloids and quartz surfaces, mass balance computation and mathematical modeling utilizing experimental breakthrough curves and deposition profiles.

The novelty in this research is that the different mechanisms affecting the retention of colloidal particles in the porous media were studied by controlling the chemical and physical conditions of the system. In Chapters 2 and 3, it is shown that the relative importance of attachment to the AWI and SWI was determined using two different bacteriophages and solutions with various pH and ionic strengths. In Chapters 4 and 5, the aim was to just focus on the effect of straining. Therefore, colloid attachment to the SWI and AWI was minimized by establishing highly unfavorable conditions for attachment to the interfaces.

Organization of the Dissertation

Following this introduction, Chapter 2 describes the transport of bacteriophages MS2 and ϕX174, used as surrogate pathogenic viruses, at various water contents and solution chemistries in terms of pH and ionic strength (IS). It was shown that the enhanced retention of ϕX174 viruses at lower water content was caused by increased attachment to the SWI and that retention by the AWI was not significant. The trend of breakthrough data of MS2 was less conclusive in resolving the role of the AWI. Although attachment of MS2 viruses to the AWI could not be ruled out in our experiments, we suspected that the increased retention of this phage under unsaturated condition was also due to enhanced attachment to the SWI. Increased attachment to the SWI under unsaturated conditions is attributed to increased mass transfer of viruses to the SWI due to a reduced diffusion length at lower water content.

In Chapter 3, the factors affecting virus adsorption onto the AWI under unsaturated conditions were investigated. This work demonstrated that electrostatic interaction of viruses with the AWI is much more important than hydrophobicity. Under unsaturated conditions, viruses captured within the column could be recovered in the column outflow by re-saturating and immediately draining the column. This finding suggests that attached viruses onto the AWI are viable and prone to return to aqueous phase upon any

disturbance.

In Chapters 2 and 3, bacteriophages were chosen to study colloid transport in porous media as the intention was to minimize the effect of physical factors like straining on colloidal transport. It is believed that straining of viruses is not significant due to their small sizes (about 30 nm).

Chapters 4 and 5 report our study where fluorescent latex microspheres (1.1 μm) are used as surrogates for bacteria. In Chapter 4, packed column experiments and mathematical modeling studies were conducted to explore the influence of water content, pore water ionic strength, and grain size on the transport of latex microspheres in porous media. Experiments were carried out under chemically unfavorable conditions for colloid attachment to both solid-water interfaces (SWI) and air-water interfaces (AWI) using negatively charged and hydrophilic colloids and solution chemistry modified with a bicarbonate buffer to pH 10. DLVO calculations and complementary batch experiments demonstrated that attachment of colloids to the SWI and AWI was insignificant across the range of the ionic strengths considered. This work demonstrated that straining – the retention of colloids in small pores and grain junctions – is the primary mechanism of colloid retention under both saturated and unsaturated conditions for the experimental conditions tested.

Chapter 5 highlights the fact that staining is not just a function of physical properties of the system such as colloid and porous media sizes. Previous research on straining has not considered the potential influence of solution chemistry and system hydrodynamics. Experimental and theoretical studies were therefore undertaken to explore the coupling of physical and chemical mechanisms of colloid straining under unfavorable attachment conditions (pH=10). Breakthrough curves and hyper-exponential deposition profiles suggest a strong dependence on the solution chemistry, the system hydrodynamics, and the colloid and collector grain size, with increasing deposition occurring for increasing ionic strength, lower flow rates, and larger ratios of the colloid to the median grain diameter.

Finally the findings and implications of this doctoral research are summarized in Chapter 6.

Chapter 2

Virus transport in saturated and unsaturated sand columns

Torkzaban, S., S.M. Hassanizadeh, J.F. Schijven, and A.M. de Roda Husman, "Virus transport in saturated and unsaturated sand columns. *Vadose Zone Journal*," 5: 877-885, 2006.

Abstract

The transport of viruses in unsaturated porous media has been a subject of great interest in recent years because of the enhanced removal of these microorganisms compared with saturated conditions. We studied the transport of bacteriophages MS2 and ϕX174, used as surrogate pathogenic viruses, at various water contents and solution chemistries in terms of pH and ionic strength (IS). The objective was to explore the interaction of viruses with the solid-water interfaces (SWI) and air-water interfaces (AWI) for a range of conditions. The experimental data were fitted with a transport model to determine the adsorption (attachment and detachment rate) parameters. Our results show that the retention of viruses in the soil column increases as water saturation decreases when the chemical conditions are favorable for adsorption (pH 7 and relatively high IS). Our analysis indicates that the enhanced retention of ϕX174 viruses at lower water contents is caused by increased attachment to the SWI and that retention by the AWI is not significant. Results obtained from a first series of experiments (pH 9 and low IS) showed insignificant attachment of MS2 viruses to both the SWI and the AWI. The MS2 breakthrough data for a second series of experiments (pH 7 and high IS) did not allow us to separate out the role of the AWI. Although attachment of MS2 viruses to the AWI cannot be ruled out in our experiments, we suspect that the increased retention of this phage under unsaturated condition was also due to enhanced attachment to the SWI. Increased attachment to the SWI under unsaturated conditions is attributed to increased mass transfer of viruses to the SWI due to a reduced diffusion length at lower water contents. Our results demonstrate that if there is any attachment to the AWI, it is reversible. When unfavorable conditions occur for attachment to the SWI, the attached viruses may be detached by moving solid-water-air contact lines.

INTRODUCTION

Groundwater is a major source for drinking water. It has the potential to become contaminated with pathogenic microorganisms from land application of raw and treated wastewater, septic wells, effluent from septic tanks, leaking sewage pipes and animal manure (Gerba and Smith, 2005). Among pathogenic microorganisms, viruses are of major concern since they are smaller than bacteria and protozoa and far more mobile in subsurface environment (Schijven and Hassanizadeh, 2000). A number of studies have documented the ability of viruses to migrate significant distances through soil (Keswich and Gerba, 1980; Goyal et al. 1984; Gerba and Rose, 1990). The transport and fate of viruses in the subsurface is governed by advection, dispersion, and inactivation, together with interaction of viruses with different interfaces. Attachment and inactivation processes mainly determine virus removal during soil passage (Keswich and Gerba, 1980; Yates et al., 1987). Virus removal rates in the saturated zone vary greatly depending upon the type of virus involved, the type of soil, water content, pH, and the salt content of the water (Gerba *et al.*, 1984; Schijven and Hassanizadeh, 2000). Unsaturated conditions have additionally been found to enhance the removal of viruses during soil passage (e.g. Jin et al., 2000; Powelson *et al.*, 1990; Powelson and Gerba, 1994; Poletika et al., 1995).

The enhanced removal of viruses in the vadose zone, as compared with the saturated zone, has been attributed to increased adsorption onto solid-water interfaces (SWI), irreversible attachment to air-water interfaces (AWI), and/or attachment to solid-water-air contact lines (SWA) (e.g. Chu et al., 2001; Lance and Gerba, 1984; Bitton et al., 1984; Powelson et al., 1990; Thompson et al., 1998). The hypothesis of irreversible attachment of viruses to the AWI was supported by visualization studies involving colloid transport in micromodels (Wan and Wilson, 1994a; Sirivithayapakorn and Keller 2003). Wan and Wilson (1994a) suggested that a wide variety of colloids, including hydrophobic and hydrophilic latex microspheres, clay particles and bacteria can irreversibly accumulate at the AWI and that this accumulation increases with increasing particle hydrophobicity and solution ionic strength (IS). Colloids that are transported to the AWI are believed to be retained by either capillary or electrostatic forces. Hence, interfacial attachment will depend on pH, IS, and colloid surface properties. An increase

in IS reduces the magnitude of the repulsive energy barrier between the negatively charged air–water interface and similarly charged mineral colloids. This produces more favorable conditions for attachment and faster rates of AWI capture (Wan and Wilson, 1994a; Saiers and Lenhart, 2003a). In contrast, Crist et al. (2004) and (2005) observed that hydrophilic latex microsphere colloids did not adsorb to the AWI, and that colloid retention occurred at the solid-water-air contact line (SWA). Wan and Tokunaga (2002) demonstrated in bubble column experiments that only positively-charged particles attached to the negatively charged AWI. This suggests that colloid immobilization at the AWI would be limited to a small subset of environmental colloids.

Several column-scale experiments were previously conducted to study the effect of unsaturated conditions on virus removal using bacteriophages MS2 and/or ϕX174 (Chu et al., 2001, 2003; Keller and Sirivithayapakorn, 2004). Chu and et al. (2001) obtained different retention results for different sand surface properties. For clean sand (treated to remove all metal oxides), they found that the slight attachment of viruses to the AWI was irreversible, possibly due to strong interfacial forces. Results for untreated sand suggested that the presence of iron oxides created favorable conditions for attachment to the SWI and dominated the removal of viruses under unsaturated conditions. Keller and Sirivithayapakorn (2004) observed that the removal of MS2 increased significantly with decreasing water content. The enhanced removal was ascribed to attachment to the AWI and straining in thin water films. Hydrophobic interaction (Schijven and Hassanizadeh, 2000) has also been suggested to contribute to the adsorption of viruses to the SWI and the AWI. However, there is insufficient evidence to show that this process is a significant contributor to virus attachment.

Although earlier studies have clearly shown that lower water contents lead to more virus retention in soil columns, the relative importance of the various mechanisms involved is still unclear. The objective of this study was to examine the effect of water content on the fate and transport of viruses in porous media, in particular their adsorption (attachment and detachment) behavior. Two sets of column experiments involving different chemical conditions and saturation levels were carried out. Two bacteriophages were employed with different hydrophobicity and surface charge properties. In the first set of experiments, a solution of high pH (9) and low IS (0.6mM) was used. For these

conditions, one should expect negligible adsorption of both bacteriophages to the SWI. They may, however, attach to the AWI. The second set of experiments was conducted using a solution of neutral pH (7) and higher IS (19mM). Under these conditions, adsorption to the SWI may become significant. The various experiments also allow us to investigate the effect of water content on SWI adsorption. A mathematical model (HYDRUS-1D) that takes into account virus attachment and detachment to two types of kinetic adsorption sites was used to study the various retention mechanisms.

MATERIALS AND METHODS

Characteristics of phages and solution chemistry

MS2 and ϕX174 were selected as model viruses. MS2 is an icosahedral phage with a diameter of 27 nm and a low isoelectric point of 3.5 (Penrod *et al.*, 1996), conversely ϕX174 is less hydrophobic than MS2 (Shields and Farrah, 1987), and has an isoelectric point of about 6.7 and a size of 23 nm (Dowd *et al.*, 1998).

Highly concentrated suspensions of MS2 and ϕX174 were prepared as described in ISO 10705-1 (2000) and ISO10705-2 (2000), respectively. These concentrated bacteriophage suspensions were used to prepare stock suspensions, diluted with 1 g/l peptone-saline to a concentration of 10^{10}-10^{11} phages per liter. The concentrated stock suspensions were subsequently used to prepare seeding suspensions of approximately 10^9 phages per liter. MS2 was assayed as described in ISO 10705-1 (2000) using host strain WG49 (ATCC 15597). Bacteriophage ϕX174 was assayed according to ISO 10705-2 (2000) using WG5 (ATCC 70078) as the host.

Tris (pKa of 8.55 at 0°c) and deionized water were used to prepare the buffer solution. In the first series of experiments, the pH of the solution was adjusted to 9 by addition of NaOH (1mM), while the ionic strength was kept low (~ 0.6mM). In the second series of experiments, the pH and IS of the buffer solution was adjusted to 7 and 19mM by addition of HCl (1mM) and NaCl, respectively. The pH and IS of each experiment are listed in Table 1.

A series of batch studies was carried out to measure inactivation of the phages in the water phase during the experiments. For this purpose, 2 liter of two different waters (pH 9 and low IS, pH 7 and high IS) were dosed with MS2 and ϕX174 at about the same

concentration as the input concentrations of the column experiments. The suspensions were regularly analyzed for a period of one month to yield inactivation rates for the two different chemical conditions.

Table 1. Experimental conditions of column experiments

Experiment	pH	Ionic strength (mM)	Saturation (%)	Pore water velocity (cm/min)	Dispersivity (cm)	seeding duration (pore volumes)
HpLi100	9	0.6	100	0.68	0.060	3.0
HpLi65	9	0.6	65	0.56	0.44	8.0
LpHi100	7	19	100	0.68	0.060	4.2
LpHi66	7	19	66	0.7	0.43	9.7
LpHi52	7	19	52	0.45	0.56	6.3

Column set-up and experiments

A schematic of the column setup is shown in Figure 1. A cylindrical PVC column with an internal diameter of 10 cm and length of 23 cm was used. A hydrophilic nylon membrane with 10 µm pore size (SaatiTech, Veniano, Italy), supported by a stainless steel plate, was used as a capillary barrier at the bottom of the column. Results of preliminary experiments (performed without sand) demonstrated that neither the column nor the end-fitting assemblies removed viruses from the suspension. Sand with a median grain size (d_{50}) of 140 µm and uniformity (d_{60}/d_{10}) of 1.6 was used as the porous medium. The sand was treated with HCl (1mM) for about 20 minutes in order to remove any attached colloids, and then rinsed thoroughly with distilled water followed by oven drying at 110 °C. The free iron oxide content on the sand surface was measured to be 45 mg Fe per kilogram sand using the procedure modified by Mehra and Jackson (1960). The sand was wet-packed in the column following the procedure of Robinson and Friedman (2001) to produce a homogeneous packing. A shaker was constructed and used to uniformly apply the buffer or the virus suspension to the inlet of the column.

16
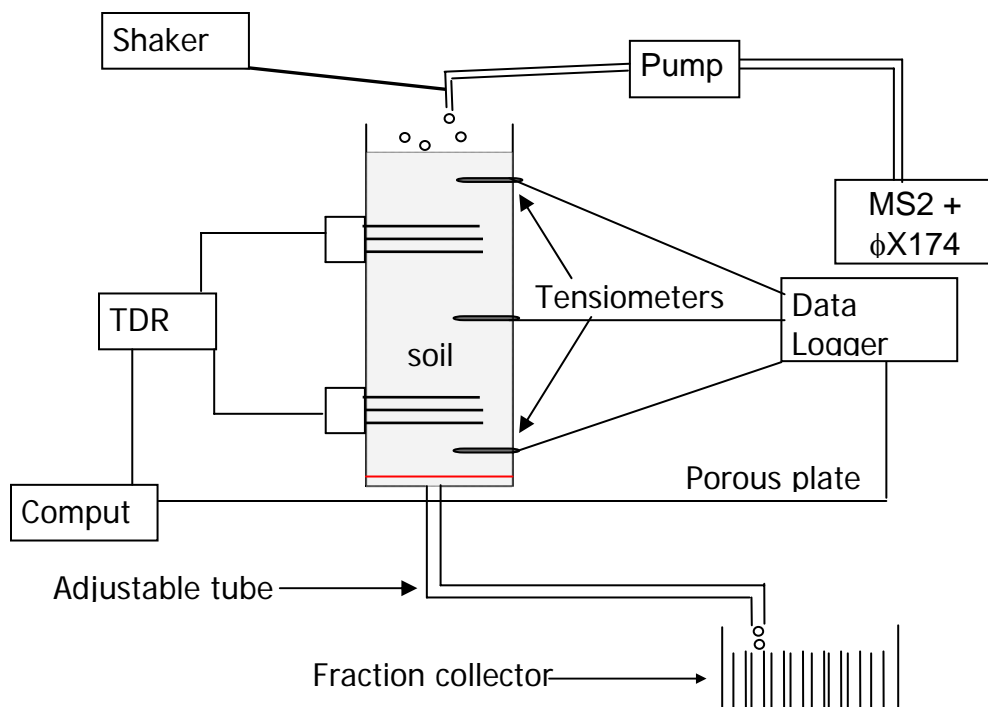
Figure 1. Schematic of the experimental column apparatus.

Capillary pressure head was measured with three mini-tensiometers (Rhizosphere Research Products, Wageningen, The Netherlands) inserted at 6, 12 and 19 cm from the upper sand surface. Two TDR probes (Soilmoisture Equipment Corp., Santa Barbara, USA) for measuring water content were also installed at 7 and 13 cm from the lower boundary. Data from the tensiometers and TDR were collected continuously using a CR10X datalogger (Campbell Scientific Ltd, Lougborough, UK) and monitored with a computer.

The column was flushed under saturated conditions with about seven pore volumes of the buffered solution to standardize the ionic strength and pH of the system. The chemical conditions were verified by measuring the pH and IS of both the influent and effluent. Unsaturated experiments were performed at various saturation levels. A uniform saturation and capillary pressure along the column was established in each experiment; deviations in water content between the upper and lower ports were less than 7%. Uniform saturation conditions were achieved at a given flow rate by gradually increasing the suction at the bottom of the column by lowering the outflow level.

Readings from the three mini-tensiometers confirmed that a unit hydraulic gradient was established along the column. Once uniform and steady-state flow was established at a given water content, the only driving force for water flow was gravity. In this case Darcy flux equals the hydraulic conductivity at that saturation level. To minimize the effect of the flow velocity on our results, we applied a hydraulic gradient in the saturated experiments such that the flow velocity was approximately the same as in one of the unsaturated experiments. Table 1 shows a summery of the various column experiments.

Prior to phage application, tracer experiments were carried out to determine the dispersion coefficient of each experiment. A solution containing 1 g/l of NaCl was applied to the column at a known water saturation. The breakthrough curve was then obtained by measuring the electrical conductivity (EC) of the outflow as a function of time. Following the salt tracer experiment and after the salt was thoroughly flushed from the column, a suspension of bacteriophages MS2 and ϕX174 containing about 10^6 plaque-forming units (pfu) per milliliter of each phage was introduced onto the column. The virus suspension was applied for 5-10 pore volumes (seeding duration) in attempts to obtain a steady-state breakthrough curves. Virus-free solution was subsequently applied to study the elution portion of the effluent curve. In most cases, the column was drained to investigate the role of a moving SWA on virus remobilizing. Several studies (Gomez-Suarez et al., 2001; Saiers et al., 2003) previously reported the detachment of bacteria and colloids from solid surfaces upon the passage of air-water interfaces, as a result of the solid-water-air contact lines (SWA).

Effluent samples were collected from the bottom of the column at regular intervals using a fraction collector, and analyzed for virus concentrations. All experiments were conducted in a cold room (5±3°C) to minimize inactivation of viruses. Five experiments were carried out at different saturation and solution chemistry levels as shown in Table 1. They were labeled by the corresponding conditions. For example, experiment HpLi100 was carried out at high pH, low IS, and 100% saturation. Experiments HpLi100 and HpLi65 were conducted for conditions in which adsorption to the SWI was expected to be minimal. This was achieved by increasing the pH of the solution to 9 and maintaining a very low IS (0.6 mM). For this pH condition, positively-charged sites on the surface of sand grains originated from iron oxides should have

reversed to become negatively charged (Elimelech *et al.*, 2000). Experiments LpHi100, LpHi66 and LpHi52 were carried out at pH 7 and IS of 19 mM where more extensive attachment to the SWI was expected due to presence of iron oxides on the surface grains (45 mg Fe Kg^{-1}).

Modelling of transport and fate of viruses under saturated and unsaturated conditions

After a certain travel time and travel distance through the porous media, viruses are removed from the soil water. Processes of major importance for the removal of viruses during this passage are adsorption and inactivation. The governing equation of one dimensional unsaturated virus transport, including terms accounting for adsorption to the SWI and the AWI, follows as:

$$\frac{\partial \theta C_l}{\partial t} = \frac{\partial}{\partial z}\left(\theta D \frac{\partial C_l}{\partial z}\right) - \frac{\partial (q C_l)}{\partial z} - \mu_l \theta C_l - r_s - r_a \tag{1}$$

where C_l is the number of free viruses per unit volume of the aqueous phase [pfuL^{-3}]; further referd to it as the free virus concentration, θ is the water content (-), D is the dispersion coefficient [L^{2}T^{-1}], q is the Darcy water flux density [LT^{-1}], μ_l is the inactivation rate coefficient for free viruses [T^{-1}], and r_s and r_a are adsorption rates to the SWI and AWI, respectively [pfuL^{-3}T^{-1}]. Note that inactivation of free viruses is assumed to be of a first- order process (Schijven and Hassanizadeh, 2000).

Virus adsorption to the soil-water interface (SWI): The following kinetic formulation for adsorption of viruses to the SWI was employed (Bales *et al.*, 1991, 1993; Schijven and Hassanizadeh, 2000):

$$\frac{\partial \rho_b C_s}{\partial t} = r_s - \mu_s \rho_b C_s = k_{att}^s \theta C_l - k_{det}^s \rho_b C_s - \mu_s \rho_b C_s \tag{2}$$

where C_s is the adsorbed virus concentration at the SWI in terms of number of viruses per unit mass of soil [pfuM^{-1}], μ_s is the inactivation rate coefficient for attached viruses [T^{-1}], ρ_s is the bulk density of the soil [ML^{-3}], and k_{att}^s and k_{det}^s are the attachment and detachment rate coefficients, respectively [T^{-1}]. Note that the attachment, detachment and inactivation rates are assumed to be linear. In case of heterogeneities in the soil properties

19

or between virus particles, more than one kinetic adsorption site may be present (Schijven and Simunek, 2001). We note that, even in the case of a homogeneous SWI, k_{att}^{s} and k_{det}^{s} are not necessarily constant since they may be affected by such factors as pH, ionic strength, organic matter content, temperature, grain size, and flow velocity (Schijven and Hassanizadeh, 2000). Under unsaturated conditions, the adsorption coefficients may also be a function of water content.

Virus adsorption to the air-water interface (AWI): The attachment of viruses to the AWI can be described by the following mass balance equation:

$$\frac{\partial aC_a}{\partial t} = r_a - \mu_a aC_a = k_{att}^{a}\theta C_l - k_{det}^{a} aC_a - \mu_a aC_a \tag{3}$$

where C_a is the adsorbed virus concentration at the AWI in terms of number of viruses per unit volume of air [pfu.L^{-3}], k_{att}^{a} and k_{det}^{a} are rate coefficients for attachment and detachment of viruses to and from the air-water interface [T^{-1}], μ_a is the inactivation rate coefficient for attached viruses [T^{-1}], and a is the air content (the volume of air per unit volume of the soil, [-]). In some cases adsorption may be nonlinear, in which case the adsorption coefficient becomes a function of C_a (e.g. in the case of blocking of attachment sites).

Parameter estimation

The governing equations (1-3) were solved numerically subject to appropriate initial and boundary conditions using the HYDRUS-1D software package (Simunek *et al.*, 1998). HYDRUS-1D simulates water, heat, and multiple solute movement in one-dimensional variably-saturated porous media. We used a modified version of HYDRUS-1D that permits consideration of two distinct sites for reversible kinetic adsorption (Schijven and Simunek, 2001). The code is coupled to a nonlinear least square optimization routine based on the Marquardt-Levenberg algorithm (Marquardt, 1963) to facilitate the estimation of solute transport parameters from experimental data.

As can be seen from Eqs (1), (2) and (3), the model contains the following parameters: the water content (θ), the average pore water velocity ($v = \dfrac{q}{\theta}$), the dispersivity ($\lambda = \dfrac{D}{v}$), three inactivation rate coefficients (μ_l, μ_s, μ_a), and the attachment and the detachment rate coefficients. Several of these parameters were estimated from independent experiments. The water content (θ) was measured directly; this parameter as explained earlier was reasonably constant in time and space. The average pore water velocity (v) was calculated from direct measurement of the water flux and the water content for each experiment. The dispersivity (λ) of the saturated and unsaturated column was estimated by inverse analysis of the breakthrough data of NaCl. As expected, the dispersivity was found to increase with decreasing saturation (Toride *et al.* 2003). We assumed that the NaCl-based dispersivity was the same as for the viruses. Small variations in the dispersivity were judged not to be important since advection was always the dominant transport process in our experiments as reflected by relatively large values of the column Peclet number, Pe=λL, where L is column length. Values of Pe in our experiments were always greater than 40.

The inactivation rate coefficient of free viruses (μ_l) as measured with the batch experiments was assumed to be applicable also to the column experiments. The inactivation rate coefficient for bacteriophages attached to the solid surface (μ_s) was furthermore assumed to be the same as μ_l. Enhanced or decreased inactivation of attached viruses has been reported (see e.g. Sakoda *et al.*, 1997; Gerba, 1984). However, the ratio of μ_l/μ_s is generally close to one (Schijven and Hassanizadeh, 2000). In any case, we fitted the saturated breakthrough curves with and without μ_s and found no significant effect on the values of attachment and detachment coefficients. The fitted value of μ_s was found to be very small and of the same order as μ_l. This is because of the short duration of our experiments (5 to 6 hours) and low temperature that we were able to assume solid phase inactivation to be insignificant. Similar results were obtained by fitting μ_a to unsaturated breakthrough curves. Therefore, μ_a was also assumed to have the same value as μ_l.

The attachment/detachment rate coefficients (k^s_{att}, k^s_{det}) for saturated column experiments, were obtained by fitting the solution of Eqs (1) and (2) to the virus breakthrough data. The very small concentration values at the tail of the breakthrough curve were found to have an insignificant effect on the fitted parameter values. Although, they can be given more weight by using log-transformed values of the breakthrough concentrations in the fitting process.

Values of k^s_{att}, k^s_{det}, determined from the saturated experiments cannot be transferred directly to the unsaturated experiments since they likely depend on water content. Therefore, unsaturated breakthrough curves were fitted with Eqs.(1), (2), and (3) to determine the rate coefficients k^s_{att}, k^s_{det}, k^a_{att}, and k^a_{det} at a given water content. Results of the fitting process were at first very much affected by initial estimates for the parameters. This problem was avoided by using the following protocol: values of k^s_{att}, k^s_{det} obtained from the saturated experiments were used as initial estimates for the corresponding parameters under unsaturated conditions. With these initial values, the breakthrough curves were fitted without log-transformation so that data from the breakthrough part of the curve and the plateau were dominant. The resulting fitted parameters were then used as initial guesses for fitting the log-transformed effluent curves. This resulted in a final set of parameter values which were still compared with the data to make sure that they fitted the entire effluent curve. A similar procedure was used for fitting saturated breakthrough data with the two-site kinetic model (k^1_{att}, k^1_{det}, k^2_{att}, and k^2_{det}) when a single site model was found to be unable to produce a reasonable fit.

RESULTS

Tracer experiments

Tracer experiments using sodium chloride were carried out to estimate dispersivity of the sand at different saturation levels. The breakthrough curves from all experiments were symmetrical with no evidence of tailing. This indicated that dead end pores and immobile water either did not exist or did not play a significant role in causing physical non-equilibrium in the transport of solute. Table 1 shows the values of dispersivity estimated by fitting the breakthrough data with Hydrus-1D, which indicates that the dispersivity increases with decreasing water contents. Figure 2 shows the fitted

breakthrough data obtained from NaCl experiment associated with LpHi52 (52% saturation) and demonstrates insignificant tailing. Tracer results from replicate saturated column experiments (HpLi100 and LpHi100) indicate that our packing procedure was reproducible.
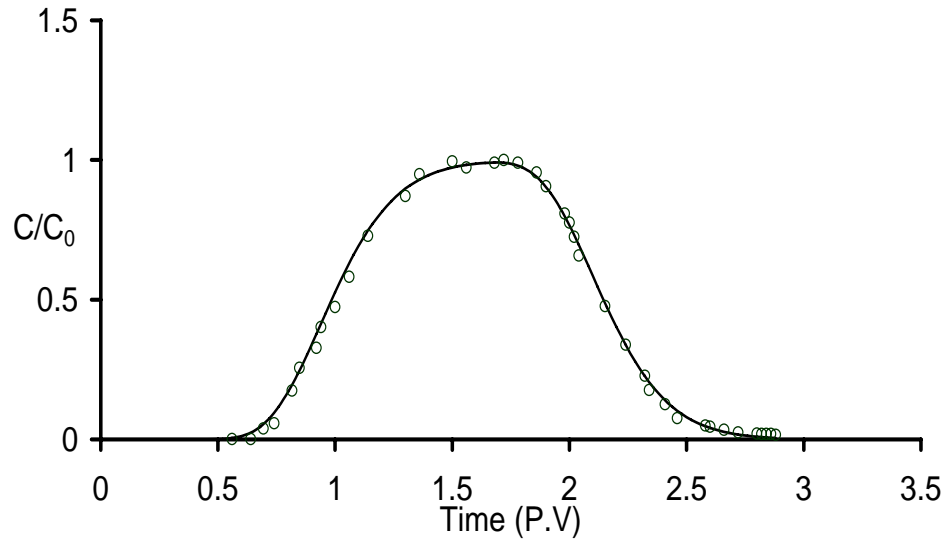
Figure 2. Measured (symbols) and fitted (lines) breakthrough curves of salt tracer (NaCl) in experiment LpHi52 (52% saturation).

Virus inactivation in batch experiments

The results obtained from batch experiments showed that there was no significant difference between inactivation rates at pH 7 and 9 for the two bacteriophages. The value of the inactivation rate coefficient of MS2 was 3.4×10^{-5} min^{-1} (0.043 day^{-1}) and that of ϕX174 was 1.3×10^{-5} min^{-1} (0.014 day^{-1}). As was mentioned, these values were also used for μ_s and μ_a.

Description of the breakthrough curves

Measured and fitted breakthrough curves for all experiments (conducted at different saturation levels and solution chemistry) are shown in Figures 3 and 4. Breakthrough curves (left) are plotted with the normalized concentration (C/C_0) on a linear scale in order to emphasize differences in the maximum values of C/C_0 between

experiments. Breakthrough curves (right) are also plotted with C/C_0 on a logarithmic scale in order to focus on the tails of the breakthrough curves.

In the series of experiments (experiments HpLi100 and HpLi65 in Figure 3) conducted at pH 9 and low IS, it can be observed that both viruses were adsorbed weakly to SWI and/or AWI. This can be deduced by examining the logarithmic plot of breakthrough curves. Notice the steep decline of the tails, and the fact that a plateau with $C/C_0=1$ was reached during the seeding period. Application of the one-site kinetic adsorption model produces a good fit of the breakthrough data for both bacteriophages even in the case of unsaturated conditions. Table 2 lists the corresponding parameter values and standard deviations.
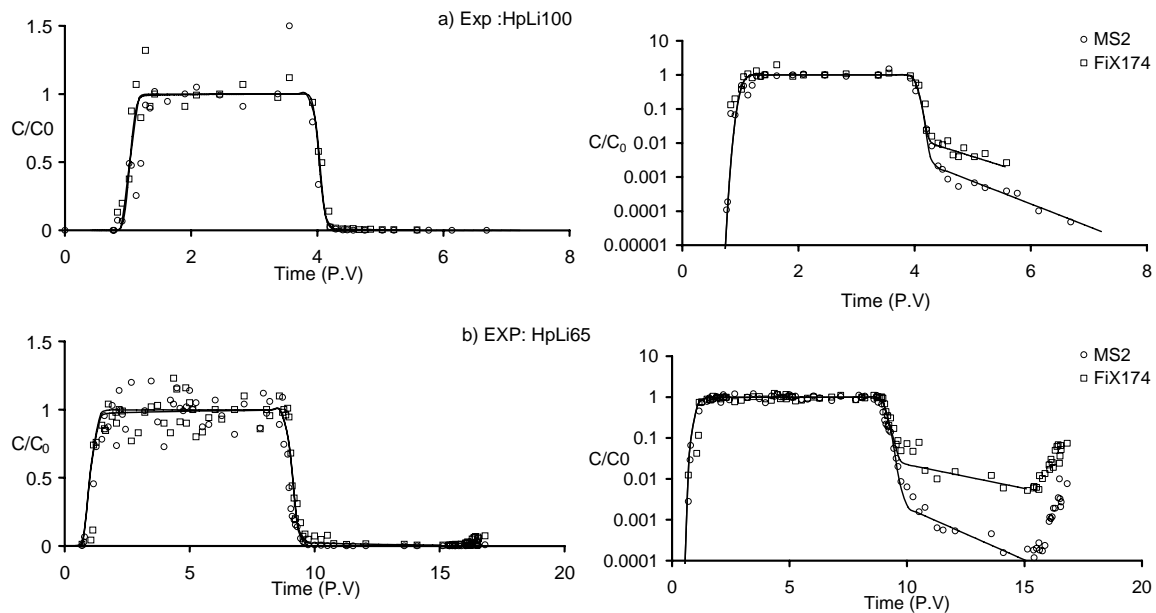
Figure 3. Measured (symbols) and fitted (lines) breakthrough curves of MS2 and ϕX174 at pH 9 and IS 0.6 mM in experiments HpLi100 (100% saturation) and HpLi65 (65% saturation). Left plots: C/C_0 on linear scale. Right plots: C/C_0 on log-scale.
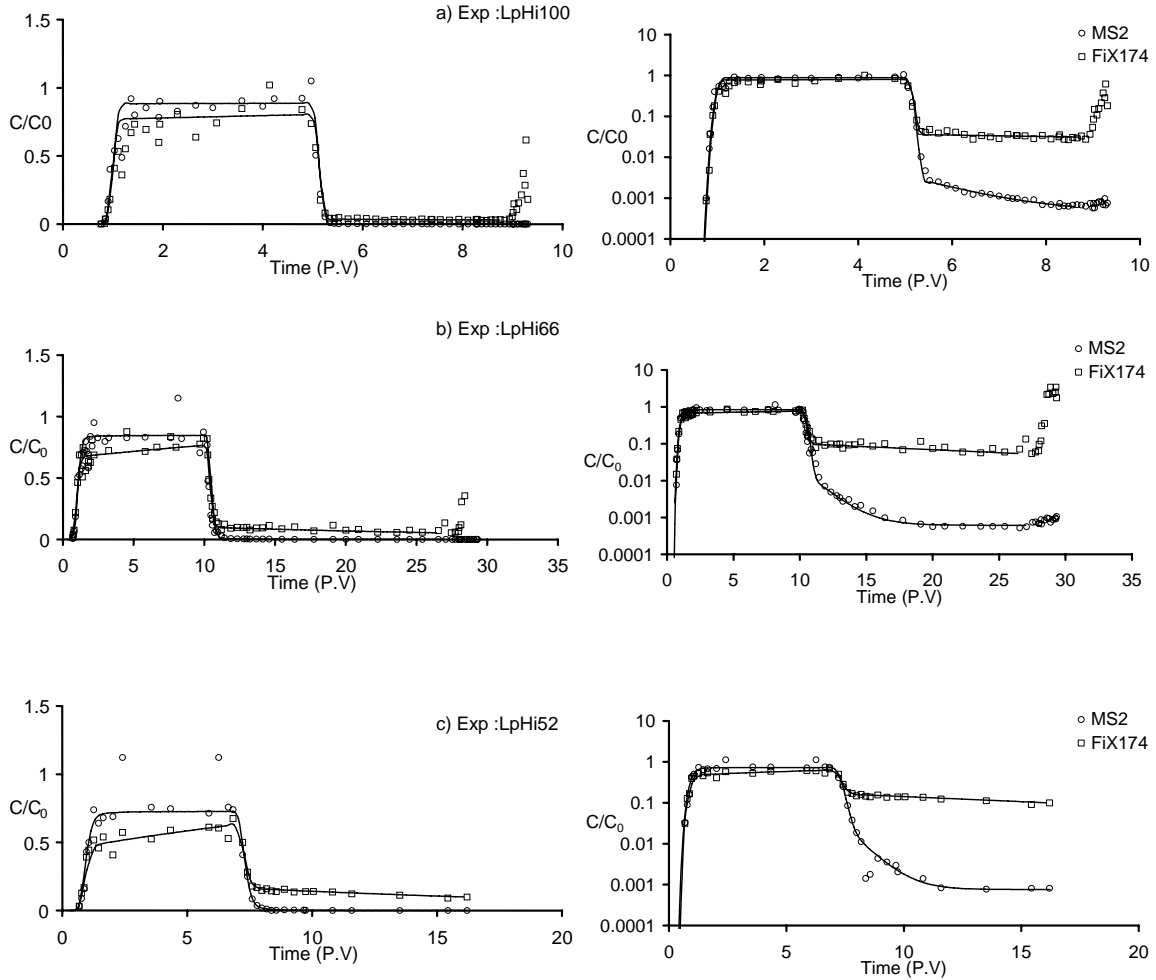
Figure 4. Measured (symbols) and fitted (lines) breakthrough curves of MS2 and φX174 at pH 7 and IS 19 mM in experiments LpHi100 (100% saturation), LpHi65 (66% saturation), and LpHi52 (52% saturation). Left plots: C/C_0 on linear scale. Right plots: C/C_0 on log-scale.

In the series of experiments conducted at pH of 7 and higher IS of 19mM, there was increased attachment as the outflow concentrations of the viruses did not reach the inflow concentration, even under saturated conditions (see plots on the left side of Figure 4). In the case of φX174, a one-site kinetic model still provided a satisfactory fit of the breakthrough curves. In the case of MS2, however, more complex transport behaviour was observed. The tails of the breakthrough curves of MS2 plotted in log-scale showed a relatively smooth transition of the declining limb to a long straight tail, even in the case

of 100% saturation (experiment LpHi100). It was therefore necessary to employ a reversible two-site kinetic adsorption model in order to fit the breakthrough curves.

Effect of solution chemistry

As can be seen from Table 2, k_{att} increases and k_{det} decreases as the solution condition becomes favorable for adsorption. In order to compare the retention capacity of the bacteriophages at different solution chemistry and saturation levels, the distribution coefficient K_D for each site was determined as the ratio of k_{att}/k_{det}. Calculated values are given in Table 3. Moreover, the mass balance of viruses was determined by comparing the number of viruses coming out of the column, calculated from integrating the area under the breakthrough curves, to the total number of seeded viruses (see Table 4). From these values, it is clear that the retention capacity increases both under saturated and unsaturated conditions as pH decreases and IS increases.

Under saturated conditions, the value of k_{att} for ϕX174 is about twenty times higher at pH 7 and higher IS (experiment LpHi100) than at pH 9 and low IS (experiment HpLi100), whereas the value of k_{det} is about twenty times lower. A similar effect is observed for unsaturated conditions (experiment HpLi65 versus LpHi66 and LpHi52). It should be noted that we cannot evaluate individually the relative roles of pH and IS. This data just suggests the combined influence of the two parameters on k_{att} and k_{det}.

Effect of water content

From Table 3, we can clearly see that when the condition is favourable for attachment the retention of both ϕX174 and MS2 tends to increase as the saturation decreases. At high pH and low IS, the effect of water content was negligible for both bacteriophages as adsorption was small. The reverse seems to be true in experiments conducted at pH 7 and higher IS. This is also reflected in the values of k_{att} presented in Table 2. The value of k_{att} for both phages increased with decreasing water content. However, there was no clear effect of water content on the value of k_{det}.

Table 2. Parameter values determined from fitting the bacteriophages breakthrough curves (average ± standard deviations)

	†$k^1_{att} \times 10^3$ (min^{-1})	$k^1_{det} \times 10^3$ (min^{-1})	$k^2_{att} \times 10^3$ (min^{-1})	$k^2_{det} \times 10^3$ (min^{-1})	R^2 (%)
Experiment			ϕX174		
HpLi100	0.43 ± 0.18	25 ± 11			89
HpLi65	0.82 ± 0.34	7.0 ± 1.4			91
LpHi100	8.2 ± 1.7	1.4 ± 0.2			88
LpHi66	13 ± 1.4	1.5 ± 0.3			90
LpHi52	15 ± 1.1	1.7 ± 0.14			94
			MS2		
HpLi100	0.10 ± 0.03	47 ± 7			96
HpLi65	0.13±0.03	30±4.6			98
LpHi100	0.10±0.03	20±1.8	3.7±1.1	0.030±0.010	98
LpHi66	0.50±0.05	22±2.3	5.1±1.2	0.010±0.006	97
LpHi52	0.80±0.02	25±2.5	6.4±1.5	0.010±0.009	94

†Superscripts 1 and 2 denote kinetic (k) interaction of type 1 and 2, respectively.

Effect of drainage

To investigate whether the bacteriophages retained in the column were attached to the SWI or to the AWI, the column was fully drained at the end of experiments HpLi65, LpHi100, and LpHi66. This was done by stopping the water influx and lowering the effluent hanging tube to gradually drain the column under gravity.

A sharp increase of outflow concentration for ϕX174 was observed after draining the column (Figures 3b, 4a and 4b). At 100% saturation (experiment LpHi100), ϕX174 particles could only have been retained at the SWI and thus were subsequently remobilized by moving the SWA contact lines during drainage. Remobilization of bacterial and clay particles attached to the SWI by moving SWA contact lines has also been reported by other researchers (Powelson and Mills, 2001; Saiers *et al.*, 2003; Sirivithayapakorn and Keller, 2003).Under unsaturated conditions (experiments HpLi65

and LpHi66), no distinction could be made between release of φX174 from the SWI or AWI.

For MS2, an increased concentration following drainage was only observed at pH 9 and low IS (experiment HpLi65, Fig.3b), but not at pH 7 and higher IS (experiments LpHi100 and LpHi66, Fig4a and 4b). We believe that at pH 9 and low IS, remobilization of MS2 by moving SWA contact lines was facilitated by the strong negative charge of MS2. In experiment LpHi100, despite the fact that more MS2 was retained, no increased concentration was observed after the drainage. This may suggests that the attached MS2 particles were strongly bound to SWI such that passing of the SWA contact lines was not able to remobilize them. This hypothesis is in agreement with the high value of k_{att} and the low value of k_{det} to the first site of adsorption. In experiment LpHi66, no increased concentration in breakthrough curve was also observed after draining the column.

Table 3. Calculated distribution coefficients (K_D)

Experiment	φX174	MS2	
	k_D	† k_D^1	k_D^2
HpLi100	0.02	0.002	
HpLi65	0.1	0.004	
LpHi100	5.8	0.005	123
LpHi66	8.6	0.02	510
LpHi52	8.8	0.03	640

†Superscripts 1 and 2 refer to the two different kinetic sites.

Table 4. Calculated mass balance (%)

Experiment	MS2	φX174
HpLi100	100	100
HpLi65	100	99
LpHi100	88	93
LpHi66	85	89
LpHi52	73	80

DISCUSSION

In line with expectations, our results clearly show that the retention of viruses in the soil increases as the water saturation decreases. This could be due to enhanced adsorption to solid-water interfaces, attachment to air-water interfaces, attachment to the solid-water-air contact lines, or a combination of these effects. Results of our experiments show that the extent of enhanced retention depends on the solution chemistry and the virus type. In particular, the isoelectric point (IP) of the virus and soil surfaces seems to be important.

Adsorption of viruses to the AWI is believed to be controlled by solution chemistry, particle surface charge, and hydrophobicity (Wan and Tokunaga, 2002; Wan and Wilson, 1994a). Studies have shown that air-water and oil-water interfaces are negatively charged for pH values larger than 2 (Li and Somansundaran 1991; Gracia *et al*. 1995; Marinova *et al*. 1996). Wan and Tokunaga (2002) demonstrated in bubble column experiments that only positively-charged particles attached to the negatively-charged AWI. Under our experimental conditions, where both MS2 and ϕX174 are negatively charged, we may expect little attachment to the AWI. Indeed, we believe that virus retention by the solid-water interface was the dominant effect and that retention by the air-water interface was insignificant.

Although it may seem difficult to differentiate between attachment to the SWI and the AWI, we believe that a careful analysis of the breakthrough curves, specially the tail part, may provide clues to the relative significance of these two attachment mechanisms. If there is attachment to both the AWI and SWI, a two-site kinetic model would likely be required to simulate the breakthrough curves under unsaturated conditions. However, in the case of ϕX174, for both high and low pH experiments and at various saturations, a one-site kinetic model could simulate breakthrough curves satisfactorily. Similar results were obtained for MS2 but only for high pH and low IS conditions. Therefore, we conclude that attachment to the AWI was negligible in these cases.

For low pH-high IS experiments, however, a two-site kinetic model was needed for simulating MS2 breakthrough curves in both saturated and unsaturated experiments (see parameters for LpHI100 in Tables 2 and 3). This suggests that there are two different adsorption sites on the SWI: a weak-adsorbing site and a strongly-adsorbing

site. If there was significant adsorption to the AWI, we believe that a three-site kinetic model would be required to simulate the breakthrough curves of MS2 in the LpHi66 and LpHi52 experiments. This was, however, not the case. We are therefore led to the conclusion that adsorption to the AWI was not significant, or that it was of the same order of magnitude as one of the adsorption sites on the SWI so that the two effects could be lumped. Although adsorption of MS2 to the AWI cannot be ruled out completely, we speculate that increased attachment under unsaturated experiments occues because of enhanced attachment to the SWI instead of the AWI. Further research is needed to prove this hypothesis.

Additional evidence on the insignificance of AWI adsorption comes from the drainage of the columns at the end of the HpLi65, LpHi100, and LpHi66 experiments. The drainage process creates AWI in the column. If there was adsorption to the AWI, drainage should create additional adsorption sites and, thus, it should produce a drop in the breakthrough concentration. In the case of ϕX174, the opposite trend was observed in , and resulted in a sharp increase in the breakthrough concentration. A similar result was obtained for MS2 in the experiment HpLi65, where adsorption to SWI was weak. No effect of drainage on the breakthrough concentration of MS2 was observed in experiments LpHi100 and LpHi66, where there was strong adsorption to the SWI.

Our results are in contrast to some earlier studies that suggest that irreversible attachment to the AWI is the main mechanism for enhanced removal of viruses and colloidal particles with decreasing water content (*e.g.* Wan and Wilson, 1994a; Powelson *et al.*, 1990; Jin *et al.*, 2000; Powelson and Mills 2001; Keller and Sirivithayapakorn 2004).Our results indicate that if there was any attachment to AWI, it certainly was not irreversible. In all cases, we needed to include relatively large detachment rate coefficients in our model (see Table 2) in order to obtain a satisfactory fit to the breakthrough curves, especially in the tail portion of the curves. Moreover, C/ C_0 values of both bacteriophages reached a plateau with the value of unity and the mass recovery was almost 100% in saturated and unsaturated experiments conducted at a high pH. This means that, for the duration of our experiments, inactivation and irreversible attachment to both the SWI and AWI were negligible.

Some authors have suggested that hydrophobic interactions are responsible for attachment of viruses to the AWI (Jin *et al*., 2000). Here again, if this were the case, we would have needed two different sites for modelling unsaturated breakthrough curves. Moreover, hydrophobic interactions should have been more pronounced at a high pH and low IS, where conditions for adsorption to the solid phase are unfavourable. This behaviour, however, was not observed. We therefore believe that hydrophobic interactions do not play a significant role in adsorption of these viruses to the AWI's.

A two-site kinetic model was needed to simulate MS2 breakthrough curves in both saturated and unsaturated experiments that were carried out at pH 7 and IS of 19 *mM*. Table 3 shows that there was a strong adsorption site and a week adsorption site, with saturated K_D values equal to 123 and 0.005, respectively. The only plausible explanation for such a strong adsorbing site under saturated conditions is the presence of iron oxide on the surface of sand (45 mg Fe/kg, see Materials and Methods). At a neutral pH, iron oxides are positively charged whereas MS2 is still negatively charged. This results in strong adsorption of MS2 to the SWI under both saturated and unsaturated conditions. The same result does not hold for ϕX174 because it has an almost neutral surface charge at a pH of 7. Indeed, breakthrough curves for ϕX174 were satisfactorily modelled using a one-site kinetic model with a relatively small distribution coefficient, even at a pH of 7 (see Table 3).

There is a clear increase in the retention of both phages as the saturation decreases. This enhanced adsorption can be explained as follows. Kinetic adsorption is the resultant of two mechanisms: diffusion of viruses from within the pores to the soil grain surfaces and then attachment to the surfaces. The reverse occurs in the case of desorption. As the saturation decreases, the water moves in smaller pores or in narrow wedge-shaped corners. As a result, the diffusion length decreases and this leads to faster adsorption kinetics. Also, at lower saturations, zones of immobile water will be formed within the soil. Diffusion into these zones will manifest itself as enhanced adsorption. Some researchers have suggested that increased attachment of viruses to the SWI is due to an increase in electrostatic and hydrophobic interactions under unsaturated conditions, as larger pores are no longer available for transport and viruses are closer to the SWI (Lance and Gerba, 1984; Chu *et al.*, 2001). However, this is unlikely to be the case, as

was also dismissed by Powelson *et al.* (1990), because the effective range of electrostatic and hydrophobic forces are on the order of nanometres and the sizes of water-filled pores is much larger.

We emphasize that our results do not exclude the possibility of significant adsorption of viruses to the AWI under other chemical conditions. More studies are needed to determine the range of chemical conditions where significant attachment to AWI may occur.

CONCLUSIONS

Column experiments were conducted to examine the fate and transport of viruses using two different bacteriophages (MS2 and ϕX174), two different solution chemistries, in terms of pH and ionic strength, and various saturation levels. The following conclusions may be drawn:

1. At lower pH and higher IS and under saturated conditions, both ϕX174 and MS2 were retained significantly by attachment to the SWI due to electrostatic interactions.
2. Under unsaturated conditions attachment of both ϕX174 and MS2 increased, whereas detachment was little affected. The increased attachment was attributed to enhanced attachment to the SWI.
3. Our results indicate that if there is any attachment to the AWI, this process is not irreversible.
4. Under unfavourable conditions for attachment to the SWI, viruses may be scoured from the SWI by moving the SWA contact lines.

Acknowledgments

Chapter 3

Role of Air-Water interfaces on retention of viruses under unsaturated conditions

Torkzaban, S., S.M. Hassanizadeh, J.F. Schijven, and H.H.J.L. van den Berg, Role of Air-Water Interfaces on retention of viruses under unsaturated conditions," *Water Resources Research*, 42, W12S14, doi:10.1029/2006WR004904, 2006.

Abstract

We investigated transport of viruses through saturated and unsaturated sand columns. Unsaturated experiments were conducted under conditions of uniform saturation and steady-state water flow. The water saturation ranged from 1 to 0.5. Bacteriophages MS2 and ϕX174 were used as surrogates for pathogenic viruses in these studies. Phosphate buffered solutions with different pH values (7.5, 6.2, 5.5, and 5) were utilized. Virus transport was modeled assuming first-order kinetic adsorption for interactions to the solid-water interface (SWI) and the air-water interface (AWI). Under saturated conditions, virus retention increased as pH decreased and a one-site kinetic model produced a good fit to the breakthrough curves. Under unsaturated conditions, a two-site kinetic model was needed to fit the breakthrough curves satisfactorily. The second site was attributed to the adsorption of phages to the AWI. According to our results, ϕX174 exhibits a high affinity to the AWI at pH values below 6.6 (the isoelectric point of ϕX174). Although it is believed that MS2 is more hydrophobic than ϕX174, MS2 had a lower affinity to the AWI than ϕX174, presumably due to the lower isoelectric point of MS2, which is equal to 3.9. Under unsaturated conditions, viruses captured within the column could be recovered in the column outflow by re-saturating and immediately draining the column. Draining of columns under saturated conditions, however, did not result in any recovery of viruses. Therefore, the recovery can be attributed to the release of viruses adsorbed to the AWI. Our results suggest that electrostatic interactions of viruses with the AWI are much more important than hydrophobicity.

Introduction

Diseases related to contamination of drinking water constitute a major stress on human health. Among pathogenic microorganisms, viruses represent the worst case as they are very small and can be infectious at very low doses. Fortunately, soil can act as a filter for many groundwater contaminants such as infectious agents. In this regard, the purification capacities of saturated soil have been known and studied for some time [Schijven and Hassanizadeh, 2000; Harvey and Harms, 2002; Ginn et al., 2002]. Column studies suggest that unsaturated soil has even a greater ability for the removal of viruses [Bales et al., 1991; Powelson and Gerba, 1994; Powelson et al., 1990; Poletika et al., 1995; Thompson and Yates, 1999; Jin et al., 2000; Chu et al., 2001]. Since groundwater recharge comes from infiltrating water that passes through the vadose zone, the unsaturated soil serves as the first line of defense in protecting drinking water supplies from pathogen contamination. Accurate knowledge of the processes that control fate and transport of viruses in unsaturated porous media is therefore needed to assess contamination potential and to design the setback distances for water production wells.

In general, flow and virus transport in the unsaturated zone are more complex than in the saturated zone for the following reasons. First, virus adsorption can take place on both solid-water (SWI) and air-water (AWI) interfaces. Adsorption of viruses to AWI is complex and our knowledge of corresponding mechanisms is yet limited. Second, transient flow conditions and variable water saturations may result in continuous re-distribution of viruses among the SWI and AWI. Also arrival of new water supplied by irrigation and precipitation may create variable chemical conditions that result in re-distribution of and (re)mobilization of viruses, as it has been reported for other colloids [El-Farhan et al., 2000; Ryan et al., 1998]. Third, water flow and transport processes in the vadose zone are complicated by preferential flow, fingering, and funneled flow [Kung, 1990a; Seyfried and Rao, 1987] that could greatly enhance the downward movement of contaminants [Kung, 1990b].

Under unsaturated conditions, viruses are believed to be present mainly in the water phase, on the AWI, and on the SWI. Virus transport in the unsaturated zone is greatly influenced by degree of water saturation [Chu et al. 2001; Jin et al. 2000; Lance and Gerba 1984; Powelson et al. 1990; Poletika et al. 1995]. The AWI is believed to be a

36

site of strong adsorption for both hydrophobic and hydrophilic colloidal particles. But, it has been reported in unsaturated column experiments that hydrophobic colloids could be retained to a greater extent than hydrophilic colloids due to increased sorption to the AWI [Corapcioglu and Choi, 1996]. Attachment of colloids onto the AWI is often considered to be irreversible due to electrostatic and capillary forces that hold the colloids at the interface [Ducker et al. 1994; Wan et al. 1994; Wan and Wilson 1994b; Wan and Tokunaga 2002; Costanza-Robinson and Brusseau 2002; Sirivithayapakorn and Keller 2003).

There is also evidence that adsorption to the SWI increases as the water saturation decreases [Bitton et al.1984; Jorgensen1985; Chu et al. 2001]. The relative importance of the water saturation effect on virus retention and transport changes from minimal to significant, as the extent of positively-charged sites on the grain surface increases [Chu et al. 2001; Torkzaban et al. 2006].

In addition to adsorption to the AWI and SWI, colloids can be retained in soil by straining. Straining is the trapping of colloidal particles in the down gradient pore throats that are too small to allow particle passage [McDowell-Boyer et al., 1986]. Traditionally straining has been considered to be an important removal mechanism when the particle-collector size ratio is greater than 0.05 [Sakthivadivel, 1996]. Bradford et al. [2003], however, recently proposed straining as a capturing mechanism when the ratio of the particle size to the average grain size is even much smaller (around 0.005). The significance of the straining is also anticipated to increase under unsaturated conditions [Bradford et al. 2002, 2003], although no published studies have examined this hypothesis. However, straining is expected to be minimal for the bacteriophages in sand due to their very small size of around 25 nm.

In this study, we have investigated the significance of attachment to the AWI and the factors that affect it. To this end, several column experiments were conducted using two different bacteriophages and solutions of various pH. In an attempt to minimize the influence of the SWI, phosphate buffer was chosen because the phosphate ions tend to block positively-charged sites on soil surfaces [Sigg and Stumm 1981]. The following issues were specifically investigated in this study: (i) attachment to the AWI; (ii) detachment from the AWI; and (iii) viability of viruses attached to the AWI.

MATERIALS AND METHODS

Phages Characteristics and Solution Preparation

Bacteriophages such as MS2 and ϕX174 are commonly used as surrogates for pathogenic viruses. MS2 is an icosahedral phage with a diameter of 27 nm and a low isoelectric point (IP) of 3.9 (Zerda, 1982). Bacteriophage ϕX174 is similar in size to MS2, but is less hydrophobic [Shields and Farrah, 1987], and has an IP of about 6.7 [Ackermann and Dubow, 1987]. Highly concentrated suspensions of MS2 and ϕX174 suspensions were used to prepare stock suspensions, diluted with 1 g/l peptone-saline to a concentration of 10^{10}-10^{11} phages per liter. These stock suspensions were then used to prepare seeding suspensions of approximately 10^8 phages per liter. MS2 was assayed as described in ISO 10705-1 [2000] using host strain WG49 (ATCC 15597). Bacteriophage ϕX174 was assayed according to ISO 10705-2 [2000] using WG5 (ATCC 70078) as the host.

A phosphate buffer solution was prepared by dissolving 0.03 g/l KH_2PO_4 and 0.12 g/l K_2HPO_4 to ultra-pure water. The ionic strength was adjusted to 19mM by adding NaCl. The pH of the buffer was adjusted by adding NaOH to achieve a pH value of 7.5, 6.2, 5.5, and 5 for four different series experiments. Phage ϕX174 will be positively charged in experiments conducted at pH levels lower than 6.7, whereas MS2 (whose IP is 3.9) is expected to remain negatively charged at all considered pH levels.

To measure inactivation of phages in the water phase, a series of inactivation experiments was carried out. In the cold room (temperature of 5^oC), two liters of each of the four different solutions mentioned above (pH=7.5, 6.2, 5.5, and 5) were seeded with MS2 and ϕX174 at about the same concentration as the input concentrations of the column experiments. These suspensions were regularly analyzed over a period of one month. In this manner, inactivation rates at the various solution pHs were determined.

Column Set-up and Experiments

A schematic presentation of the column setup is shown in Figure 1. A cylindrical PVC column with an internal diameter of 10 cm and length of 23 cm was packed with sand. A hydrophilic nylon membrane with 10 μm pore size (SaatiTech, Veniano, Italy), supported by a stainless steel plate, was used at the bottom of the soil column to prevent

air phase breakthrough. Results of auxiliary experiments (performed without sand) demonstrated that neither the column body nor the end-fitting assemblies retained the viruses. Sand with a median grain size (d_{50}) of 140 μm and the uniformity (d_{60}/d_{10}) of 1.6 was used as the porous medium. The sand was treated with HCl (1mM) for about 20 minutes in order to remove any attached colloids, and then rinsed thoroughly with distilled water followed by oven drying at 110 °C. The free iron oxide content on the sand surface was measured to be 45 mg Fe. kg^{-1} as determined by the modified procedure of Mehra and Jackson (1960).

The column was wet-packed with the water level kept a few centimeters above the soil surface. Care was taken to ensure uniform packing by pouring the sand in small quantities. After each incremental addition of sand, the new sand layer was gently mixed with the previous layer and then the column was tapped to minimize any layering and to liberate any entrapped air. A shaker connected to the inlet tube was used to uniformly apply the buffer solution or the virus suspension on the upper surface of the column, which was covered by a filter paper.

Capillary pressure head was measured with three mini-tensiometers (Rhizosphere Research Products, Wageningen, The Netherlands) inserted at 6, 12 and 19 cm from the upper sand surface. Two TDR probes (Soilmoisture Equipment Corp., Santa Barbara, USA) for measuring water saturation were also installed at 4 and 15 cm from the upper boundary. Data from the tensiometers and TDR were collected continuously using a CR10X data logger (Campbell Scientific Ltd, Lougborough, UK) and were monitored with a computer.

Both saturated and unsaturated virus transport experiments were carried out. Each time the column was flushed under saturated condition with about thirty pore volumes of the buffered solution to mask any positively charged regions on grain surfaces. This was verified by measuring the pH of the influent and effluent, as the ligand exchange between phosphate and surface ferric ions releases hydroxides from the surface to the solution.
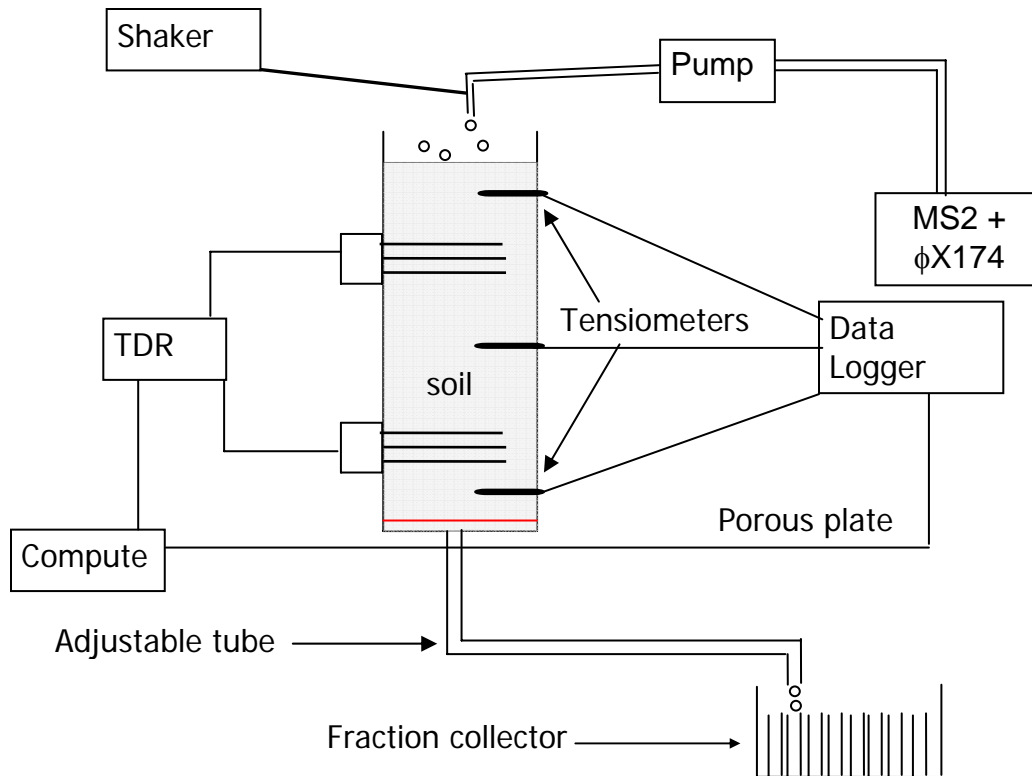
Figure 1. Schematic representation of experimental apparatus.

Unsaturated experiments were performed at various water saturation levels. A uniform saturation and capillary pressure along the column was established in each experiment through the following procedure. To establish a desired saturation, the water inflow rate was reduced to the hydraulic conductivity corresponding to that saturation. Then, the pressure head at the bottom of the column was gradually reduced to the value corresponding to the matrix potential at the desired saturation. This resulted in a unit hydraulic head gradient, i.e. constant capillary pressure, which implies a constant saturation along the column. Readings of tensiometers and TDR probe's verified the uniformity of saturation. To minimize hysteresis effects, we gradually decreased the bottom pressure head (by adjusting the position of the drip point of a hanging water tube) to achieve unit-gradient flow. To minimize the effect of water velocity in our results, we applied a hydraulic gradient in the saturated experiments such that the average water velocity was almost the same as in one of the unsaturated experiments. Table 1 shows general specifications of the four series of experiments.

After establishing a specified saturation and water chemistry, transport experiments were carried out in five stages: tracer experiment using NaCl, flushing of NaCl from the sand, seeding of phages, leaching out phages, and re-saturating and drainage (in case of unsaturated experiments) of the column. These stages are described below.

Prior to phage application, tracer experiments were carried out to determine the dispersion coefficient under corresponding column conditions. A solution containing 1 g/l of NaCl was fed to the column at a given water saturation and the breakthrough curve was obtained by measuring the electrical conductivity (EC) of the outflow. Following the salt tracer experiment, the column was flushed with the buffered solution in order to wash out the salt. This was verified by measuring EC of influent and effluent. Next a suspension of bacteriophages MS2 and ϕX174 containing about 10^6 plaque-forming units (pfu) of each phage per milliliter was introduced into the column. Virus suspension was applied for 5-10 pore volumes (seeding duration) in trying to obtain a steady-state breakthrough curve. Then virus-free solution was applied to obtain the declining limb and the tail of the breakthrough curve. Finally, the column drainage was carried out to investigate the effect of moving solid-water-air (SWA) contact lines on virus

Table 1. Experimental conditions of column experiments

Series No.	Saturation %	pH	Average velocity (cm/min)	Volumetric water content (%)	Dispersivity (cm)	Seeding duration (pore volume)
I	100	7.5	0.68	41	0.06	4.6
	50	7.5	0.46	21	0.56	7.24
II	100	6.2	0.68	41	0.06	8.90
	68	6.2	0.73	28	0.29	8.4
	50	6.2	0.46	21	0.56	10.4
III	100	5.5	0.68	41	0.06	7.4
	50	5.5	0.46	21	0.56	4.8
IV	100	5	0.68	41	0.06	8.90

remobilization. In the case of unsaturated experiments, the column was gradually re-saturated by raising the hanging water tube. However, there was always some air trapped inside the sand after re-saturation. The re-saturation process eliminated the continuous AWI's before draining the column, and released any viruses attached to them back into the solution.

Effluent samples were collected from the base of the column at regular intervals with a fraction collector (Fisher Scientific) and analyzed for virus concentrations. Effluent mass balances of both bacteriophages were calculated for each experiment. All experiments were conducted in a cold room (5 ± 3°C) to minimize inactivation of viruses.

Four series of experiments were carried out at different saturation and pH values, as shown in Table 1. The first series (series I) of experiments were conducted at pH 7.5. In this case, both bacteriophages are negatively charged (the IP's of MS2 and φX174 are about 3.9 and 6.7, respectively). The rest of experiments, namely series II (pH=6.2), III (pH=5.5), and IV (pH=5), were carried out at a pH in which φX174 is positively charged and MS2 is negatively charged.

Transport Models

As the viruses migrate through the porous medium, they are removed from the water. Processes of major importance for removal of viruses during this passage are adsorption and inactivation. Advection and dispersion only cause spreading of viruses and thereby attenuation of virus concentrations. The governing equation for three-dimensional unsaturated virus transport includes two terms to account for adsorption to the SWI and the AWI as follows:

$$\frac{\partial C_l}{\partial t} + v\,\frac{\partial C_l}{\partial x} = \lambda v\,\frac{\partial^2 C_l}{\partial x^2} - \mu_l C_l - \frac{r_s}{nS} - \frac{r_a}{nS} \tag{1}$$

here, C_l [pfu L^{-3}] is the number of free viruses per unit volume of the aqueous phase, n [-] is porosity, S[-] is the water saturation, λ [L] is the dispersivity, v [LT^{-1}] is the average water velocity, μ_l [T^{-1}] is the inactivation rate coefficient for free viruses, r_s and r_a [pfu L^{-3} T^{-1}] are adsorption rates to the SWI and AWI, respectively. Note that the inactivation of free viruses is assumed to be of first order [Schijven and Hassanizadeh, 2000].

Virus Adsorption to the Soil-Water Interface (SWI)

The following kinetic formulation for describing adsorption of viruses to the SWI has been employed [Bales et al., 1991, 1993; Schijven and Hassanizadeh, 2000]:

$$\frac{\partial \rho_b C_s}{\partial t} = r_s - \mu_s \rho_b C_s = k_{att}^s n S C_l - k_{det}^s \rho_b C_s - \mu_s \rho_b C_s \tag{2}$$

where C_s [pfu M^{-1}] is concentration of viruses adsorbed to the SWI in terms of number of viruses per unit mass of soil, μ_s [T^{-1}] is the inactivation rate coefficient for attached viruses, ρ_s [M L^{-3}] is the bulk density of the soil, k_{att}^s and k_{det}^s [T^{-1}] are the attachment and detachment rate coefficients, respectively. Note that attachment, detachment, and inactivation rates are assumed to be linear. In case of heterogeneities in soil properties or within virus population, there may be more than one kinetic adsorption site present [Schijven and Simunek, 2001]. It should be noted that, even in the case of homogeneous SWI, k_{att}^s and k_{det}^s are not necessarily constant, as they may be affected by factors such as pH, ionic strength, organic matter, temperature, grain sizes, and velocity [Schijven and Hassanizadeh, 2000]. Under unsaturated conditions, the adsorption coefficients may also be a function of water saturation.

Virus Adsorption to the Air-Water Interface (AWI)

The attachment of viruses to the AWI can be described by the following mass balance equation:

$$\frac{\partial a C_a}{\partial t} = r_a - \mu_a a C_a = n S k_{att}^a C_l - k_{det}^a a C_a - \mu_a a C_a \tag{3}$$

here a [-] is the air content, that is, the volume of air per unit volume of the soil, C_a [pfu L^{-3}] is the adsorbed virus concentration to the AWI in terms of number of viruses per unit volume of air. The rate coefficients k_{att}^a and k_{det}^a [T^{-1}] are for attachment and detachment of viruses to and from the air-water interface and μ_a [T^{-1}] is the inactivation rate coefficient for attached viruses. In nonlinear adsorption, the adsorption coefficient could be a function of C_a (e.g. in the case of blocking of the attachment sites). But that possibility is not considered here.

It would have been more appropriate to quantify the concentration of viruses adsorbed to the AWI in terms of number of viruses per unit area of the AWI. But, then we need to know specific areas of the AWI, that is, area of the AWI per unit volume of the soil. Such a quantity is, however, very difficult to measure and we did not have the means to measure it. Therefore, we have chosen for air content as a substitute for specific interfacial areas. The two are known to be related. It should be noted that the air content is related to water saturation by $a = n (1 - S)$.

The model parameters were determined by fitting the measured concentrations of bacteriophages in the outlet of the column with the solution of the governing equations (1-3). The governing equations were solved numerically subject to appropriate initial and boundary conditions using the software package HYDRUS-1D [Simunek *et al.*, 1998]. We used a modified version of HYDRUS-1D that permits consideration of two distinct sites for reversible kinetic adsorption [Schijven and Simunek, 2002]. The code is coupled to a nonlinear least square optimization routine based on the Marquardt-Levenberg algorithm [Marquardt, 1963] to facilitate the estimation of solute transport parameters from experimental data.

RESULTS and DISCUSSION

Virus Inactivation in the Aqueous Phase

The results obtained from the batch inactivation experiments showed that there was no significant difference between inactivation rates at the various pH values (i.e. 7.5, 6.2, 5.5, and 5) for the two bacteriophages. The value of the inactivation rate coefficient of MS2 was 3.3×10^{-5} min^{-1} (0.042 day^{-1}) and that of ϕX174 was 1.5×10^{-5} min^{-1} (0.015 day^{-1}). It is worth mentioning that we have included inactivation terms in our model for sake of being thorough, but that the experiments were designed to minimize the effect of inactivation. This was done by performing the experiments at a relatively low temperature (5 ^{o}C) and for a relatively short duration

Breakthrough Curves and Parameter Estimation

Figures 2 through 5 present measured concentration measurements as a function of time for MS2 and ϕX174 obtained from four series of experiments. At the top right corner of each figure, the breakthrough data are plotted with the normalized concentration (C/C_0) on a linear scale in order to highlight differences in maximum values of the C/C_0 between experiments. In the main plot, the breakthrough curves are plotted with the C/C_0 on a logarithmic scale in order to focus on the tailing region of the breakthrough curves.

Figures 2 through 5 reveal a systematic trend of increasing retention with decreasing pH and water saturation. As it was mentioned earlier, at the end of unsaturated experiments, the columns were re-saturated and then drained. As a result, there is a sudden raise in concentrations of bacteriophages at the end of the unsaturated breakthrough curves. The drainage of saturated columns, however, did not result in a rise in the outflow concentration.

As it can be seen from the governing equations, we need to determine the following parameters: water saturation (S), average pore water velocity (v), longitudinal dispersivity (λ), inactivation rate coefficients, and attachment and detachment rate coefficients. Some of these parameters were estimated from independent experiments. Water saturation (S) was measured directly and it was reasonably constant in time and space. The average pore water velocity (v) was calculated from direct measurement of water flux and water saturation.
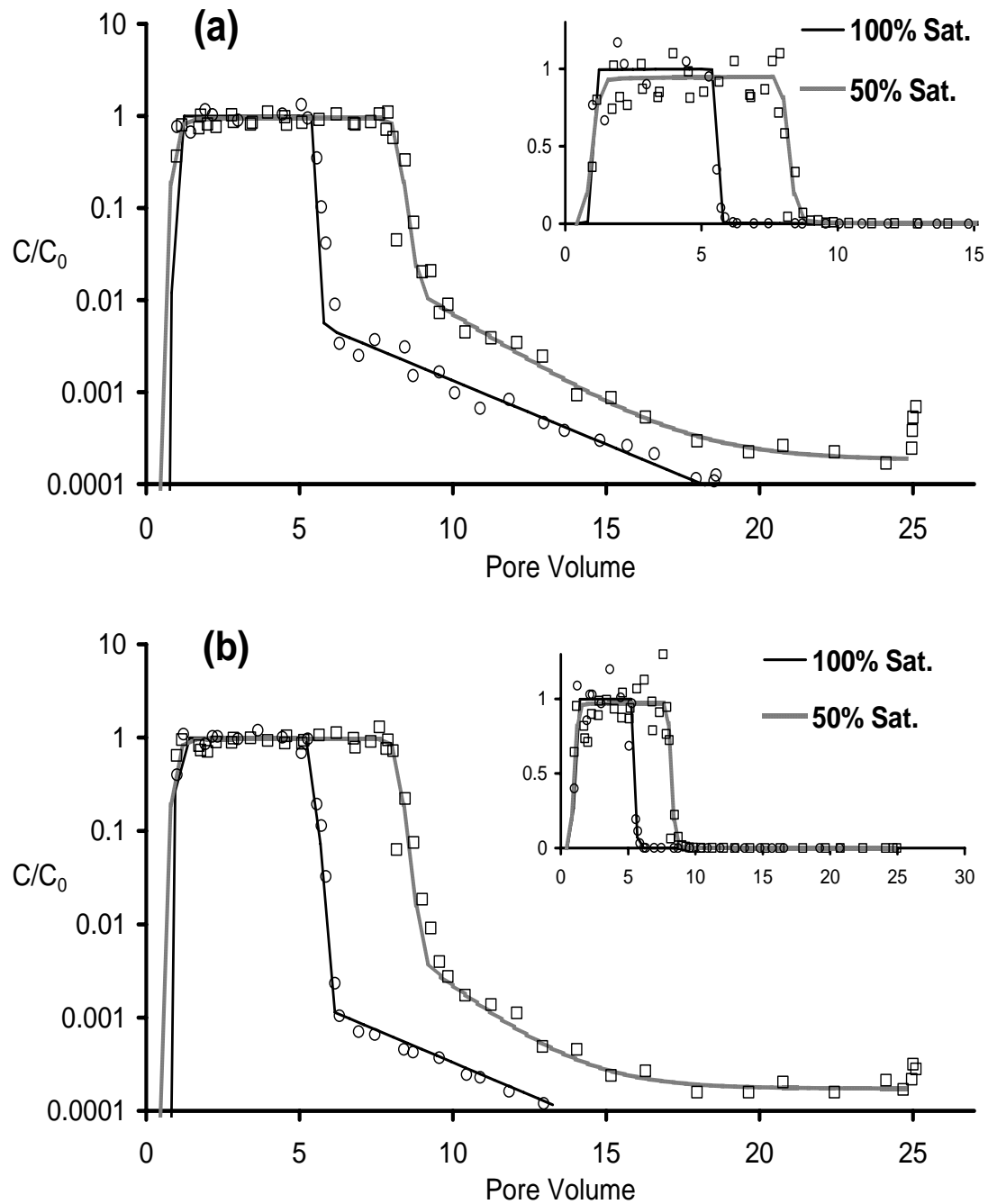
Figure 2. Measured (symbols) and fitted (lines) breakthrough curves (C/C_0 on log-scale) of experiment series I (at pH 7.5 and 100 and 50 % saturations). Right top corner plots: C/C_0 on linear scale; (a) φX174 and (b) MS2.
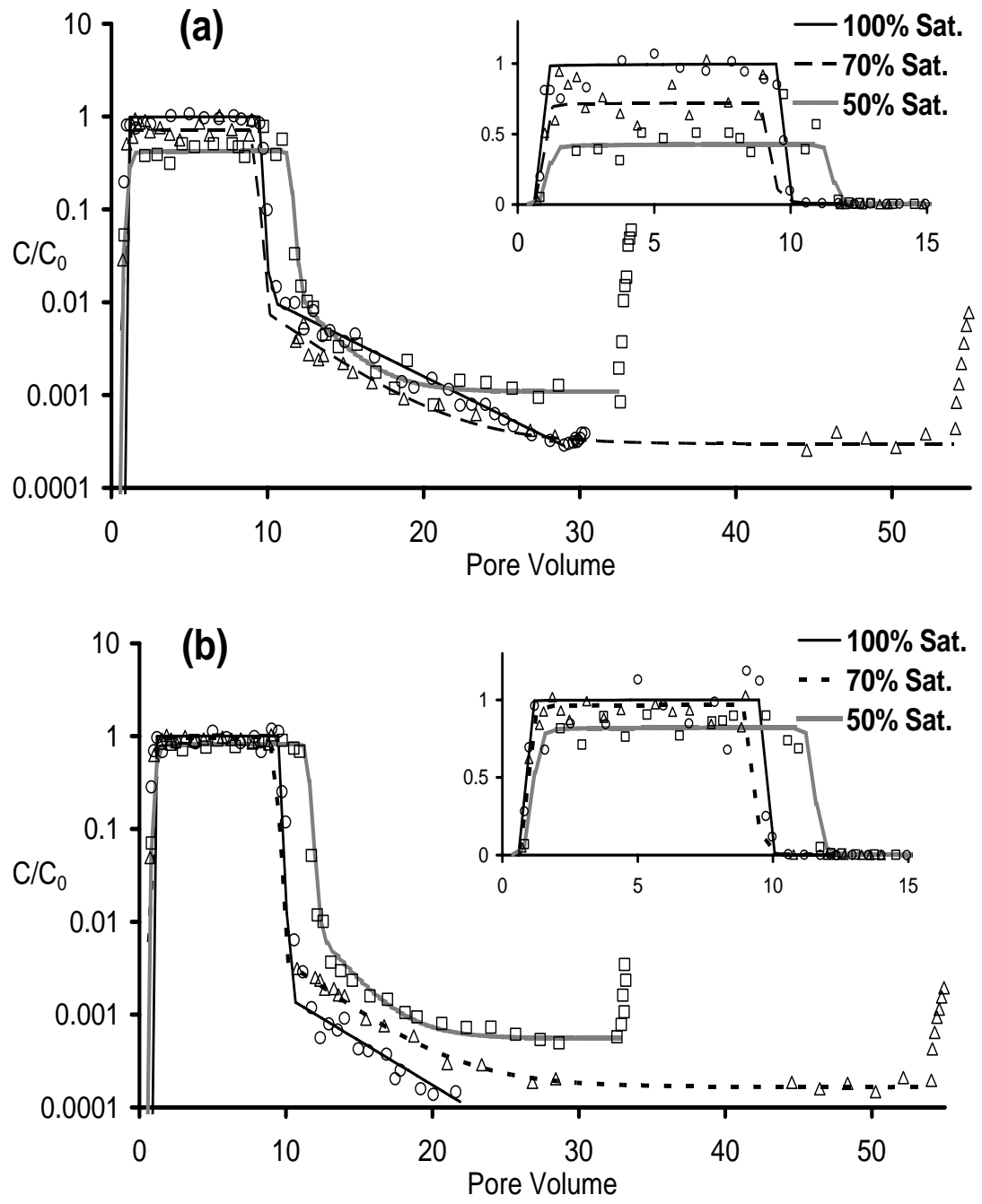
Figure 3. Measured (symbols) and fitted (lines) breakthrough curves (C/C_0 on log-scale) of experiment series II (at pH 6.2 and 100, 68, and 50 % saturations). Right top corner plots: C/C_0 on linear scale; (a) φX174 and (b) MS2.

The dispersivity (λ), for both saturated and unsaturated columns, was estimated by inverse analysis of breakthrough data of the NaCl tracer. The breakthrough curves from all experiments were symmetrical with no evidence of tailing as also observed by Torkzaban et al. [2006]. This indicated that dead end pores and immobile water either did not exist or did not play a significant role in causing physical non-equilibrium in the transport of solutes. Table 1 shows the values of dispersivity estimated by fitting the breakthrough data with HYDRUS-1D. It is evident that dispersivity increases as saturation decreases. We have assumed that the NaCl-based dispersivity is the same as for viruses. Because advection was the dominant transport mechanism in our experiments (the smallest value of Peclet number was more than 40), possible variations in viral dispersivity were not expected to be significant in our experiments.

The inactivation rate coefficient of free viruses (μ_l) was measured through the bulk batch experiments and was assumed to be applicable in the modelling of the virus breakthrough curves. The inactivation rate coefficient for bacteriophages attached to the solid surface (μ_s) was assumed to be equal to μ_l, because fitting saturated breakthrough curves with and without μ_s had no significant effect on the value of attachment and detachment coefficients. Inactivation was found to be insignificant because of the short duration of the column experiments. Similar results were obtained when fitting inactivation rates for unsaturated breakthrough curves. Therefore, μ_a was also assumed to have the same value as μ_l.

For saturated column experiments, attachment/detachment rate coefficients (k^s_{att}, k^s_{det}), were obtained by fitting the solution of equations (1) (with r_a set equal to zero) and (2) to the virus breakthrough data. In order to account for the effect of the very small concentration values at the tailing region of the breakthrough curves, we used log-transformed values of the breakthrough curves in the fitting process [Schijven and Simunek, 2002].
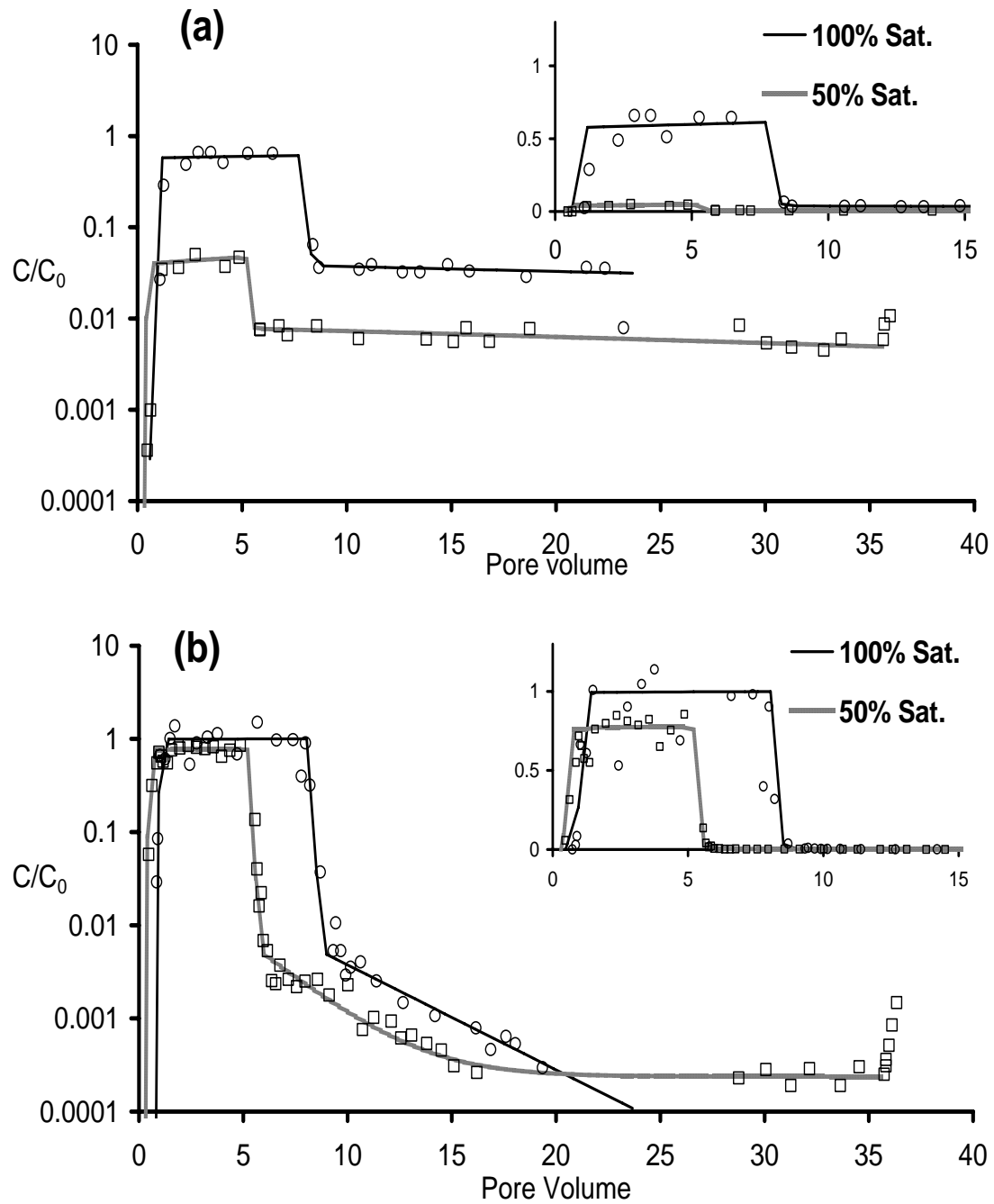
Figure 4. Measured (symbols) and fitted (lines) breakthrough curves (C/C_0 on log-scale) of experiment series III (at pH 5.5 and 100 and 50 % saturations). Right top corner plots: C/C_0 on linear scale; (a)ϕX174 and (b) MS2.
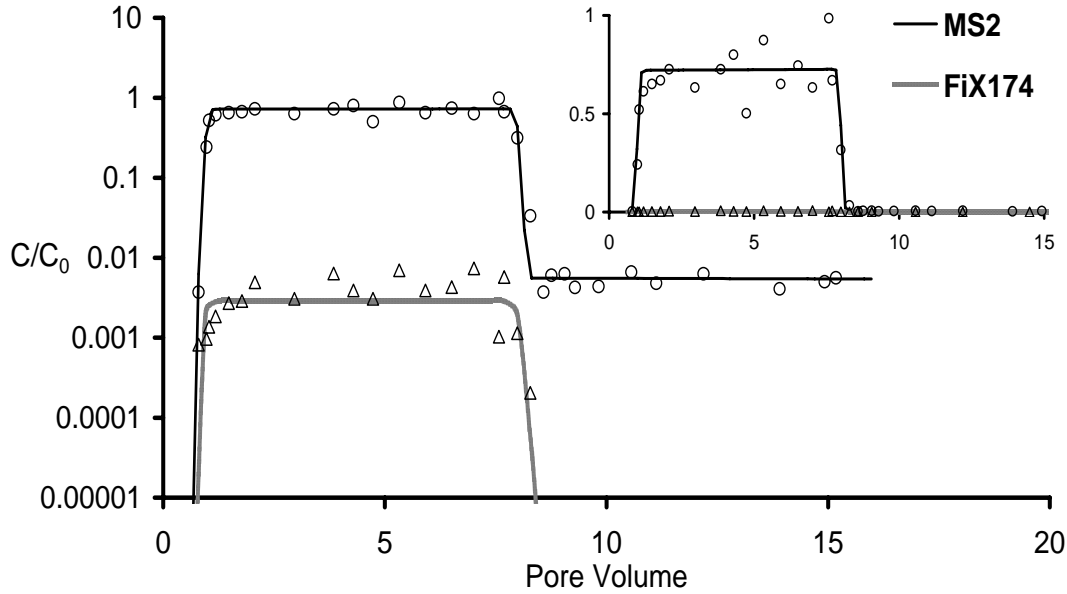
Figure 5. Measured (symbols) and fitted (lines) breakthrough curves (C/C_0 on log-scale) of experiment series IV (at pH 5 and 100% saturation). Right top corner plots: C/C_0 on linear scale.

Values of k^s_{att} and k^s_{det}, determined from the saturated experiments cannot be transferred directly to the unsaturated experiments as they are known to depend on water saturation [Saiers and Lenhart 2003a; Torzkaban et al., 2006). Therefore, unsaturated breakthrough curves were fitted to the solution of equations (1), (2), and (3) to determine rate coefficients k^s_{att}, k^s_{det}, k^a_{att}, and k^a_{det} at a given water saturation.

Fitted breakthrough curves from all experiments, conducted at different saturation levels and pH, are shown in Figures 2 till 5. It can be observed that application of a one-site kinetic model produces a good fit of the breakthrough data of both bacteriophages for the experiments conducted under saturated conditions. In contrast, a two-site kinetic model was required in order to fit the breakthrough curves obtained under unsaturated conditions. Table 2 lists the corresponding parameter values and standard deviations.

Role of SWI in Virus Adsorption

As can be seen from Tables 2 (a) and 2(b), k_{att}^{s} increases as the solution pH decreases and the reverse is seen for k_{det}^{s}. Thus, in order to compare the retention capacity for the bacteriophages at different solution chemistry and saturation levels, the distribution coefficient, K_D, for each site was determined as the ratio of k_{att}/k_{det} [Schijven and Hassanizadeh, 2000]. Calculated values are given in Table 3. It is clear that the retention capacity increases significantly as the water saturation and/or pH decrease. The calculated mass balance for both phages also shows a significant increase in retention as the pH decreased from 7.5 to 5 (see Table 4).

Bitton et al. [1984] and Jorgensen [1985] postulated that the increased retention of viruses under unsaturated conditions is promoted by the closer proximity of the viruses to the solid surfaces. Lance and Gerba, [1984] and Chu *et al.*, [2001], however, have suggested that increased attachment of viruses to the SWI is due to a more pronounced effect of electrostatic and hydrophobic interactions under unsaturated conditions, as larger pores are no longer available for transport and viruses are closer to the SWI.

Table 2a. Parameter values for ϕX174 determined from fitting the bacteriophages breakthrough curves. (Average ± Standard Deviations for the fitted parameters)

Series No.	Saturation %	pH	Interaction with AWI		Interaction with SWI	
			$k_{att}^{a} \times 10^3$ (min⁻¹)	$k_{det}^{a} \times 10^3$ (min⁻¹)	$k_{att}^{s} \times 10^3$ (min⁻¹)	$k_{det}^{s} \times 10^3$ (min⁻¹)
				ϕX174		
I	100	7.5	-	-	0.21±0.04	6.5±0.5
	50	7.5	1.1±0.01	0.01±0.01	0.30±0.01	9.1±0.8
II	100	6.2	-	-	0.90±0.03	5±0.7
	68	6.2	8.1±1.0	0.0048±0.001	1.25±0.2	5.8±0.7
	50	6.2	15±1.2	0.0058±0.001	1.83±0.2	6.7±1.2
III	100	5.5	-	-	21	0.5
	50	5.5	80±2.3	0.003±0.0007	51±2.1	0.7±0.08
IV	100	5	-	-	185±3.1	0.0001±0.0001

Table 2b. Parameter values for MS2 determined from fitting the bacteriophages breakthrough curves. (Average ± Standard Deviations for the fitted parameters)

Series No.	Saturation %	pH	Interaction with AWI		Interaction with SWI	
			$k_{att}^{a} \times 10^3$ (min^{-1})	$k_{det}^{a} \times 10^3$ (min^{-1})	$k_{att}^{s} \times 10^3$ (min^{-1})	$k_{det}^{s} \times 10^3$ (min^{-1})
				MS2		
I	100	7.5	-	-	0.05±0.003	9.5±1.3
	50	7.5	0.6±0.06	0.017±0.01	0.12±0.07	12±1.4
II	100	6.2	-	-	0.06±0.004	6.5±0.8
	68	6.2	1.1±0.02	0.020±0.003	0.16±0.01	8.5±1.4
	50	6.2	1.5±0.06	0.0063±0.001	0.20±0.06	9.5±1.6
III	100	5.5	-	-	0.2±0.01	5.1±0.5
	50	5.5	9.7±1.1	0.005±0.001	0.43±0.1	7±1.2
IV	100	5	-	-	10±0.8	0.1±0.002

We believe that this is unlikely to be the reason, as was also dismissed by Powelson *et al.* [1990], because the effective range of these forces is in the order of nanometers and the sizes of water-filled pores is much larger. Torkzaban et al. [2006] suggested that increased attachment to the SWI at lower saturations can be attributed to a reduction in the diffusion length within the pores at lower saturations. Moreover as water saturation is reduced, there may also be an increase in the ratio of the soil-water area to the water volume; thus, resulting in enhanced adsorption.

It is interesting to note that we were always able to produce a good fit of the saturated breakthrough data for both bacteriophages using a one-site kinetic model. This is in contrast to results of Torkzaban et al. [2006] who had to employ a two-site kinetic model even for saturated experiments in the case of MS2 for pH values around 7. They explained their results by the fact that the sand grain surfaces contained 45 mg of iron oxides per kg of sand, thus creating two different types of adsorption sites on the sand grains. Although we have used the same sand, we did not see any improvement in our simulation results by inclusion of a second sorption site.

Table 3. Calculated distribution coefficients (K_D)

Series No.	Saturation %	pH	$\dagger K_D^s$	K_D^a	K_D^s	K_D^a
				MS2	ϕX174	
I	100	7.5	0.005		0.03	
	50	7.5	0.01	35.3	0.03	110
II	100	6.2	0.009		0.18	
	68	6.2	0.018	55	0.21	1687
	50	6.2	0.02	238	0.27	2586
III	100	5.5	0.04		42	
	50	5.5	0.06	1940	73	26666
IV	100	5	100		1850000	

†Superscripts *s* and *a* refer to the SWI and AWI.

We believe that the difference lies in the use of phosphate buffer solution in the current series of experiments. In fact, phosphate can effectively mask positively-charged patches on soil grains and eliminate their effect on virus transport. For example, it has been shown that phosphate competes with natural organic mater through binding to surface ferric sites forming a strong complex [Chi and Amy 2004]. There is ample experimental evidence that phosphate adsorption to metal oxides is chemisorption and occurs by ion exchange with singly-coordinated surface hydroxides [Yates and Healy, 1975; Parfitt et al., 1976].

Our results also show that draining the soil column at the end does not lead to the release of viruses adsorbed to the SWI. In other words, the moving solid-water-air contact lines (SWA) were not able to detach significant numbers of viruses from the SWI. In contrast, Gomez-Suarez et al. [2001] and Saiers et al. [2003] reported detachment of bacteria and colloids as a result of moving the SWA contact lines. This may suggest that in our experiments, the attached viruses were strongly bound to the SWI such that passing of the SWA contact lines was not able to remobilize them.

Table 4. Calculated mass balance (%)

Experiment		MS2	φX174
I	100% Sat	99.9	100
	50% UnSat	97.5	95
II	100% Sat	100	99.5
	68% UnSat	96.8	78.5
	50% UnSat	92	43.6
III	100% Sat	99	78.5
	50% UnSat	77.1	8.6
IV	100% Sat	72	0.29

Role of AWI in Virus Adsorption

Examining breakthrough curves in Figures 2-5 and fitted parameter values shown in Tables 2, 3, and 4, we can identify the presence of two distinct adsorption sites for both φX174 and MS2 in unsaturated column experiments. The first adsorption site is attributed to the SWI and the second site is believed to be for the AWI. From Table 3, it is obvious that the adsorption capacities of both viruses increased as the pH decreased. This result is attributable to the fact that as pH decreases, the viruses, especially φX174, become more positively charged, whereas the AWI is still negatively charged at pH values larger than two [Li and Somansundaran 1991; Gracia et al. 1995]. Wan and Tokunaga [2002] demonstrated in bubble column experiments that only positively-charged particles attached to the negatively-charged AWI. At high pH values, both bacteriophages are negatively charged. Therefore their affinity for adsorption to AWI is low. Indeed, Torkzaban et al., [2006] observed no significant retention of MS2 and φX174 under unsaturated conditions when the pH of the solution was nine.

As pH decreases, the electrostatic repulsion between phages and the AWI decreases, resulting in increased adsorption to the AWI. This effect is expected to be more pronounced for φX174 than for MS2 due to differences in their IP (6.7 compared to 3.9). The mass recovery data (in Table 4) shows more retention for φX174 than MS2 as the degree of saturation decreases. In fact, results of our experiments show that the

affinity of ϕX174 to the AWI is much larger than that of MS2 (see Table 3). As pH decreased to values lower than the IP of ϕX174, the role of the AWI becomes dominant in virus retention because of the increased attraction between ϕX174 viruses and the negatively-charged AWI. In contrast, repulsive forces between the MS2 and AWI always exist for the considered pH range (7.5-5) as both are negatively charged. Hydrophobicity is apparently not the controlling factor for virus adsorption to the AWI, as ϕX174 is less hydrophobic than MS2. Hydrophobic colloids have been reported to have a higher affinity to the AWI than hydrophilic colloids [Wan and Wilson, 1994a; Wan et al., 1994]. Our results indicate that, in the cases of viruses, the effect of electrostatic interactions is much more important than the hydrophobicity.

Results of experiments conducted at pH=6.2 show that adsorption of phages to the AWI increases as water saturation decreases. We believe the explanation for this apparent enhanced adsorption, similar to the increased adsorption to the SWI at lower saturations, lies in the fact that the diffusion length, and thus the time needed for viruses to reach the AWI, decreases. Moreover, it is obvious that the amount of air-water interfacial area increases as the water saturation decreases.

Irreversible attachment to the AWI has been suggested as the main mechanism for enhanced removal of colloids, including viruses, in low saturations in many studies [*e.g.* Wan and Wilson, 1994a; Powelson *et al.*, 1990; Jin *et al.*, 2000; Powelson and Mills 2001; Keller and Sirivithayapakorn 2004]. However, our results clearly show that the attachment to the AWI is reversible, because we needed to assign a non-zero value to detachment rate coefficients in our model (see Table 2) in order to obtain a satisfactory fit to the breakthrough curves, especially in the tail part of the curves. Indeed, if the tails of the breakthrough curves were not measured, one might be led to believe that the attachment to the AWI is irreversible. In other words, one may obtain a satisfactory fit to the breakthrough curves using either an irreversible adsorption model or a reversible adsorption model with significant inactivation. However, such a fit will be most probably giving unacceptable results for the tail part of the breakthrough curves.

It has been reported that some viruses such as MS2 and ϕX174 are rapidly inactivated once they attach to the AWI [Trouwborst et al., 1974; Jin et al., 2000; Chu et al., 2001]. In contrast, our results do not show a significant inactivation rate at the AWI

for our bacteriophages at the considered temperature. This can be deduced from the flat tail of the breakthrough curves under unsaturated conditions and also from the sudden rise in virus concentrations after re-saturation (i.e. eliminating the AWI) and draining the column. The rise in concentrations after drainage suggests that the attached viruses on the AWI were still viable. It is worth noting that the sharp rise was not very pronounced for the unsaturated column in the third series of experiments (Fig. 4), despite the fact that a large portion of viruses had remained in the column. This may be due to the high affinity of the bacteriophages (especially ϕX174) to the SWI so that when they were released into solution from the AWI (after re-saturation) they attached again to the SWI. Our study shows that although retention of viruses may be high under constant unsaturated conditions, adsorbed viruses to the AWI may be released to solution during episodic wetting events that occur in the vadose zone. This finding was also reported by Powelson and Mills [2001], who found that constant unsaturated conditions resulted in significantly higher bacteria removal than transient unsaturated flow.

The works of Wan and Tokunaga [1997] and Lenhart and Saiers [2002] suggest that film straining represents the most important deposition mechanism for hydrophilic colloids under conditions of low ionic strength and low to intermediate moisture content. The water film thickness we calculated, on the basis of the equations proposed by Wan and Tokunaga [1997], was about 30 nm in our unsaturated columns, which is about the same as the size of MS2 and ϕX174. If film straining was playing an important role in our experiments, the effect should have been the same for both viruses regardless of the pH and virus type. We, however, observed more retention of ϕX174 than MS2 especially in lower pHs. Therefore, we do not believe that film straining played a major role in virus retention in our study. For a similar reason, we also do not believe that conventional straining (i.e., trapping of colloidal particles in pores that are too small to allow particle passage) had a significant contribution to the virus retention in our study.

CONCLUSIONS

Column experiments were conducted to examine the fate and transport of viruses as a function of water saturation and pH. This was examined using two different

bacteriophages, four different solutions in terms of pH, and under various saturation levels. The following conclusions may be drawn:

(1) adsorption capacities of the viruses to the SWI and AWI increase as the pH decreases; (2) the effect of electrostatic interactions is more important than the effect of hydrophobicity in case of adsorption to the AWI; (3) virus adsorption to both the SWI and AWI increases as the water saturation decreases; and (4) attachment to the AWI is reversible.

Chapter 4

Colloid transport in unsaturated porous media: The role of water content and ionic strength on particle straining

Torkzaban, S., S. A. Bradford, M. Th. Van Genuchten, S. L. Walker," Colloid transport in unsaturated porous media: The role of water content and ionic strength on particle straining" *Journal of Contaminant Hydrology* (under review).

Abstract

Packed column and mathematical modeling studies were conducted to explore the influence of water saturation, pore-water ionic strength, and grain size on the transport of latex microspheres (1.1 μm) in porous media. Experiments were carried out under chemically unfavorable conditions for colloid attachment to both solid-water interfaces (SWI) and air-water interfaces (AWI) using negatively charged and hydrophilic colloids and modifying the solution chemistry with a bicarbonate buffer to pH 10. DLVO calculations and complementary batch experiments were conducted and demonstrated that partitioning of colloids to the SWI and AWI was insignificant across the range of the ionic strengths considered. The breakthrough curve and final deposition profile were measured in each experiment indicating colloid retention was highly dependent on the suspension ionic strength, water content, and sand grain size. In contrast to conventional filtration theory, most colloids were found deposited close to the column inlet, and hyper-exponential deposition profiles were observed. A mathematical model, accounting for time- and depth-dependent straining, produced a reasonably good fit for both the breakthrough curves and final deposition profiles. Experimental and modeling results suggest that straining – the retention of colloids in low velocity regions of porous media such as grain junctions – was the primary mechanism of colloid retention under both saturated and unsaturated conditions. The extent of stagnant regions of flow within the pore structure is enhanced with decreasing water content, leading to a greater amount of retention. Ionic strength also contributes to straining, because the number of colloids that are held in the secondary energy minimum increases with ionic strength. These weakly associated colloids are prone to be translated to stagnation regions formed at grain-grain junctions, the solid-water-air triple point, and dead-end pores and then becoming trapped.

Introduction

Colloid movement through porous media is of great significance in a number of environmental fields including contaminant transport, soil profile development, and subsurface migration of pathogenic microorganisms. Pathogenic microorganisms such as bacteria and viruses (often referred to biocolloids) pose a high risk to water resources through land application of raw and treated wastewater, septic systems, leaking sewage pipes, and animal manure (Hurst, 1980; Powelson et al., 1993; Redman et al., 2001). Colloid transport in porous media is also of concern due to colloid-facilitated transport of a wide variety of inorganic and organic contaminants that adsorb onto these particles and travel significant distances (de Jonge et al., 1998; Ryan et al., 1998; McGechan and Lewis, 2002). Hence, comprehensive knowledge of the transport of colloidal particles in subsurface environments is essential for predicting biological and chemical contaminant fate. Considerable research has been devoted to the fate and transport of colloids in saturated porous media (reviews are given by Schijven and Hassanizadeh, 2000; Harvey and Harms, 2002; de Jonge et al., 2004); however, colloid transport in the unsaturated (vadose) zone, which often act as a first natural layer against the pollution of groundwater, has received little systematic research and the governing mechanisms are poorly understood.

Mechanisms of colloid retention in unsaturated porous media include adsorption (attachment/detachment processes) to solid-water interfaces (SWI) (reviews are given by Ryan and Elimelech, 1996, Schijven and Hassanizadeh, 2000), air-water interfaces (AWI) (e.g. Wan and Wilson, 1994a), straining (McDowell-Boyer et al., 1986; Bradford et al. 2002, 2003), and film straining (Wan and Tukonaga, 1997; Saiers and Lenhart, 2003a). Attachment to the SWI involves colloid collision with and attachment to grain surfaces, and consequently depends on the chemical and physical characteristics of the colloids and soil surfaces as well as the solution chemistry (Ryan and Elimelech, 1996, Walker et al., 2004). The AWI present within unsaturated porous media is also believed to serve as a collector for colloid particles, reportedly in an irreversible manner, retained by either capillary or electrostatic forces (Wan and Wilson, 1994b; Schafer et al., 1998). Colloid attachment to the AWI, therefore, depends on pH, ionic strength, and colloid surface properties (DeNovio et al. 2004; Torkzaban et al. 2006b). Additionally, Wan and

Tokunaga (2002) demonstrated that only positively charged colloidal particles attached at the AWI, and Crist et al. (2004, 2005) observed in three-dimensional porous media that negatively charged hydrophilic colloids did not attach to the AWI.

Straining involves the retention of colloids in the smallest regions of the pore space (McDowell-Boyer et al., 1986; Cushing and Lawler 1998; Bradford et al. 2002, 2003, 2006a) such as those formed near grain-to-grain contact points. It should be noted that retention of colloids near to grain-to-grain contact points has also been referred to in the literature as wedging (Herzig et al., 1970; Johnson et al., 2007). In the smallest regions of the pore space the water velocity is very low and these locations can be considered as zones of relative flow stagnation. Straining may also occur in pore throats that are too small to allow the passage of multiple colloids (Herzig et al., 1970; Bradford et al., 2002), a process often referred to as bridging (Ramachandran and Fogler, 1999). Criteria for colloid straining in porous media has traditionally been assumed to be simply a function of the ratio of colloid to collector diameters (d_p/d_g) and the pore size distribution of the medium (Herzig et al., 1970; McDowell-Boyer et al., 1986; Bradford et al., 2002, 2003). Herzig et al., (1970) computed that when d_p/d_g exceeds 0.05, straining significantly contributes to retention of colloids in porous media. Recently, a few researchers have suggested that the theoretical criteria of Herzig et al. (1970) underestimates the extent of straining in colloid retention and that straining can be occurring at d_p/d_g as low as 0.002 (Bradford et al., 2002; Bradford et al., 2003; Li et al., 2004).

In unsaturated media, straining has received relatively less attention (Gargiulo et al., 2007). In fact, straining may be more pronounced in unsaturated versus saturated porous media because capillary forces constrain water flow within the smaller regions of the pore space. Furthermore, unsaturated systems also contain solid-water-air triple points at the intersection of solid-water and air-water interfaces. Triple points and grain-grain contact points share many similarities in that these locations are both low velocity zones. In this work, we consider retention at the triple point as an additional form of straining. Moreover, the extent to which saturated and especially unsaturated colloid straining is sensitive to changes in the chemical properties of the system (i.e. aqueous phase, colloids, and collectors) remains poorly understood (Bradford et al., 2006a;

Bradford et al., 2007). In addition to straining, film straining (Wan and Tokunaga, 1997) is another potential retention mechanism needing further investigation. Film straining is the removal of colloids in partially saturated porous media occurring as a result of the physical restrictions to colloid transport through water films with thicknesses smaller than the diameter of the colloids.

Previous studies on unsaturated colloid transport have mainly focused on the determination of the colloid concentration in the effluent (e.g. Saiers and Lenhart. 2003a; Torkzaban et al., 2006a, 2006b). Breakthrough concentrations are typically simulated by using a variety of parameters to best fit the data that consider SWI and/or AWI adsorption rate coefficients, and/or film straining coefficients. Few studies have reported the shape of the colloid deposition profiles for unsaturated conditions. Bradford et al. (2003) demonstrated in saturated colloid transport experiments that breakthrough curves can be adequately fit using a variety of models such as an attachment and detachment model, or an attachment and straining model. The study showed that consideration of both breakthrough curves and deposition profiles in model fitting is vital to gain insight on the controlling deposition mechanisms.

The objective of this work was to explore the effects of water content and solution ionic strength on colloid transport and retention. Highly unfavorable attachment conditions were employed to ensure a high repulsive energy barrier against attachment and therefore the retention mechanisms involved were not attachment by simply chemical interactions, but rather by straining. To minimize colloid attachment to both the SWI and AWI, the experiments were conducted using hydrophilic, negatively charged microspheres in a buffered solution such that the SWI and AWI were negatively charged. Unfavorable attachment conditions were confirmed to exist through complementary batch experiments and DLVO calculations. The breakthrough data and final deposition profile were measured and simulated using the HYDRUS-1D code that accounts for time and depth-dependent deposition processes. Fitted model parameters were used to gain insight into the various mechanisms controlling colloid transport in unsaturated systems.

MATEIALS AND METHODS

Tracer, Colloid, and Sand Materials

The background electrolyte solution utilized in this study consisted of deionized water buffered to pH 10 (1.67 mM $NaHCO_3$ + 1.67 mM Na_2CO_3). Sodium nitrate (0.2 mM, Fisher Scientific) was used as a conservative tracer to characterize the hydrodynamic properties of the porous medium. Carboxylate-modified latex (CML) colloids (Molecular probes, Inc., Eugene, OR) were selected as model colloid particles. These spherical particles have been employed in previous colloid transport studies reported in the literature (Wan and Wilson, 1994a, 1994b). CML was chosen due to the high density of carboxylic acids on the colloid surface creating a negatively charged-hydrophilic surface. Colloid diameter was 1.1 µm with a particle density (ρ_p) of 1.055 g cm^{-3} and a particle surface charge density (ρ_q) of 0.0175 meq/g. The values of ρ_p and ρ_q were provided by the manufacturer. The concentration of colloid suspension (2.5 – 2.8×10^7 N_c ml^{-1}; where N_c denotes number of colloids) was selected to minimize any permeability reductions of the porous media.

Two different sizes of Ottawa aquifer sand (U.S. Silica, Ottawa, IL) were used in this study. These sands are designated hereafter as 3550 and MIX having median grain sizes (d_{50}) of 360 and 240 µm, respectively. The uniformity index ($U_i = d_{60} / d_{10}$ where x % of the mass was finer than d_x) of the 3550 and MIX sands was measured to be 1.88 and 3.06, respectively. The capillary pressure - saturation curves for these Ottawa sands were previously reported by Bradford and Abriola (2001). Ottawa sands typically consist of 99.8% SiO_2 (quartz) and trace amounts of metal oxides, are spheroid in shape, and have rough surfaces. Quartz and iron oxides possess a net negative charge at pH 10 (Tipping, 1981; Redman et al., 2004), and any attractive electrostatic interactions between the CML colloids and the porous media is expected to be minimized at this pH.

Experimental set-up

The column experiment was designed to accurately establish a steady state and unit hydraulic gradient along the column in case of unsaturated transport (Figure 1). A stainless steel column with internal diameter and length of 5 and 10 cm, respectively, was selected for this study. A hydrophilic nylon membrane with 10 µm pore size (SaatiTech, Veniano, Italy), supported by a aluminum end-plate, was used as a capillary barrier at the bottom of the column. The nylon membrane had a bubbling pressure of 70 cm-H_2O.

Results of preliminary experiments (performed without sand) demonstrated that neither the column body nor the nylon membrane retained the colloids.

The column was wet-packed with the water level maintained a few centimeters above the sand surface. After the addition of sand, the column was vibrated to ensure a uniform packing and to liberate any trapped air bubbles. Prior to each experiment, the column was flushed upward under saturated conditions with about seven pore volumes of the pH 10 electrolyte solution to free the effluent from background colloids in the sand. The flow was then reversed and the column was rinsed with additional two pore volumes before starting the transport experiments. The solution chemistry conditions were verified by measuring the pH and ionic strength of the influent and effluent solutions.

A sprinkling apparatus equipped with 7 stainless steel needles was connected to a high performance liquid chromatography (HPLC) pump (Barnant Company, Barrington, IL) and used to evenly distribute the influent over the sand surface. Capillary pressure head was measured with two stainless steel miniature tensiometers (Chemiquip Products Co., West New York, NJ) inserted at 2 and 8 cm from the upper sand surface. Data from the tensiometers were collected continuously using a CR10X datalogger (Campbell Scientific Ltd, Lougborough, UK) and monitored with a keyboard display (CR10KD). The average water content of the column (under steady-state unit gradient flow conditions) was monitored gravimetrically with an electronic balance (Sartorius Master Series, LP Models, Germany) and is listed in Table 1 and 2. The lower boundary condition was controlled using a hanging water column to impose a constant suction. Unsaturated transport experiments involved draining the saturated column to the desired water saturation level by reducing the inflow water rate to the hydraulic conductivity corresponding to that saturation. Simultaneously, the pressure head at the bottom of the column was gradually reduced until the readings of the tensiometers showed the same values. This resulted in a unit hydraulic head gradient, i.e. constant capillary pressure, which implies a constant saturation level along the column. In some experiments, to eliminate the effect of variations in water velocity in our results, a hydraulic gradient was applied in the saturated experiments such that the average water velocity was the same as in the unsaturated experiments. Table 1 and 2 indicates the parameters of each column experiment.
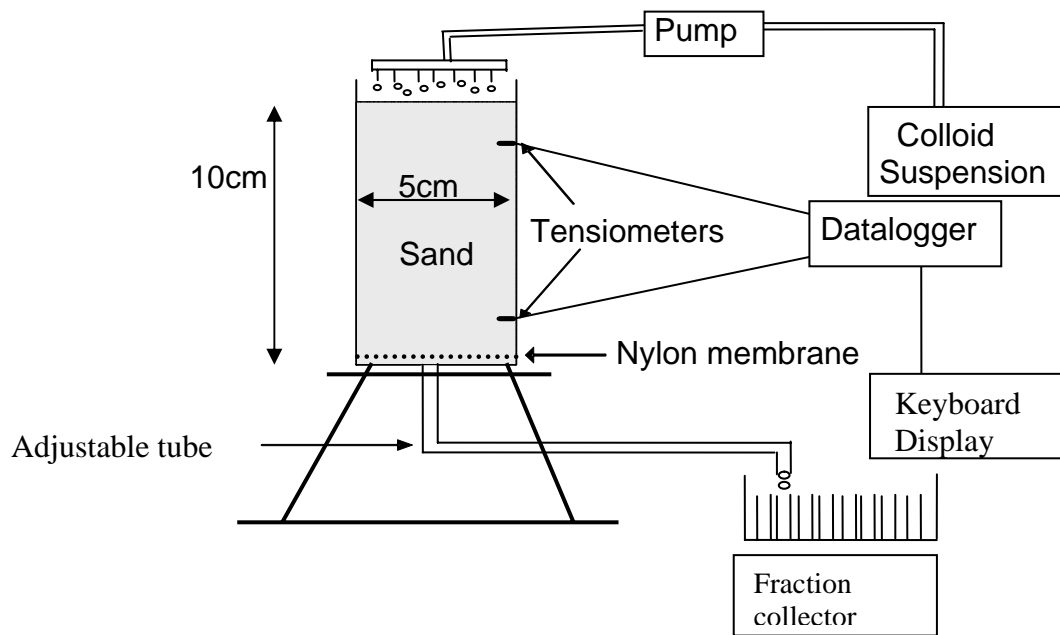
Figure 1. Schematic representation of experimental set-up.

Transport Experiment Protocol

Column transport experiments were systematically conducted to investigate the transport and deposition behavior of the 1.1 μm CML microspheres under saturated and unsaturated conditions at three different ionic strengths (IS=6, 30, and 60 Mm at a pH of 10). After establishing a specified saturation and water chemistry, transport experiments were carried out in six stages. These stages are described in greater detail below:

Stage 1: Prior to colloid application, tracer experiments were carried out to determine the dispersivity for each saturated condition. A solution containing 0.2 mM $NaNO_3$ was fed into the column at given water saturation and the breakthrough curve was obtained by measuring the absorbance of the effluent at 204 nm using a spectrophotometer (Perkin Elmer LC95 UV/VIS spectrometer, Irvine, CA).

Stage 2: Following the tracer experiment, the influent was switched to the background electrolyte solution in order to flush out the remnant nitrate. This was verified by measuring the absorbance of the effluent. This step also served the purpose of equilibrating the column with the electrolyte to be used in the subsequent colloid transport experiment.

Table 1. Experimental conditions for column experiments in 3550 sand (Li, Mi, and Hi stand for low, medium, and high ionic strength. Lv, Mv, and Hv stand for low, medium, and high velocity).

EXP.	Saturation	Ionic	Ave. Water	Dispersivity	Pulse Duration
Li100	100	6	0.6	0.08	7.12
Mi100		30	0.35		5.01
Hi100Lv			0.35		4.63
Hi100Mv	100	60	0.56	0.08	5.94
Hi100Hv			0.87		5.43
Li70		6			7.08
Mi70	70	30	0.85	0.4	5.09
Hi70		60			5.51
Li50		6			7.12
Mi50	50	30	0.6	0.6	5.04
Hi50		60			5.94
Li40		6			7.05
Mi40		30	0.37	0.8	5.03
Hi40	40	60			4.64

Table 2. Experimental conditions for column experiments in MIX sand (Li, Mi, and Hi stand for low, medium, and high ionic strength).

EXP.	Saturation	Ionic	Ave. Water	Dispersivity	Pulse
Li100		6	0.28		3.8
Mi100	100	30	0.39	0.1	2.7
Hi100		60	0.56		5.4
Li80		6			3.3
Mi80	80	30	0.35	0.22	3.0
Hi80		60			4.2
Li60	60	6	0.23	0.5	3.5
Mi60		30			2.8

Stage 3: A colloid suspension ($2.5 - 2.8 \times 10^7$ N_c ml^{-1}) was introduced into the column at a constant rate. The colloid suspension was applied for a given number of pore volumes (pulse duration) as listed in Table 1. equilibrating the column with the electrolyte to be used in the subsequent colloid transport experiment.

Stage 4: Colloid-free electrolyte solution was applied to the column at the same flow rate until the effluent colloid concentration returned to baseline level. Effluent samples were collected at selected intervals by a fraction collector and analyzed for colloid concentration using a spectrometer (Perkin Elmer LC95 UV/VIS spectrometer, Irvine, CA) at 480 nm.

Stage 5: Following completion of the colloid transport experiments, the spatial distribution of deposited colloids in a sand column was determined (Bradford et al., 2002). The sand was carefully excavated in 1 cm increments and each increment was placed in a 50 mL polypropylene centrifuge tube containing 30 mL of the background electrolyte solution. The tubes were very slowly shaken for a few minutes to liberate reversibly retained colloids. The concentration of colloids in the supernatant solution was measured using a fluorometer (Turner Quantech Fluorometer, Dubuque, IA) following an experimental protocol outlined previously (Bradford et al., 2002). Water and sand were poured into an aluminum dish and placed in an oven for several hours to volatilize all of the remaining water. The volume of water and mass of sand in each tube was determined from mass balance by measuring the weight of the empty tubes, water and sand tubes, and dry sand.

Stage 6: A colloid mass balance was conducted at the end of the column experiment using effluent concentration data and the deposited colloids in the column. The calculated number of effluent and retained colloid particles was normalized by the total number of particles injected into a column.

Batch Experiments

Batch experiments were conducted by placing 10 g of sand and 10 ml of a known initial concentration of colloid suspension into a polypropylene centrifuge tubes with the temperature kept at approximately 20 °C. Three different ionic strength solutions (6, 30, 60 mM) buffered at pH 10, corresponding to the chemical conditions in column experiments, were used for making colloid suspension. The suspension and sand were allowed to equilibrate for 2 hours by gently rotating the tubes end over end (15 rpm) on a tube rotator (Fisher Scientific, San Diego, CA). The 2-h equilibration time was chosen to mimic the duration of the column experiments. A control experiment without colloids was also run for measuring the background concentration of colloids introduced from the sand. The initial and final concentrations of colloids in the suspension were determining using the spectrophotometer (Perkin Elmer LC95 UV/VIS spectrometer, Irvine, CA) after setting the tube to rest for a few minutes. All experiments were performed in duplicate.

Electrokinetic Characterization of Colloids

The zeta potential of the colloids was measured using a ZetaPals instrument (Brookhaven Instruments Cooperation, Holtsville, NY). The measurements were carried out three times for each condition and the average values were -110, -85, -71 mV for the colloids suspended in 6, 30, and 60 mM ionic strength solutions, respectively. The AWI has been reported to be negatively charged over a very wide range of ionic strength and pH (Li and Somansundaran 1991; Gracia et al., 1995). According to results obtained by Li and Somasundaran (1991), the zeta potential of air bubbles in NaCl solution at pH 10 and a solution ionic strength with a range of 0.01-100 mM varies from -90 to -50 mV. The zeta potential of quartz sand surfaces in pH 10 solution has been reported previously to be approximately -70 mV (Elimelech et al., 2000). These values were used in calculations for electrostatic forces presented later in this paper.

Application of Colloid Transport Model for Saturated and Unsaturated Systems

The HYDRUS-1D code (Simunek et al., 2005) is a finite element model for simulating the one-dimensional movement of water, heat, and multiple solutes in variably saturated media. The code numerically solves the Richards' equation for saturated-

unsaturated water flow and Fickian-based advection-dispersion equations for the nonlinear equilibrium and kinetic reactions between colloids and the SWI. The code is coupled to a non-linear least square optimization routine based upon the Levenberg-Marquardt algorithm (Marquardt, 1963) to fit model parameters to breakthrough curve and/or deposition profile information. Relevant aspects of the code that were used to simulate the colloid transport data are described below.

The transport of colloids through the sand columns was described using the one-dimensional form of the advection-dispersion equation (ADE) that accounts for colloid deposition in the column:

$$\frac{\partial C}{\partial t} = \lambda v \frac{\partial^2 C}{\partial z^2} - v \frac{\partial C}{\partial z} - r_d \tag{1}$$

where C is the number of colloids per unit volume of the aqueous phase ($N_c L^{-3}$), λ is the dispersivity (L), v is the average pore water velocity (LT^{-1}), and r_d is the mass transfer rate of colloids in aqueous phase to/from the deposited phase ($N_c L^{-3} T^{-1}$) given by:

$$\rho_b \frac{\partial S_d}{\partial t} = r_d = \theta K_d \psi_s C - \rho_b K_{\text{det}} S_d \tag{2}$$

where ρ_b is the soil bulk density (ML^{-3}), θ is the volumetric water content (-), K_d is the colloid deposition coefficient (T^{-1}), ψ_s is a dimensionless deposition function for deposited colloids (-), S_d is the concentration of deposited colloids in the column ($N_c M^{-1}$), and K_{det} is the first order detachment rate coefficient (T^{-1}).

A simple and flexible form for ψ_s is used in the model to account for time and depth-dependent deposition behavior as (Bradford et al., 2002, 2003):

$$\psi_s = \left(1 - \frac{S_d}{S_{\max}}\right)\left(\frac{d_{50} + z}{d_{50}}\right)^{-\beta} \tag{3}$$

where d_{50} is the median grain size of the porous medium (L), β is a parameter that accounts for the spatial distribution of retained colloids (-), S_{max} is the maximum concentration of deposited colloids ($N_c M^{-1}$), and z is the down gradient distance from the porous medium inlet (L). The first term on the right hand side of this equation is used to account for time-dependent deposition in a manner similar to Langmuirian blocking (Adamcyzk, 1994). When the value of S_{max} is large then this term approaches a value of

69

1 and time-dependent deposition behavior becomes irrelevant. The second term on the right hand side of the above equation is used to describe depth-dependent deposition behavior; i.e., hyper-exponential profiles with decreasing deposition rates with increasing depth. When β goes to zero, then depth-dependent deposition is not considered. Bradford et al. (2003) reported that the value of β=0.432 gave a good description of the spatial distribution of retained colloids when significant straining occurred; hence this value was used in the simulations reported in this paper.

Based on the theoretical approach presented above, mechanisms of colloid deposition such as straining, film straining, and attachment to the SWI and AWI are lumped together in a single exchange term, r_d. Below we present experimental evidence to help identify the relative importance of each of these deposition mechanisms for our experimental conditions, and to provide more evidence for our model formulation.

RESULTS and DISCUSSION

Tracer Experiments

Breakthrough curves for the conservative tracer under both saturated and unsaturated conditions were well-described by the classical ADE (equation 1). Figure 2 shows an observed and ADE-simulated nitrate breakthrough curve in 3550 sand at 50% water saturation. Other nitrate breakthrough curves for unsaturated systems gave similar results. Table 1 and 2 report the value of dispersivity obtained by fitting the experimental data with the HYDRUS-1D model. The dispersivity values increase with decreasing water content similar to what has been reported in the literature (Toride et al., 2003). Figure 2 also demonstrates that the tracer exhibits small amounts of tailing in the declining limb of the breakthrough curve under unsaturated conditions. Similar, breakthrough tailing behavior has also been reported in literature (Pardilla et al., 1999; Toride et al., 2003), and is believed to occur as a result of immobile regions (inaccessible to flow) existing in unsaturated porous media. Although the physical non-equilibrium model, which accounts for both mobile and immobile regions, can provide a superior description to the tracer breakthrough curve than the simple advection-dispersion model (Cherrey et al., 2003), we decided to utilize the ADE model to be consistent with subsequent colloid transport modeling. We do believe, however, that immobile regions

may play an important role on colloid transport and this will be discussed in greater detail later on in the paper.
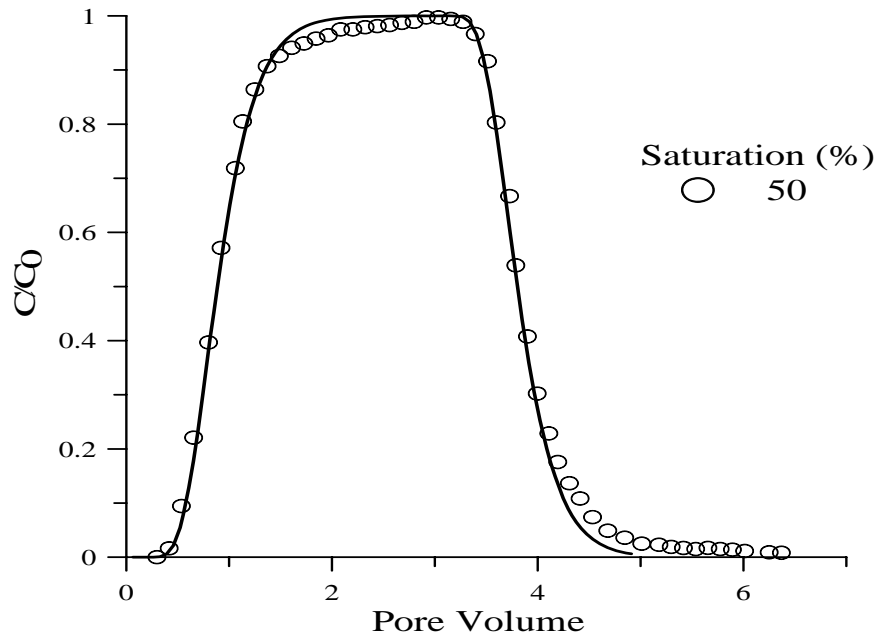
Figure 2. Measured (symbols) and fitted (lines) breakthrough curves of tracer (NaNO$_3$) in an experiment carried out in 3550 sand and 50% saturation.

Colloid Transport

Figures 3-5 present measured and fitted breakthrough curves for column experiments conducted with varying water contents and solution ionic strengths in 3550 (Figs. 3a-b and 4a-c) and MIX (Figs. 5a-c) sands, respectively. In these figures the normalized effluent concentration is plotted versus the number of pore volumes passed through the column. After approximately 1 pore volume, the injected colloids break through the column and are detected in the effluent. The influent was switched to a colloid-free solution after a given number of pore volumes listed in Table 1 and 2. For both sands, lower water contents tended to result in lower peak effluent concentrations and greater colloid retention (see Figs. 3a-b, 4a-c, 5a-c, and Tables 3 and 4). However, this effect was more pronounced with increasing ionic strength. For each water content and sand combination, increasing the ionic strength resulted in lower peak effluent concentrations, indicating greater retention of colloids.

71

The breakthrough curves shown in Figure 4 (a-c) obtained in the experiments conducted with 3550 sand and ionic strength of 60 mM indicate that average water velocity also has a significant effect on the colloid retention. The mass recovery in the effluent decreased from 52% to 23% when the average water velocity decreased from 0.87 to 0.35 cm/min, as shown in Tables 3 and 4. All of the breakthrough curves for colloids exhibited an increasing trend: i.e. during the period of continued colloid addition, the effluent concentration increased with time. This suggests the filling of deposition sites occurred with time. The apparent tailing behavior of the breakthrough curves implies a low detachment rate of retained colloids.

Figs. 6a-d and 7a-b present the observed and simulated colloid deposition profiles at various water saturation levels and IS in 3550 (Figs. 6a-d) and MIX (Figs. 7a-b) sands, respectively. The data are presented here as normalized concentration (number of colloids recovered in the sand, N_c, divided by the total number of colloids injected into the column, N_{ct}) per gram of dry sand and are plotted as a function of distance from the column inlet. The data indicate that the highest retention occurred near to the column inlet and that the profile shape was hyper-exponential with depth.

Consistent with the breakthrough curves, Table 3 and 4 indicates that the percent recovery of colloids in the sands enhanced with decreasing water content and increasing ionic strength. The total percent recovery for colloids in the effluent and sands ranged from 87-105% (Table 3 and 4). This signifies that most of retained colloids in the column were recovered – either by elution or simply resuspension of the sand after the column experiments.

Application of HYDRUS-1D Model

To quantitatively compare the experiments, breakthrough and deposition data were simulated by fitting with the solutions of equations (1) and (2). Tables 3 and 4 summarize the fitted parameters and R^2 values for all column experiments. Application of the transport and deposition model produced a good fit to the breakthrough data with R^2 values close to one as seen in Table 3 and 4 for all of the experiments conducted. For both sand sizes, the values of K_d and S_{max} increased with ionic strength. The same behavior for K_d and S_{max} was observed for decreasing water content but it was more

72

pronounced in higher ionic strength solutions. The values of K_{det} in Tables 3 and 4 were typically several orders of magnitude lower than K_d. It can also be observed in Figs. 6a-d and 7a-b that this model predicted the deposition profile behavior reasonably well.
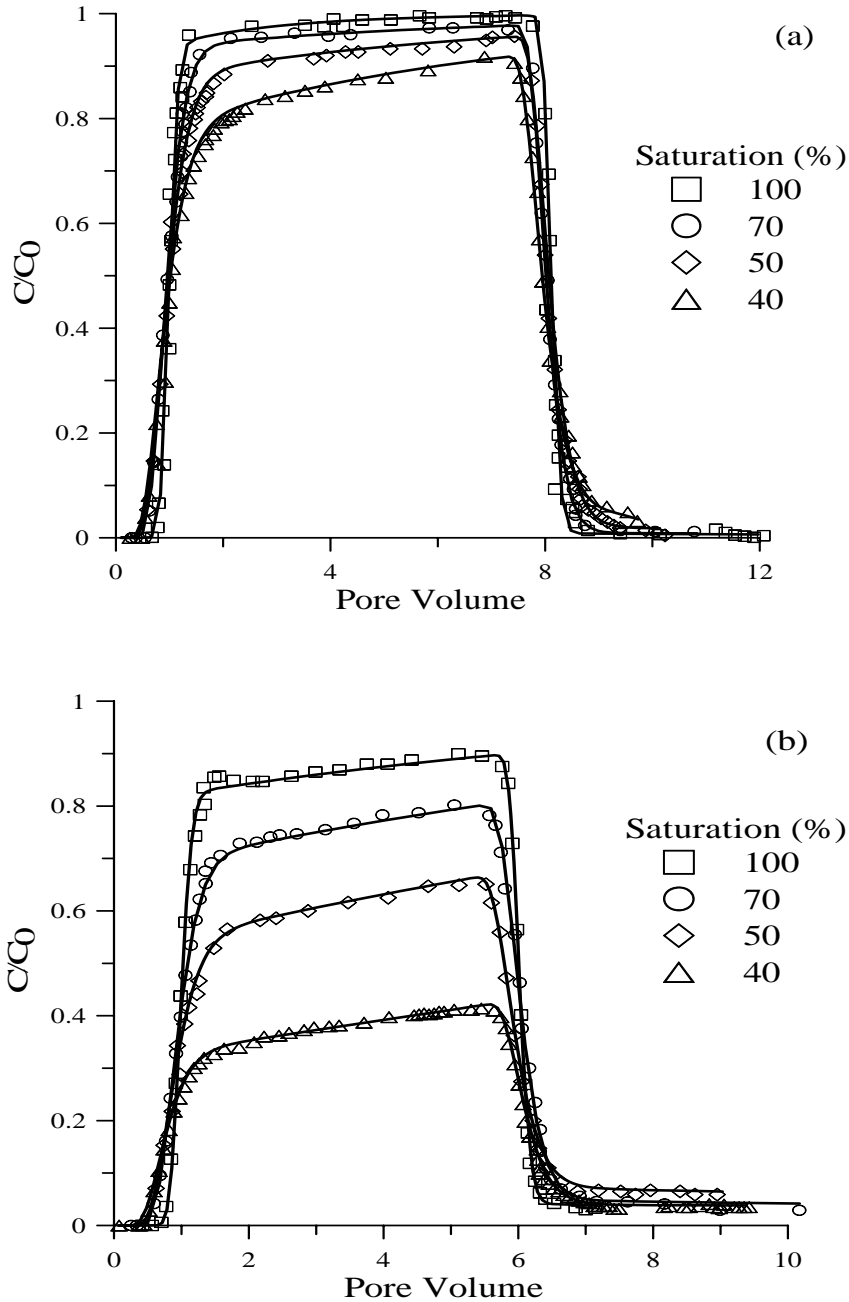
Figure 3. Observed and simulated breakthrough curves of colloids for various saturation levels in 3550 sand and ionic strength of 6mM (Fig. 3a) and 30 mM (Fig. 3b)

74
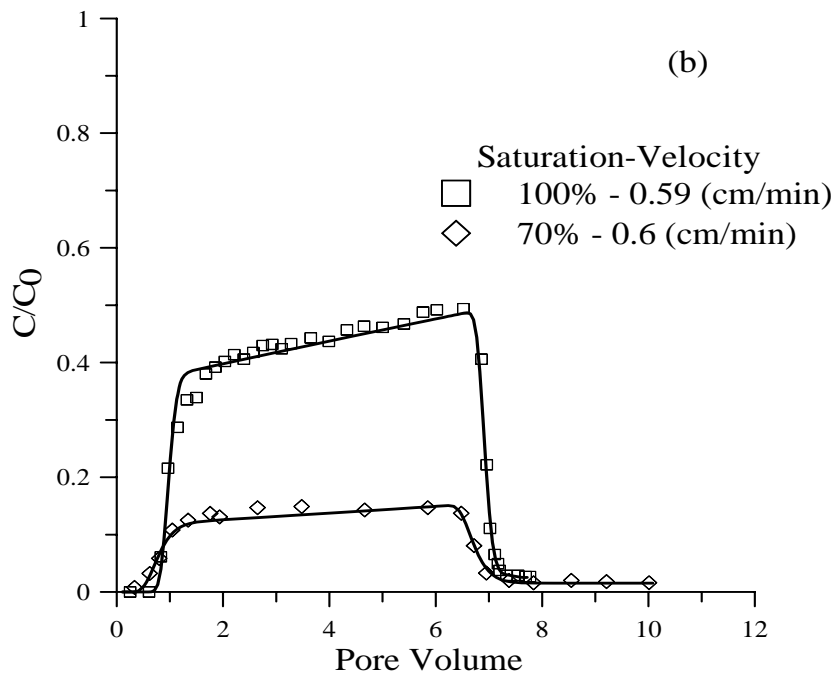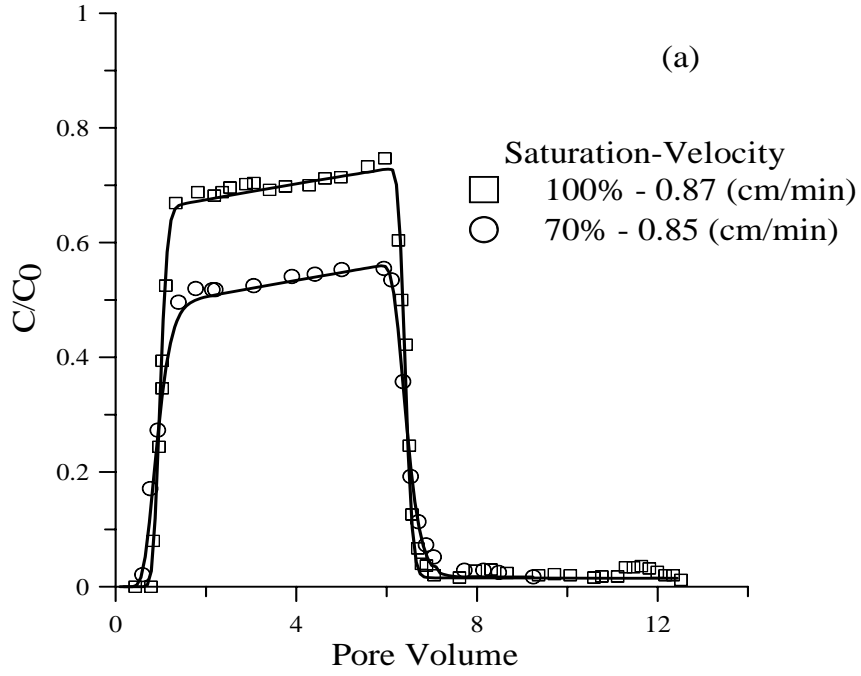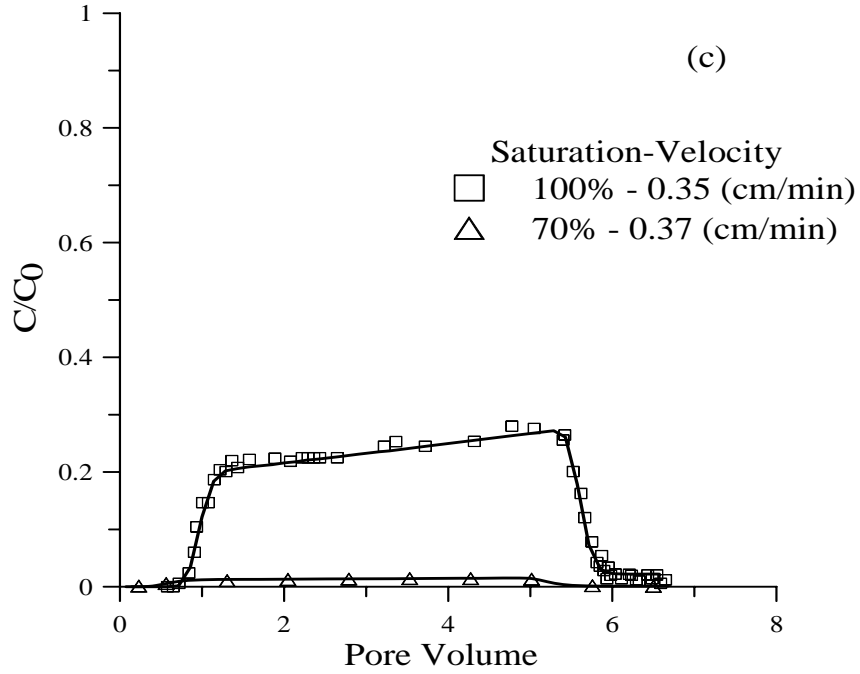
Figure 4. Observed and simulated breakthrough curves of colloids for various saturation levels in 3550 sand at an ionic strength of 60mM. The average water velocity was approximately the same in saturated and unsaturated conditions.
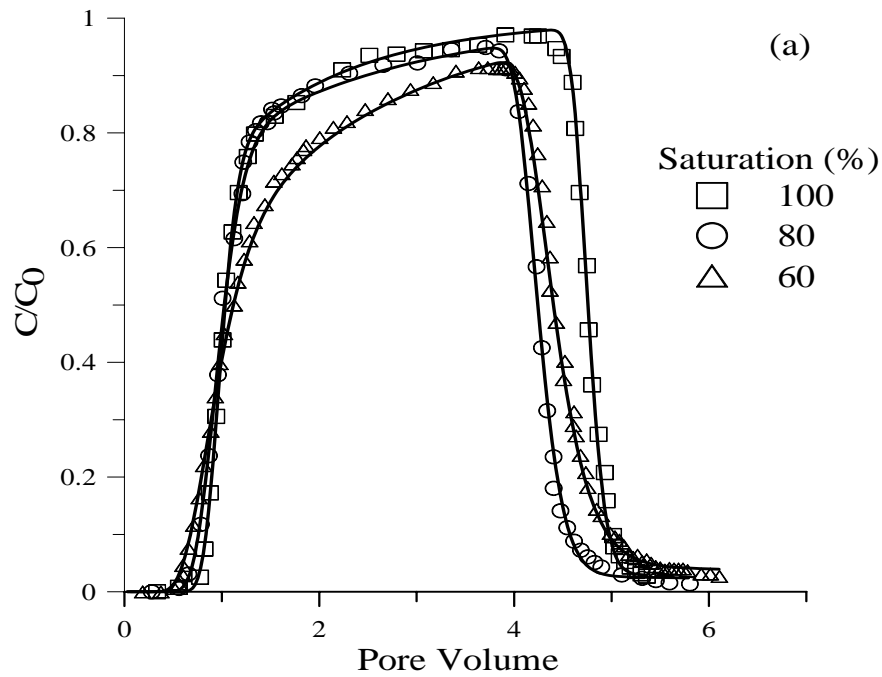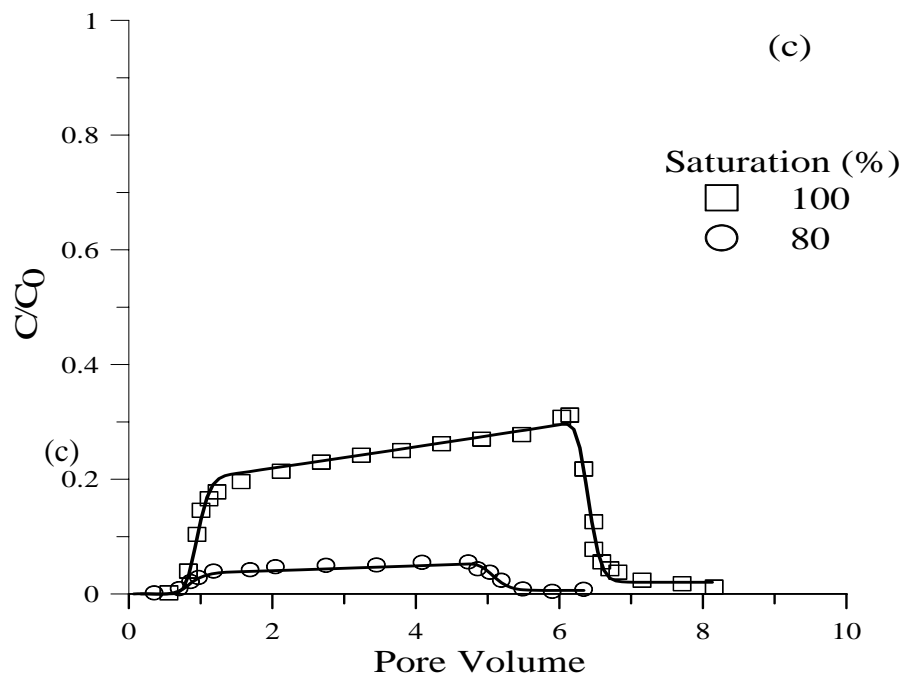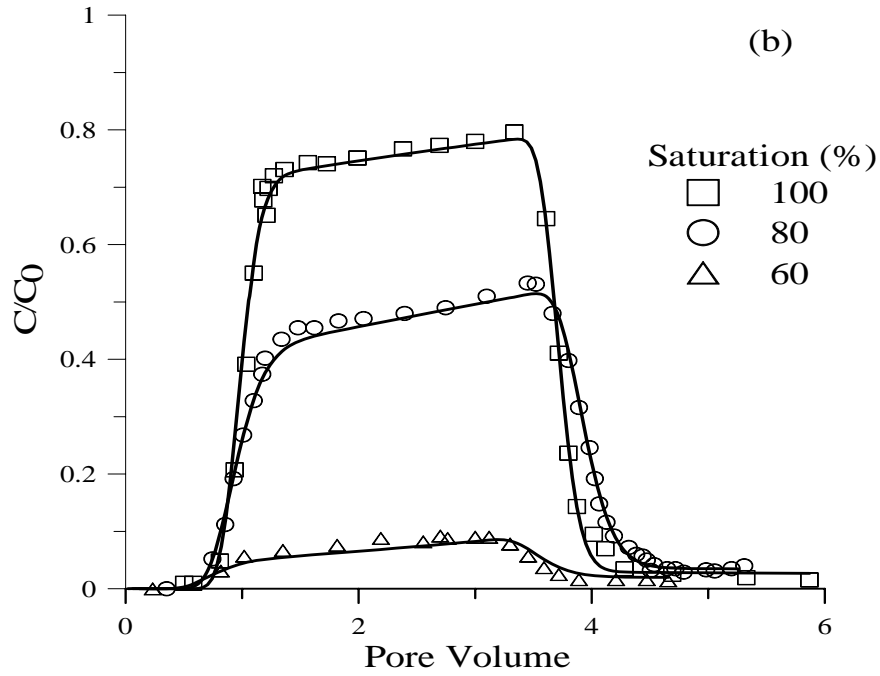
Figure 5. Observed and simulated breakthrough curves of colloids for various saturation levels in MIX sand at an ionic strength of 6 mM (Fig. 5a), 30 mM (Fig. 5b), and 60 mM (Fig. 5c)

(a)

Saturation (%)
□ 100
○ 70
◇ 50
△ 40

$N_c N_{ct}^{-1} g^{-1}$ of sand

(b)

Saturation - Velocity
□ 100% - 0.87 (cm/min)
○ 70% - 0.85 (cm/min)

$N_c N_{ct}^{-1} g^{-1}$ of sand

77
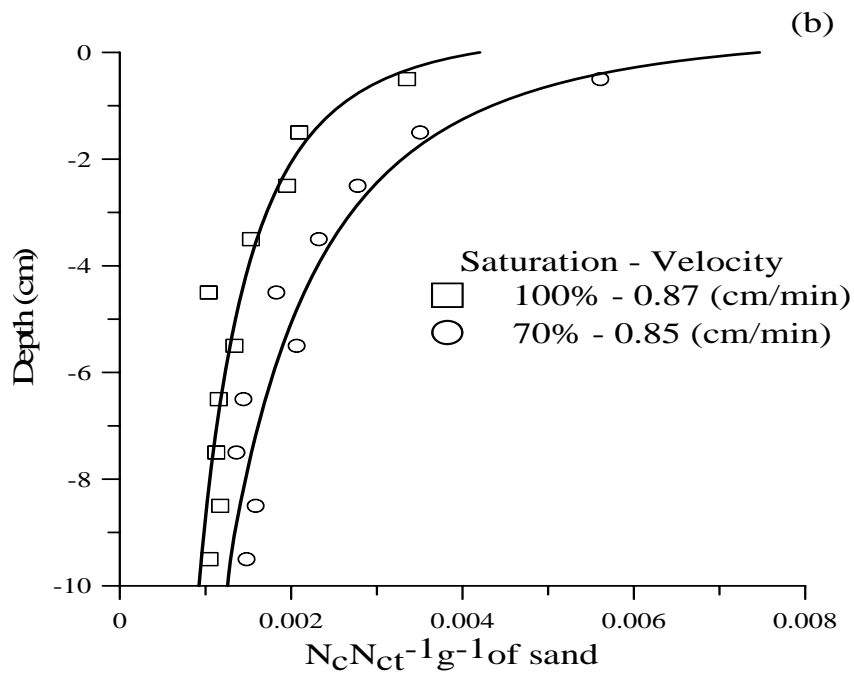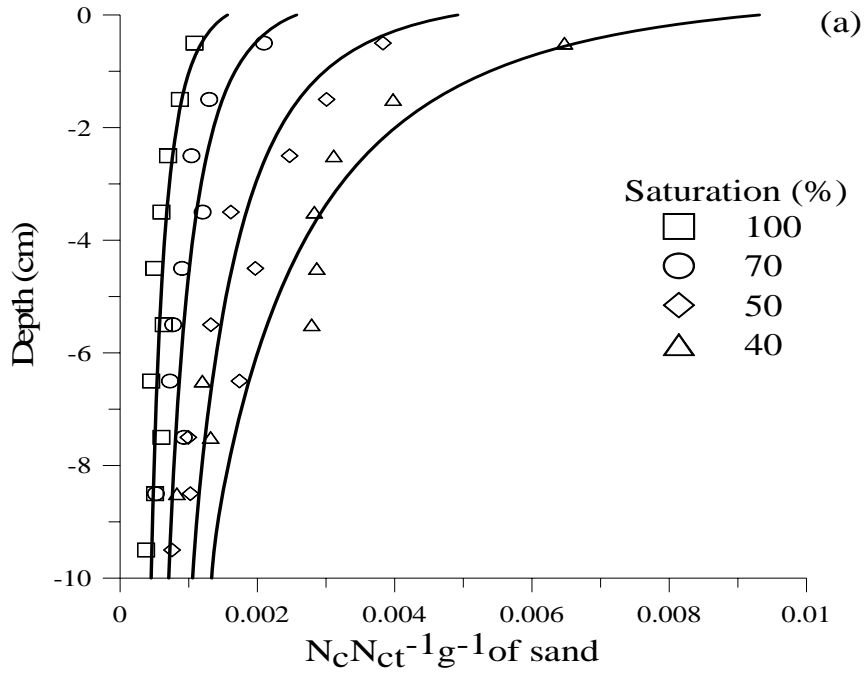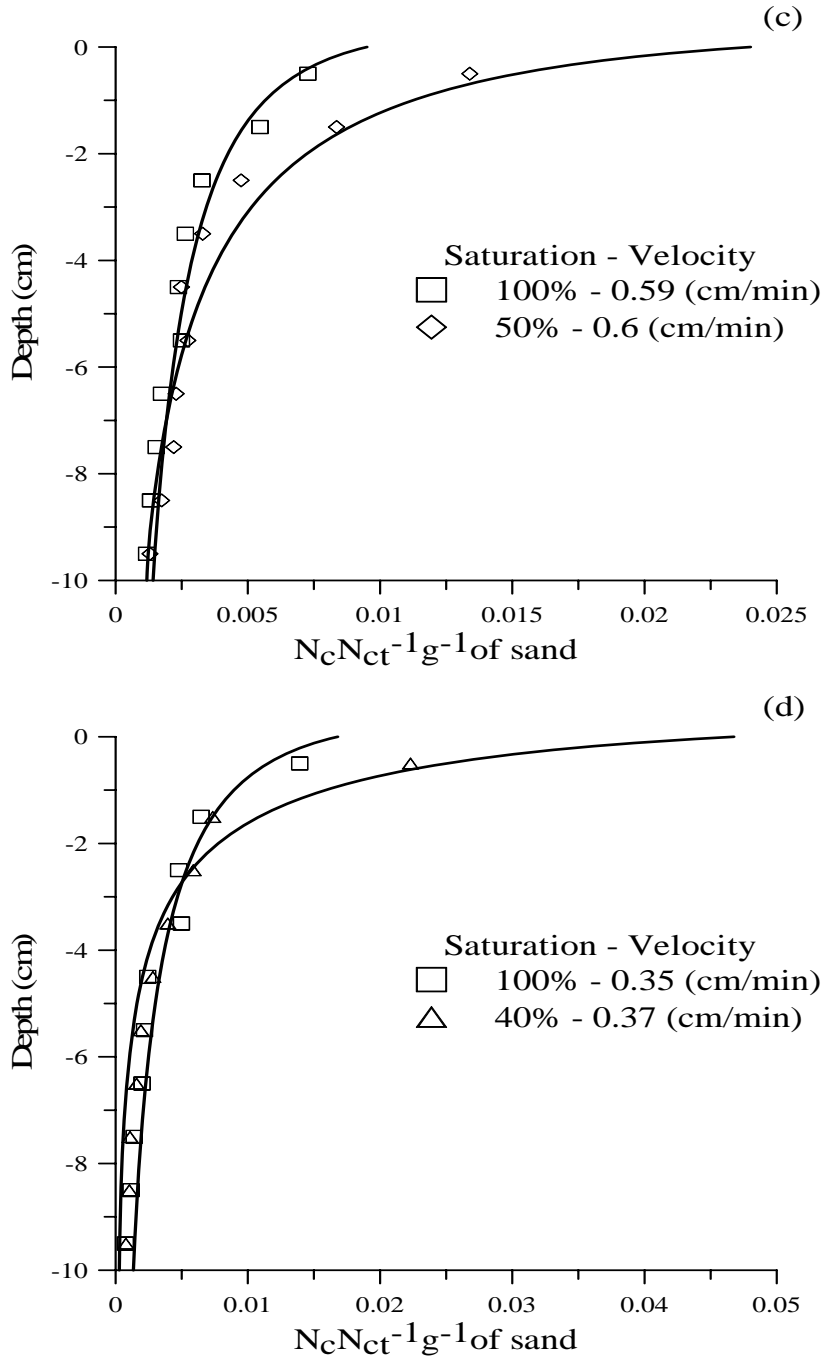
Figure 6. Observed and simulated deposition profiles of colloids for various saturation levels in 3550 sand and ionic strength of 30mM (Fig. 6a) and 60 mM (Figs. 6b-d). The average water velocity in saturated was the same as unsaturated conditions in experiments conducted at ionic strength of 60 mM.
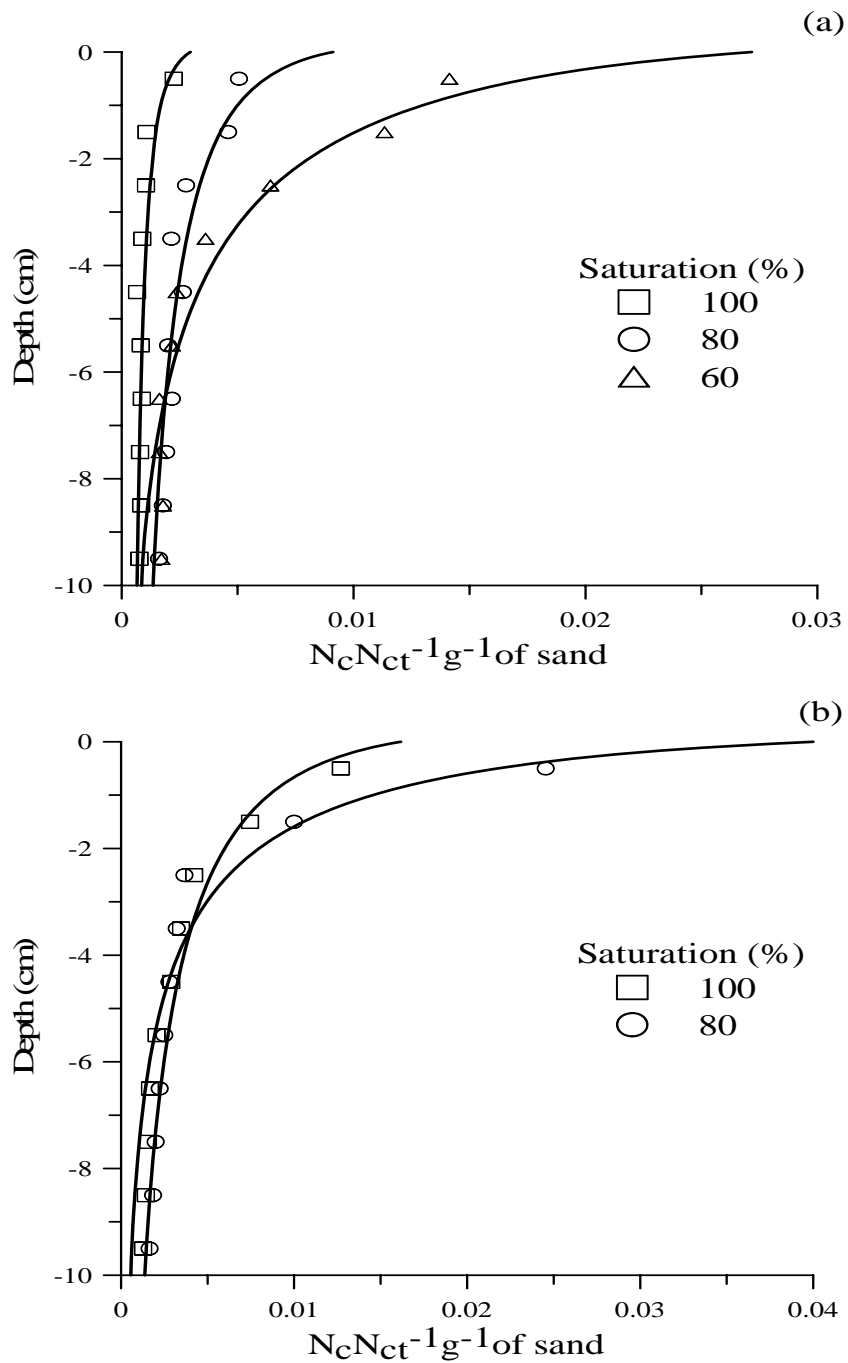
Figure 7. Observed and simulated deposition profiles of colloids for various saturation levels in MIX sand and ionic strength of 30mM (Fig. 7a) and 60 mM (Fig. 7b).

Batch Experiments and DLVO Calculations

Batch experiments were conducted to determine the potential for colloid attachment to the sand without the influence of pore structure. These experiments were conducted under a range of selected experimental conditions (20°C, pH=10, ionic strength=6, 30, and 60 mM), and were consistent with unfavorable conditions for attachment. The difference between the initial and final concentrations of colloids in solution was less than one percent. This suggests that the presence of any chemical heterogeneity on the quartz sands had negligible effect on irreversible colloid attachment. To better understand the chemical interactions between colloids and the SWI the total interaction energy was calculated using classic Derjaguin-Landau-Verwey-Overbeek (DVLO) theory (Derjaguin, 1954). In this case, the total interaction energy consists of the sum of attractive van der Waals (Gregory et al., 1981) and repulsive electrostatic (Hogg et al., 1966) interactions, and was approximated as a sphere-plate interaction. Zeta potential values were used in the place of surface potential values in the DLVO calculations, and the Hamaker constant for the CML colloids-water-sand system was set equal to 4.04×10^{-21} (Bergendahl and Grasso, 1999). As noted earlier, the measured zeta potential of the colloids becomes less negative with increasing ionic strength which is due to compression of the electrostatic double layer. The same behavior is likely for both the AWI and SWI; however for purposes of DLVO calculations, we assumed these values to be constant over the range of ionic strengths. Figure 8 presents the total interaction energy between the colloids and quartz surface upon close approach over the range of solution chemistry conditions tested in transport experiments. These calculations indicate the presence of a significant energy barrier to attachment in the primary energy minimum and a shallow secondary energy minimum at greater distance from the SWI. The depth of the secondary energy minimum increases with ionic strength ranging from 0.3 kT at 6mM to 2.9 kT at 60 mM, with corresponding separation distances of 46 to 10 nm, respectively. Note that k is the Boltzmann constant and T is the temperature in degrees Kelvin. These DLVO calculations corroborate with the batch experiment finding that there is a negligible amount of colloid adsorption to sand particles.

Similar DLVO calculations were also made to predict the interaction energy between the CML colloids and the AWI. As noted earlier, the zeta potential of the colloids and the AWI is negative resulting in a repulsive electrostatic interaction between the colloids and AWI. In contrast with the SWI, the value of the Hamaker constant for the AWI-CML colloids-water system is negative (-1.2×10^{-20} J; e.g. see Israelachvili, 1992) leading to a repulsive van der Waals interaction for these colloids as they approach the AWI. Hence, colloid attachment to the AWI is predicted to be even less favorable for the AWI than for the SWI.

Table 3. Fitted model parameters in 3550 sand and various solution ionic strengths. Also included in this table are the effluent (M_e), sand (M_S), and the total (M_T) mass percentage recovered for the experimental systems and also the coefficient of linear regression.

EXP.	S_{max}	K_{str}	K_{det}	M_E	M_S	M_T	R2
Li100	0.03	0.01	0.004	98	N.m[†]	>98	98
Mi100	0.65	0.019	0.0024	87.6	11.7	99.3	99
Hi100Hv	1.8	0.1	0.001	53	52	105	97
Hi100Mv	3.6	0.16	0.0008	32	55	87	97
Hi100Lv	5.5	0.26	0.0005	23	67	90	98
Li70	0.07	0.015	0.003	97	N.m	>97	97
Mi70	0.74	0.084	0.004	78	20	98	96
Hi70	2.5	0.17	0.0008	54	44	98	97
Li50	0.1	0.02	0.0024	93	N.m	>93	94
Mi50	1.3	0.1	0.003	66	22	88	96
Hi50	8.4	0.39	0.00063	22	75	97	97
Li40	0.16	0.024	0.002	87	N.m	>87	97
Mi40	1.8	0.13	0.0008	38	61	99	96
Hi40	12	0.6	0.0002	1.5	86	87.5	95

[†] N.m: Not measured

81

Table 4. Fitted model parameters in MIX sand and various solution ionic strengths. Also included in this table are the effluent (M_e), sand (M_S), and the total (M_T) mass percentage recovered for the experimental systems and also the coefficient of linear regression.

EXP.	S_{max}	K_{str}	K_{det}	M_e	M_S	M_T	R^2
Li100	0.075	0.024	0.003	92	N.m[†]	>92	92
Mi100	0.78	0.042	0.002	77.6	19.2	96.8	97
Hi100	5	0.29	0.0006	25	63	88	93
Li80	0.08	0.027	0.003	91	N.m	>91	94
Mi80	1.5	0.1	0.0012	49	55	104	98
Hi80	11	0.4	0.0004	5	82	87	97
Li60	0.09	0.035	0.002	86	N.m	>86	98
Mi60	2.7	0.26	0.001	9	94	103	96

[†] N.m: Not measured
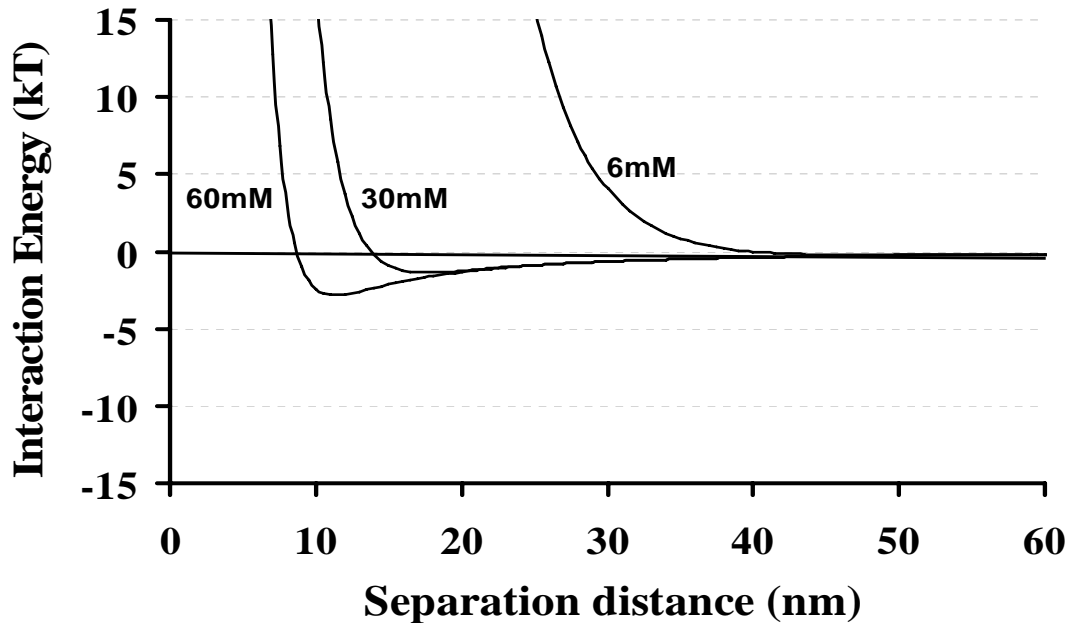
Figure 8. Calculated DLVO interaction energies as a function of separation distance and ionic strength (indicated next to each curve) for colloids. Interaction energies were calculated using the zeta potentials as surface potentials. The Hamaker constant for the colloid-water-sand media was assumed to be $4.04 \times 10\text{-}21$ (Bergendahl and Grasso, 1999).

Implications for Colloid Transport and Retention

Experimental evidence in this study has demonstrated that attachment to the SWI is not the dominant mechanism responsible for colloid retention. The first piece of indirect evidence is the batch experiments which found no significant colloid attachment to the sand. Additionally, the experimental protocol for determining the deposition profiles was based upon the rapid release of colloids into solutions, and the high recoveries were not consistent with the low detachment rates that were observed in the column experiments. If the colloids were irreversibly attached to the SWI, they should have remained on the grain surface even after suspending the sand in the same solution that was used for the transport experiments. The next piece of evidence is the fact that colloid retention occurred in the column, even under conditions when DLVO calculations indicate the presence of a substantial energy barrier against colloid attachment. Finally, the colloid deposition profiles resulting from the column experiments were not consistent with first-order attachment-detachment model predictions. Specifically, the value of β (Eq. 3) was greater than zero, indicating depth-dependent deposition rather than first-order attachment.

Recently in the literature, non-exponential deposition profiles in saturated conditions has attributed to charge variability of the porous media (Johnson and Elimelech, 1995), heterogeneity in colloid surface charge characteristics (Bolster et al., 1999; Li et al., 2004), and deposition of colloids in a secondary energy minimum (Redman et al., 2004; Tufenkji and Elimelech, 2005b). These factors may be involved, however, these mechanisms cannot fully explain the experimental data presented in this paper. The experiments were conducted in a solution at a pH 10, which should minimize any effect of charge heterogeneity on the sand surface because the isoelectric points of most metal oxides fall below this pH (Elimelech et al., 2000). The results of our batch experiments do not support the existence of any significant heterogeneity on the grain or colloid surfaces. Furthermore, the colloids may be held in secondary minima; however, this cannot explain the observed depth- and grain size- dependent deposition. Therefore, another retention mechanism must also be involved.

83

Retention of colloids under unsaturated conditions has also been attributed to partitioning at the AWI and/or film straining (e.g. Wan and Wilson 1994a; Wan and Tokunaga 1997; Lenhart and Saiers, 2002; Saiers and Lenhart, 2003a). However, attachment to the AWI is not believed to play a significant role in the reported unsaturated experiments, as both the AWI and colloids were negatively charged even in the highest ionic strength solution (see Table 2) and the van der Waals interaction was repulsive. It has been well documented that hydrophilic-negatively charged colloids are unlikely to attach to the negatively charged AWI (e.g. Wan and Tokunaga 2002; Christ et al. 2004, 2005; Torkzaban et al. 2006a, 2006b). Torkzaban et al. (2006a) investigated viral transport under a range of water saturation levels at pH 9 and reported no retention of viruses in the unsaturated columns. Crist et al. (2004, 2005) visually demonstrated that hydrophilic latex colloids did not adsorb on the AWI using a real-time pore-scale microscopic method.

It is also unlikely that film straining plays a major role in the reported colloid retention as the l.1 µm latex colloids are too large to be bound within a thin film. These thin water films have calculated thicknesses around 50 nm during steady-state water flow over an order of magnitude thinner than the diameter of the colloids used in this study (Zevi et al., 2005). Moreover, film straining is theoretically independent of solution ionic strength and flow velocity (Wan and Tokunaga, 1997). In contrast, notably more colloid retention is observed in higher ionic strength solutions and for lower water velocities.

Straining of colloids provides a plausible explanation and mechanism for the observed colloid deposition behavior. Strained colloids become trapped in the smallest regions of the pore space where the flow velocity is reduced. These nearly immobile regions (Patzek and Silin, 2001; Patzek and Kristensen, 2001) include the small pore spaces formed at grain-to grain contacts, dead-end pores, and the three-phase contact line of the solid-water- air interface (in case of unsaturated conditions). Fluorescent microscopy and x-ray microtomography studies have demonstrated that colloids accumulate in the narrow region of the pore spaces near the contacts of irregularly shaped sand grains under unfavorable attachment conditions (Bradford et al., 2005, 2006a, Xu et al., 2006; Li et al., 2006; Yoon et al., 2006). In these studies, pore-space constrictions apparently served as locations for colloid retention by straining, whereas few colloids

appeared to be immobilized far from the grain-to- grain contacts. Colloid retention in the pore network is further supported by Hoek and Agarwal (2006) who reported that DLVO forces act on colloids up to 5 times more in small pore spaces (surface roughness) than with a single flat surface. Straining, as the mechanism of colloid retention, is also supported by mass balance calculations and the fact that once the sand is resuspended in the solution and the pore structure eliminated, the colloids return to solution.

Straining has recently been demonstrated to be a strong function of DLVO and hydrodynamic forces (Bradford et al., 2006a; Bradford et al., 2007). Colloids that are weakly associated with the SWI via the secondary energy minima experience significant hydrodynamic forces (e.g. fluid drag, lift forces) due to fluid flow. The shear force acting on the colloid surface held in the secondary energy minimum is different than that acting on the colloid surface in the bulk fluid. Consequently, at close range to the SWI the colloids experience a combination of forces (hydrodynamic forces, electrical double-layer repulsion, and London-van der Waals) that creates a torque and hence rotation on the surface. (Cushing and Lawler 1998; Bergendahl and Grasso 2000). It has been proposed that weakly associated colloids with the SWI via the secondary energy minimum can be translated and/or funneled by these fluid drag forces to low velocity regions of the pore structure or "straining sites" (Bradford et al., 2007). Indeed, recent experimental evidence by Kuznar and Elimelech (2007) demonstrates that colloids captured in the secondary energy minimum can be translated along the collector surface via hydrodynamic forces and be retained in low velocity regions. Based on this argument, more colloids will be retained in a secondary energy minimum as the ionic strength is increased and these colloids will subsequently be funneled to straining sites.

The coupled effects of DLVO and hydrodynamic forces on straining also can explain the observed decrease in colloid retention with increasing fluid velocity. In this case, enhanced hydrodynamic forces may overcome the electrostatic and van der Waals interactions and detach colloids from the grain surface, and thereby minimize the amount of straining. It is also likely that the extent of relatively stagnation regions decreases as the water velocity increases (Patzek and Silin, 2001; Patzek and Kristensen, 2001). This is consistent with our observations and modeling results presented by Cushing and Lawler (1998). In contrast with the column experiments, there is no pore structure in the

batch experiments. Therefore, the hydrodynamic shear forces as the result of rotation prevented colloid attachment to the sand grains in the batch experiments.

It was anticipated that the magnitude of straining would be enhanced with decreasing sand size and water saturation level due to greater amount of low velocity regions. Both of these expected trends were verified by our experimental observations. The extent of retention of colloids increased with ionic strength and decreasing soil grain size for all of the various saturation levels tested. This is especially true for the higher ionic strength conditions (Figs.5b-c) where very little breakthrough of colloids occurred. Comparison of the breakthrough curves for all of the ionic strength conditions reveals a decrease in peak effluent concentrations with water content. All these results provide substantial direct and indirect evidence that straining is an important removal mechanism for the CML colloids in the Ottawa sands investigated.

The comparison of experimental and modeled results also suggests that straining is the underlying mechanism in colloid deposition in both the saturated and unsaturated systems tested. The concentration of retained colloids enumerated after the column experiments was found to exhibit a hyper-exponential spatial distribution through the length of the column. This indicates the deposition coefficient was depth-dependent, a trend that has previously been associated with straining (e.g., Bradford et al., 2002, 2003, and 2006b).

Conclusions

Experimental and theoretical studies were conducted to determine the role of solution chemistry and water content on colloid retention under unfavorable attachment conditions. To better understand the underlying mechanism on colloid retention, the experimental conditions were selected to minimize the potential for colloid attachment (solution pH of 10, quartz sands, and highly negatively charged colloids that were hydrophilic). DLVO calculations, mass balance information, and batch experiments confirmed our assumption that attachment to the SWI and AWI was not the dominant mechanism in colloid retention. All the observations discussed above provide convincing evidence that straining was the primary mechanism of colloid retention in our column experiments. The straining rate in a given porous media is apparently a complicated

mechanism, coupled with such parameters as pore size distribution, hydrodynamics, solution chemistry and water content. Specific findings are highlighted below.

- Straining increases in magnitude with increasing ionic strength due to an increased force (secondary energy minimum) and number of colloids that are funneled to and retained in small pores formed adjacent to grain-grain junctions.

- Straining increases in magnitude with decreasing water content due to an increase in the extent of stagnant regions of flow within the pore media.

- Increasing the flow rate of a system tends to decrease the amount of straining of colloids as a result of the increased fluid drag force that acts on weakly-attached colloids on the SWI and also decreased flow stagnation regions

- The shape of the colloid deposition profile is highly sensitive to the physical (grain size, water content, and flow rate) and chemical (solution IS and pH) properties of a system due to the interrelation of these parameters on colloid straining.

Additional research is required to better understand and quantify the coupling of physical and chemical processes that influence colloid straining in saturated and unsaturated porous media. This information is believed to be essential for predicting colloid transport and fate in many natural environments.

Acknowledgments

Chapter 5

Coupling of physical and chemical mechanisms of colloid straining in saturated porous media

Abstract

Filtration theory does not include the potential influence of pore structure on colloid removal by straining. Conversely, previous research on straining has not considered the possible influence of chemical interactions. Experimental and theoretical studies were therefore undertaken to explore the coupling of physical and chemical mechanisms of colloid straining under unfavorable attachment conditions (pH=10). Negatively charged latex microspheres (1.1 and 3 µm) and quartz sands (360, 240, and 150 µm) were used in packed column studies that encompassed a range in suspension ionic strengths (6-106 mM) and Darcy water velocities (0.1-0.45 cm min^{-1}). Derjaguin-Landau-Verwey-Overbeek (DLVO) calculations and torque analysis suggest that attachment of colloids to the solid-water interface was not a significant mechanism of deposition for the selected experimental conditions. Effluent concentration curves and hyper-exponential deposition profiles were strongly dependent on the solution chemistry, the system hydrodynamics, and the colloid and collector grain size, with greater deposition occurring for increasing ionic strength, lower flow rates, and larger ratios of the colloid to the median grain diameter. Increasing the solution ionic strength is believed to increase the force and number of colloids in the secondary minimum of the DLVO interaction energy profile. These weakly associated colloids can be funneled to small regions of the pore space formed adjacent to grain-grain junctions. For select systems, the ionic strength of the eluant solution was decreased to 6 mM following the recovery of the effluent concentration curve. In this case, only a small portion of the deposited colloids was recovered in the effluent and the majority was still retained in the sand. These observations suggest that the extent of colloid removal by straining is strongly coupled to solution chemistry.

Introduction

      Considerable research has been devoted to the fate and transport of microbes (biocolloids) and colloids in porous media (reviews are given by Schijven and Hassanizadeh, 2000; Harvey and Harms, 2002; Jin and Flury, 2002; Ginn et al., 2002). The bulk of existing colloid literature considers deposition to be controlled by attachment of colloids on grain surfaces. Mass transfer of colloids to the solid-water interface occurs via diffusion, interception, and sedimentation (Yao et al., 1971). Attachment involves collision with and subsequent retention of colloids at the solid-water interface. Once a colloid approaches the solid-water interface, attachment depends on a combination of forces and/or torques that act on the colloid (Cushing and Lawler, 1998; Bergendahl and Grasso, 1998; Li et al., 2005) at this location. These forces include gravity and buoyancy, hydrodynamic drag and lift, electrical double-layer repulsion (or attraction), and London-van der Waals interaction.

      In the presence of an energy barrier (unfavorable attachment conditions) the transport and deposition behavior of colloids is frequently found to be inconsistent with clean bed filtration theory (CFT) predictions (Albinger et al., 1994; Glynn et al., 1997; Camesano and Logan, 1998; Bolster et al., 1999; Redman et al., 2001; Bradford et al., 2002; Tufenkji et al., 2003; Li et al., 2004; Tong et al., 2005; Li and Johnson, 2005; Tufenkji and Elimelech, 2005ab). Specifically, the deposition coefficient has commonly been observed to exhibit depth dependence and the concentration of retained colloids does not decrease exponentially with distance as CFT would predict. Deviation between CFT predictions and experimental data has been reported to be increasingly significant for larger colloids and finer textured porous media (Bradford et al., 2002; and Tufenkji and Elimelech, 2005a). Bradford et al. (2003) reported that filtration theory predictions no longer adequately describe the measured deposition profiles when the ratio of the colloid diameter to the median grain diameter is greater than around 0.005.

      Filtration theory assumes a model collector (such as Happel's sphere-in-cell model which is an isolated collector in an assemblage of collectors) that neglects the actual pore structure and pores formed by grain-grain contacts which occur in porous media. However, recent experimental and theoretical research has indicated that the pore structure can play an important role in colloid deposition under unfavorable attachment conditions (Cushing and Lawler, 1998; Bradford et al., 2002, 2003, 2004, 2005, 2006abcd; Li et al., 2004, 2006ab; Tufenkji et al., 2004;

Bradford and Bettahar, 2005 and 2006; Foppen et al., 2005). This removal likely occurs by straining, which is the retention of colloids in the smallest regions of the soil pore space formed adjacent to points of grain-grain contact (Cushing and Lawler, 1998). Pore spaces occurring at grain contacts provide optimum locations for colloids that are weakly associated with the solid phase (secondary energy minima) to be retained because of reduced hydrodynamic forces, pore size limitations, and enhanced DLVO interactions (Hoek and Agarwal, 2006).

Most published research on straining has focused on the role of physical factors such as the relative size of the colloid and porous medium and little attention has been given to the potential interrelated influence of solution chemistry and hydrodynamics on straining. Attachment under unfavorable conditions is known to be highly dependent on solution chemistry (e.g., Li et al., 2004; Tufenkji and Elimelech, 2004 and 2005a), and system hydrodynamics (Wang et al., 1981; Tan et al., 1994; Kretzschmar et al., 1997; Compere et al., 2001; Li et al., 2005). Under such attachment conditions, hydrodynamic forces may be sufficient to overcome the weak association of colloids in the secondary energy minimum of the DLVO interaction energy distribution (Kuznar and Elimelech, 2006). In this case, attached colloids may be lifted from the solid surface and detach, or they may roll or slide down gradient on the grain surface to locations where the hydrodynamic shear is less significant. Bergandahl and Grasso (1998) demonstrated that rolling is often the primary mechanisms for hydrodynamic motion of detached colloids. It is logical to anticipate that some of the colloids rolling on the grain surface may be retained in straining locations (i.e., smallest regions of the pore space formed at grain-grain contact points). One can therefore expect that solution chemistry and hydrodynamic forces will play an important interrelated role in straining.

The objective of this research is to investigate the role of solution chemistry and system hydrodynamics on colloid transport and straining. Negatively charged latex microspheres and quartz sands were used in packed column studies that encompassed a range of solution IS (6-106 mM) and Darcy water velocity (0.1-0.45 cm min^{-1}). All experiments were conducted using electrolyte solution buffered to a pH of 10 to ensure highly unfavorable attachment conditions. Data analysis and interpretation was aided through DLVO calculations of the total interaction energy between the colloids and quartz surfaces, analysis of torques, mass balance computation, and experimental effluent concentration curves and deposition profiles.

Material and Methods

Colloids

Yellow-green fluorescent latex microspheres (Molecular Probes, Eugene, OR) were used as model colloid particles in the experimental studies (excitation at 505 nm, and emission at 515 nm). Two sizes of microspheres were used in the transport experiments, 1.1 and 3.0 μm. The uniformity of the colloid size was verified using with a Horiba LA 930 (Horiba Instruments Inc., Irvine, CA 92614) laser scattering particle size and distribution analyzer and by inspections of suspensions under an epi-fluorescent microscope. The microspheres had carboxyl surface functional groups, a density of 1.055 g cm^{-3}, and are reported as hydrophilic by the manufacturer. The initial influent concentration (C_i) for the 1.1 and 3.0 μm colloids for the experiments was 2.7×10^{10} and 1.3×10^9 N_c L^{-1} (where N_c denotes number of colloids), respectively. Several experiments with the 1.1 μm colloids were also conducted at a lower initial concentration of $C_i = 6.8 \times 10^8$ N_c L^{-1}.

Sand

Aquifer material used for the column experiments consisted of various sieve sizes of Ottawa sand (U.S. Silica, Ottawa, IL). The porous media were selected to encompass a range in grain sizes, and are designated by their median grain size (d_{50}) as: 360, 240, and 150 μm. Specific properties of the 360, 240, and 150 μm sands include: the coefficient of uniformity (d_{60}/d_{10}; here 10 and 60% of the sand mass is finer than d_{10} and d_{60}, respectively) of 1.88, 3.06, and 2.25; and intrinsic permeabilities of 6.37×10^{-11}, 1.12×10^{-11}, and 4.68×10^{-12} m^2, respectively. Ottawa sands typically consist of 99.8% SiO_2 (quartz) and trace amounts of metal oxides, have spheroidal shapes, and contain relatively rough surfaces. An estimate of the pore-size distribution for these sands can be obtained by using Laplace's equation of capillarity and measured capillary pressure - saturation curves presented by Bradford and Abriola (2001).

Electrolyte Solution Chemistry

The background electrolyte solutions utilized in the column studies consisted of deionized water with a buffered pH of 10 achieved with 1.7 mM NaHCO$_3$ and 1.7 mM Na$_2$CO$_3$ (Cherrey et al., 2003). This solution chemistry was chosen to create a stabilized mono-dispersed suspension

with the selected colloids. In particular, at a pH of 10 quartz and iron oxides possess a net negative charge (Tipping, 1981; Redman et al., 2004), and any attractive electrostatic interactions between the colloids and porous media is expected to be minimized at this pH. The ionic strength (IS) of the eluant, resident, and tracer solutions in the transport experiments was varied using this same pH 10 solution by changing the amounts of added NaCl (eluant and resident solutions) or NaBr (tracer). Unless specifically indicated, the concentrations of NaCl (resident and eluant solutions) and NaBr (tracer) in solution were maintained over the course of an experiment at 6, 31, 56, 81, or 106 mM. On select experiments the IS of the eluant solution was lowered to 6 mM NaCl for an additional 2.1-3.3 pore volumes after recovery of the effluent concentration curve (the first 8-10 pore volumes). All of the colloid tracer solutions consisted of the pH 10 NaBr solution (IS of 6, 31, 56, 81, or 106 mM), and the previously indicated initial colloid concentration.

Column Experiments

Procedures and protocols for the packed column experiments are reported in detail by Bradford et al. (2002). Only an abbreviated discussion is provided below. Kontes Chromaflex chromatography columns (Kimble / Kontes, Vineland, NJ) made of borosilicate glass (15 cm long and 4.8 cm inside diameter were equipped with an adjustable adapter at the top) were used in the transport studies. The columns were wet packed (water level kept above the sand surface) with the various sands. Table 1 provides porosity (ε) values and column length (L_c) for each experimental system. The colloid suspension was pumped upward through the vertically oriented columns at a steady flow rate, after which a three-way valve was used to switch to the background solution. The average Darcy velocities (q) and colloid pulse duration in terms of pore volumes (PV) for the various experiments are given in Table 1. Effluent samples were collected and analyzed for colloid concentration using a Turner Quantech Fluorometer (Barnstead / Thermolyne, Dubuque, IA). The average of three measurements were used to determine each colloid concentration (reproducibility was typically within 1% of C_i).

Following completion of the colloid transport experiments, the spatial distribution of retained colloids in each packed column was determined. The saturated sand was carefully excavated into 50 ml Falcon centrifuge tubes containing excess eluant solution of the same IS and

pH that was used in the transport experiment. The tubes were slowly shaken for 15 minutes using a Eberbach shaker (Eberbach corporation, Ann Arbor, Michigan) to liberate reversibly retained colloids. The concentration of the colloids in the excess aqueous solution was measured with the fluorometer, using the same experimental protocol as followed for the effluent samples. The volume of solution and mass of sand in each tube was determined from mass balance.

A colloid mass balance was conducted at the end of each column experiment using effluent concentration data and the final spatial distribution of retained colloids in the sand. The calculated number of colloids in the effluent and retained in the sand was normalized by the total number of injected particles into a column. Table 1 presents the calculated colloid mass percentages that were recovered for all the experiments in the effluent (M_{eff}), sand (M_{sand}), and the total ($M_{total}=M_{eff}+M_{sand}$) system.

DLVO Calculations

DLVO theory (Derjaguin and Landau, 1941; Verwey and Overbeek, 1948) was used to calculate the total interaction energy (sum of London-van der Waals attraction and electrostatic double-layer repulsion) for our 1.1 and 3 μm colloids upon close approach to quartz surfaces (assuming sphere-plate interactions) for the various solution chemistries (pH=10, and IS=6, 31, 56, 81, and 106 mM). In these calculations, constant-potential electrostatic double layer interactions were quantified using the expression of Hogg et al. (1966) and zeta potentials in place of surface potentials. Retarded London-van der Waals attractive interaction force was determined from the expression of Gregory (1981) utilizing a value of 4.04×10^{-21} J for the Hamaker constant (Bergendahl and Grasso, 1999) to represent our polystyrene latex-water-quartz system. The zeta potential of the quartz at pH 10 and for IS ranging from 6 to 106 mM was estimated using results presented in Elimelech et al. (2000) and Redman et al. (2004). Zeta potentials for our 1.1 and 3 μm colloids in the various solution chemistries that were used in the DLVO calculations were calculated from experimentally measured electrophoretic mobilities using a ZetaPals instrument (Brookhaven Instruments Corporation, Holtsville, NY).

Table 1. Column properties (Darcy velocity, q; porosity, ε; and column length, L_c; and colloid

pulse duration, T_o) and the effluent (M_{eff}), sand (M_{sand}), and the total (M_{total}) mass percentage recovered for the experimental systems.

IS	d_c	d_{50}	q	ε	L_c	T_o	M_{eff}	M_{sand}	M_{total}
mM	μm	μm	cm min⁻	-	cm	min	%	%	%
6	3	360	0.096	0.35	12.9	75	60.3	37.2	97.5
6	3	240	0.104	0.32	12.3	75	14.3	71.5	85.8
6	3	150	0.096	0.35	12.8	75	6.0	84.7	90.7
6	3	360	0.506	0.33	12.5	15	38.1	47.5	85.6
6	3	240	0.466	0.33	12.4	15	6.4	86.6	93.0
6	3	150	0.463	0.36	13.1	15	1.4	86.7	88.1
6	1.1	360	0.107	0.32	12.2	75	102.9	3.6	106.5
31	1.1	360	0.107	0.35	12.8	75	97.9	22.0	119.9
56	1.1	360	0.099	0.34	12.6	75	43.5	39.6	83.1
81	1.1	360	0.085	0.34	12.6	75	42.9	60.2	103.1
106	1.1	360	0.101	0.33	12.4	75	0.6	89.6	90.2
6	1.1	240	0.089	0.28	11.6	75	100.0	4.6	104.6
31	1.1	240	0.093	0.30	12.0	85	82.5	13.4	95.9
56	1.1	240	0.104	0.30	12.0	75	32.1	53.7	85.8
81	1.1	240	0.092	0.31	12.1	75	25.9	79.2	105.1
106	1.1	240	0.098	0.33	12.5	75	0	99.5	99.5
6	1.1	150	0.104	0.33	12.5	75	94.9	14.2	109.1
31	1.1	150	0.098	0.35	12.8	85	86.7	16.1	102.8
56	1.1	150	0.099	0.35	12.8	75	21.3	70.3	91.6
81	1.1	150	0.084	0.35	12.9	75	16.4	85.6	102.0
106	1.1	150	0.101	0.34	12.7	75	0	91.4	91.4
56	1.1	360	0.230	0.34	12.6	37.3	45.4	41.7	87.1
56	1.1	240	0.289	0.35	12.8	37.3	27.2	56.6	83.8
56‡	1.1	150	0.229	0.34	12.7	37.3	18.8	62.8	81.6
56	1.1	360	0.479	0.33	12.4	15	80.3	18.5	98.8
56	1.1	240	0.411	0.32	12.3	15	67.1	43.2	110.3
56‡	1.1	150	0.446	0.36	13.0	15	52.1	50.0	102.1
56/6†	1.1	360	0.216	0.35	12.8	112.5	46.0	43.1	89.1
56/6†	1.1	240	0.197	0.36	13.1	112.5	32.4	64.3	96.7
56/6†‡	1.1	150	0.198	0.35	12.9	112.5	25.1	69.3	94.4
106/6†	1.1	360	0.250	0.33	12.4	112.5	38.7	90.0	128.7
106/6†	1.1	240	0.256	0.32	12.3	112.5	12.3	91.6	104.0
106/6†	1.1	150	0.257	0.35	12.7	112.5	10.7	115.8	126.5
6‡	1.1	150	0.215	0.36	13.0	37.5	83.3	7.1	90.4

† - The IS of the colloid suspension and eluting solution was 56 or 106 mM for the first 8.2 to 12.4 pore volumes, followed by an additional 2.1 to 3.2 pore volume flush of 6 mM solution.
‡ - Published in Bradford et al. (2006d)

Applied and Resisting Moments

Bergendahl and Grasso (1999, 2000) provide a mathematical framework to examine the influence of hydrodynamics on colloid detachment in porous media. These authors found that detachment occurred primarily by rolling when the applied moment from hydrodynamic shear overcame the resistance associated with rolling. Lifting and sliding of attached colloids were much less significant mechanisms of detachment and were therefore not considered herein. The detachment of retained polystyrene colloids in glass beads was well predicted by this model. We utilize this approach to determine the conditions when detachment of colloids retained in the DLVO secondary minima is likely.

The resisting torque for colloids attached in the DLVO secondary minima (T_{res}; ML^2T^{-2}; M, L, and T denotes units of mass, length, and time, respectively) to fluid flow is given as:

$$T_{res} = a_0 F_{DLVO} \qquad (1)$$

where F_{DLVO} [MLT^{-2}] is the DLVO force of adhesion and a_o [L] is the contact radius. To obtain F_{DLVO} in terms of interaction energy the Derjaguin and Langbein approximations (Israelachvili, 1992) were employed. Specifically, the value of F_{DLVO} was estimated as $\Phi_{2min}{}^*/d_o$; where $\Phi_{2min}{}^*$ [ML^2T^{-2}] is the absolute value of the secondary minima interaction energy and d_o [L] is the separation distance between the colloid and the solid surface. The value of a_o is by given by Li et al. (2005) as:

$$a_0 = \left(\frac{4 r_c F_{DLVO}}{K_i} \right)^{\frac{1}{3}} \qquad (2)$$

where r_c [L] is the colloid radius and K_i [$ML^{-1}T^{-2}$] is the elastic interaction constant. Bergendahl and Grasso (2000) employed a values of K_i=4.014x10^9 N m^{-2} for glass beads and polystyrene colloids and we assume this values for the calculations discussed herein. The above analysis provides a conservative (larger) estimate of T_{res} because colloids attached in the secondary minima have been treated in an analogous fashion as those in the primary minima.

The torque applied to attached colloids as a result of the fluid drag force (T_{app}; ML^2T^{-2}) is given as (Bergendahl and Grasso, 2000):

$$M_{app} = 10.205 \pi \mu_w r_c^3 \left(\frac{\partial v}{\partial r} \right) \qquad (3)$$

where μ_w [M L^{-1} T^{-1}] is the water viscosity, and $\dfrac{\partial v}{\partial r}$ [T^{-1}] is velocity shear rate that acts on attached colloids. The value of the shear rate can be calculated for simple pore geometries. For example if we consider the porous media as a bundle of capillary tubes of different sizes, then the shear rate (at R-r_c; where R [L] is the radius of a given capillary tube) in a given capillary tube can be derived from Poiseuille's Law as:

$$\frac{\partial v}{\partial r} = \frac{\Delta p}{2 \mu_w L_{ct}} \left(R - r_c \right) \tag{4}$$

where Δp [N L^{-2}] is the pressure difference across the capillary tube, and L_{ct} [L] is the capillary tube length. Equation (4) indicates that the shear rate is proportional to the capillary tube radius and the pressure gradient. It follows from Eq. (3) that T_{app} is also proportional to these variables.

For a given conductivity and Darcy velocity in a porous medium, the value of $\Delta P/L_{ct}$ in Eq. (4) can be estimated using Darcy's Law for horizontal flow. In the experiments discussed herein the value of $\Delta P/L_{ct}$ ranged from 15696 (360 sand when q=0.1 cm min^{-1}) to 961478 (150 sand when q=0.45 cm min^{-1}) N m^{-3}. It should also be mentioned that the maximum velocity and the average water flux in a given sized capillary tube are proportional to the square of the tube radius (e.g., Jury et al., 1991). Hence, for a given pressure gradient higher flow rates and average water fluxes occur through larger than smaller capillary tubes.

Results and Discussion

Impact of Solution Chemistry on Colloid Retention

Table 1 summarizes experimental conditions and mass balance information for all column experiments. Values of M_{total} typically ranged from 83 to 110%. Three column experiments had values of M_{total} that were somewhat higher (<129%), presumably due to background interference of natural colloids in these sands that impacted values of M_{sand}. Recall that deposition profiles were obtained after excavating the sand from the column, and gently shaking the sand in excess eluant solution of the same solution chemistry that was used in the transport experiment. Values of M_{total} close to 100% in Table 1 therefore indicates that the retained colloids were only weakly associated with the Ottawa sands for the selected solution chemistries. In further support of these

97

findings, Torkzaban et al. (2006) conducted batch experiments with the same 1.1 µm colloids and sands, and similar solution chemistries (up to 60 mM) and found negligible sorption of these colloids onto the sand grains, suggesting only minimal association with these surfaces.

Table 2 provides values of zeta potential for the modified carboxyl latex colloids and quartz in the various solution chemistries that were employed in this study. The zeta potential for the colloids was determined directly from measured electrophoretic mobilities, whereas those for the quartz sands were estimated from published literature (Elimelech et al., 2000; Kuznar and Elimelech, 2006). The zeta potential for the colloids and quartz decreased with increasing IS, but were still highly negatively charged for the selected solution chemistries. Table 2 also provides calculated values of the repulsive energy barrier height (Φ_{max}) and the depth of the secondary minima ($\Phi_{2min} = \Phi_{2min}^*/k_bT_k$; where k_b is the Boltzmann constant and T_k is the temperature in degrees Kelvin) for the same experimental conditions. For the 1.1 µm colloid, as the IS of the solution was increased the height of the repulsive energy barrier decreased from 5700 to 50 k_bT_k and attachment in the primary minima is therefore not expected for these conditions. The value of Φ_{2min} also decreased with increasing IS from -0.2 to -7.2 k_bT_k, this indicates that the 1.1 µm colloids are only weakly associated with the quartz surface via the secondary energy minima, even in the highest IS solution examined (106 mM).

Based upon the predictive calculations shown in Table 2, colloid diffusion and hydrodynamic drag forces are likely sufficient to overcome the weak association of colloids in the secondary minimum (e.g., Redman et al., 2004; Walker et al., 2004; Brow et al., 2005). Calculated applied and resisting torques for colloid detachment provide further support for this hypothesis.   Table 2 gives values of T_{res} for the various solution chemistry and colloids considered herein, whereas Table 3 shows values of T_{app} for 1.1 and 3 µm colloids in several different sized capillary tubes (ranging in radius from 100 to 2.5 µm) at the minimum ($\Delta P/L_{ct}$ =15696 N m^{-3} for the 360 sand when q=0.1 cm min^{-1}) and maximum ($\Delta P/L_{ct}$ = 961478 N m^{-3} for 150 sand when q=0.45 cm min^{-1}) value of the pressure gradient that was achieved in our column experiments.

Table 2. Total interaction energy parameters (energy barrier,Φ_{max}; and secondary minima, Φ_{2min}) obtained from DLVO calculations for planar quartz surfaces and latex microspheres for

experimental solution chemistries (see Material and Methods section for details of the calculations). The zeta potential for colloids (ζ_c) and grains (ζ_g) were measured or estimated from the literature (Elimelech et al., 2000; Redman et al., 2004). Also included is the calculated resisting moment (M_{res}) according to Eq. (1).

d_c (μm)	IS (mM)	ζ_c (mV)	ζ_g (mV)	Φ_{max} (k_bT_k)	Φ_{2min} (k_bT_k)	M_{res} (Nm)
1.1	6	-104	-80	8722	-0.2	2.1E-24
1.1	31	-104	-54	2895	-1.2	2.3E-23
1.1	56	-104	-53	2695	-2.2	5.2E-23
1.1	81	-78	-52	2218	-3.4	9.2E-23
1.1	106	-64	-52	1823	-4.6	1.4E-22
3.0	6	-76	-80	11833	-0.6	1.3E-23

The value of T_{app} decreased as the radius of the capillary decreased and the size of the colloid decreased, and increased with increasing velocity (pressure gradient). Comparison of values for T_{res} (Table 2) and T_{app} (Table 3) indicate that T_{res} is always less than T_{app} (by several orders of magnitude). Colloid detachment will occur via rolling when $T_{app}>T_{res}$, hence, these values predict that colloid detachment will always occur for our experimental conditions. The above analysis, however, does not consider the potential influence of pore and colloid size limitations on colloid retention. Colloids that interact with the solid phase can still be retained, if they roll along the surface of the solid and come to a region of the pore space where $T_{app}<T_{res}$ and/or there are physical limitations that are imposed on colloid transport by the size of the colloid and the pore space; i.e, a straining location adjacent to grain-grain contact points.

Table 3. The applied moment (M_{app}) for 1.1 and 3 μm colloids in several different sized capillary tubes (ranging in radius from 100 to 2.5 μm) at the minimum $\Delta p /L_{ct} = 15696$ N m^{-3} for the 360

sand when q=0.1 cm min^{-1}) and maximum $\Delta p /L_{ct}$ = 961478 N m^{-3} for 150 sand when q=0.45 cm min^{-1}) value of the pressure gradient that was achieved in our column experiments according to Eqs. (3) and (4).

	$\Delta p /L_{ct}$ - Minimum		$\Delta p /L_{ct}$ - Maximum	
	1.1 (:m)	3.0 (:m)	1.1 (:m)	3.0 (:m)
r_c (:m)	M_{app} (Nm)	M_{app} (Nm)	M_{app} (Nm)	M_{app} (Nm)
2.5	7.8E-20	7.9E-19	4.9E-18	4.9E-17
5.0	1.8E-19	2.9E-18	1.1E-17	1.8E-16
10.0	3.9E-19	7.2E-18	2.4E-17	4.4E-16
50.0	2.1E-18	4.2E-17	1.3E-16	2.6E-15
100.0	4.3E-18	8.6E-17	2.6E-16	5.2E-15

Figure 1 presents breakthrough curves (Fig. 1a) and deposition profiles (Fig. 1b) when the IS was 6 mM, the pH was 10, and the ratio of the colloid diameter (d_c) to the median grain size (d_{50}) was varied from 0.007 to 0.02. Breakthrough curves are plotted herein with relative concentrations (C/C_i) on the y-axis and pore volume on the x-axis. Deposition profiles are plotted herein with the relative number (N_c/N_{tc}; where N_c is the number of retained colloids and N_{tc} is the total number of colloids injected into the porous medium) per gram of dry sand on the x-axis and dimensionless distance from the column inlet (distance from inlet divided by the column length) on the y-axis.   As noted previously, DLVO calculations presented in Table 2 indicate that deposition in the primary or secondary minima was not expected for these colloids and porous media under these experimental conditions. As d_c/d_{50} increased, however, more deposition was observed, especially in the sand adjacent to the column inlet. These results are consistent with previous studies which observed enhanced colloid straining with increasing values of d_c/d_{50} (e.g.,

Bradford et al., 2003). Micromodel photos presented by Bradford et al. (2005) provide visual confirmation that similarly sized colloids were retained by straining in these Ottawa sands.

Figure 2 presents effluent concentration curves for 1.1 μm modified carboxyl latex microspheres in 360 (Fig. 2a; d_c/d_{50} =0.003), 240 (Fig. 2b; d_c/d_{50} =0.005), and 150 (Fig. 2c; d_c/d_{50} =0.007) μm Ottawa sand for a range of IS (6 mM to 106 mM) and a Darcy velocity of approximately 0.1 cm min^{-1}. Figure 3 presents the corresponding deposition profiles for these systems. A systematic decrease in the peak effluent concentration and an increase in the colloid deposition is observed with increasing IS in Figs. 2 and 3. Many other researchers have reported a similar dependence of colloid transport on IS under unfavorable attachment conditions (e.g., Li et al., 2004; Tufenkji and Elimelech, 2004 and 2005a). This has commonly been attributed to changes in the DLVO total interaction energy between colloids and collector grains. Specifically, at higher ionic strengths the energy barrier to deposition in the primary minima decreases and the depth of the secondary minima increases (see Table 2). Enhanced attachment with increasing IS has therefore been attributed to surface charge variability of the grain surfaces and colloids, and interactions associated with the secondary minima (e.g., Tufenkji and Elimelech, 2004 and 2005a).

Inspection of Fig. 3 reveals that most of the enhanced deposition with increasing IS occurs at the inlet of the column. This trend is similar to that seen in Fig. 1b for increasing d_c/d_{50}. Comparison of Figs. 3a, 3b, and 3c reveal that the shape of the deposition profile is also highly dependent on the grain size of the sand. For a given IS, the deposition profiles tend to exhibit a more gradual change in retained concentration with depth for the coarser textured sand. Conversely, as the sand size is decreased the profiles tend to become more hyper-exponential for a given IS. Comparison with Fig. 2, as well as effluent mass balance information presented in Table 1, further indicates that the magnitude of colloid deposition depends on both the sand size and the IS. When the IS was 6 or 31 mM the amount of deposition was relatively insensitive to the grain size. Conversely, when the IS was 56 or 81 mM the role of grain size on deposition is much more pronounced; i.e, increasing with decreasing sand size. When the IS was 106 mM the role of grain size is only apparent by distinct differences in the shape of the deposition profiles (Fig. 3), because most of the colloids are retained in the sands. The above information provides

evidence that the physical and chemical phenomena controlling deposition are inextricably related.

Additional experiments were conducted to better understand the relative roles of grain size and solution composition on colloid deposition. In these experiments the column was flushed with an additional 2.1 to 3.2 pore volumes of 6 mM solution before excavation of the sand and determination of the deposition profiles. Figure 4 presents the measured effluent concentration curves (Fig. 4a) and deposition profiles (Fig. 4b) for 1.1 μm colloid transport experiments conducted in 150, 240, and 360 μm Ottawa sand when the IS was initially 56 mM and then switched to 6 mM (referred to as 56/6 mM). Also included in this figure for reference is an 1.1 μm colloid transport experiment conducted in 150 μm sand when the IS was maintained at 6 mM. In all cases, the Darcy water velocity was approximately 0.2 cm min^{-1}. Figure 5 presents similar information as in Fig. 4, however the experiments reported in Fig. 5 involved an initial IS of 106 mM before switching to 6 mM solution (referred to as 106/6 mM). Table 1 provides additional information about specific experimental conditions.

It is observed in Figs. 4a and 5a that a second peak in the effluent concentration curve occurred when the solution IS was changed from the higher value (56 or 106 mM) to 6 mM as a result of colloid release. This behavior has typically been ascribed to release of colloids associated with the solid surface via the secondary minima (Franchi and O'Melia, 2003; Hahn and O'Melia, 2004; Hahn et al., 2004). Secondary minima association alone cannot explain the observed behavior.

The first piece of evidence is that the corresponding deposition profile (Figs. 4b and 5b) are not exponential, even after a flushing step with an additional 2.1 to 3.2 pore volumes of 6 mM solution. Second, mass balance calculations indicate that the total amount of colloids recovered in the effluent only accounts for a small percentage of the injected colloid mass. For the 56/6 mM systems shown in Fig. 4a only 46, 32, and 25% of the injected colloids were recovered in the effluent for the 360, 240, and 150 μm sand, respectively. Similarly, for the 106/6 mM systems
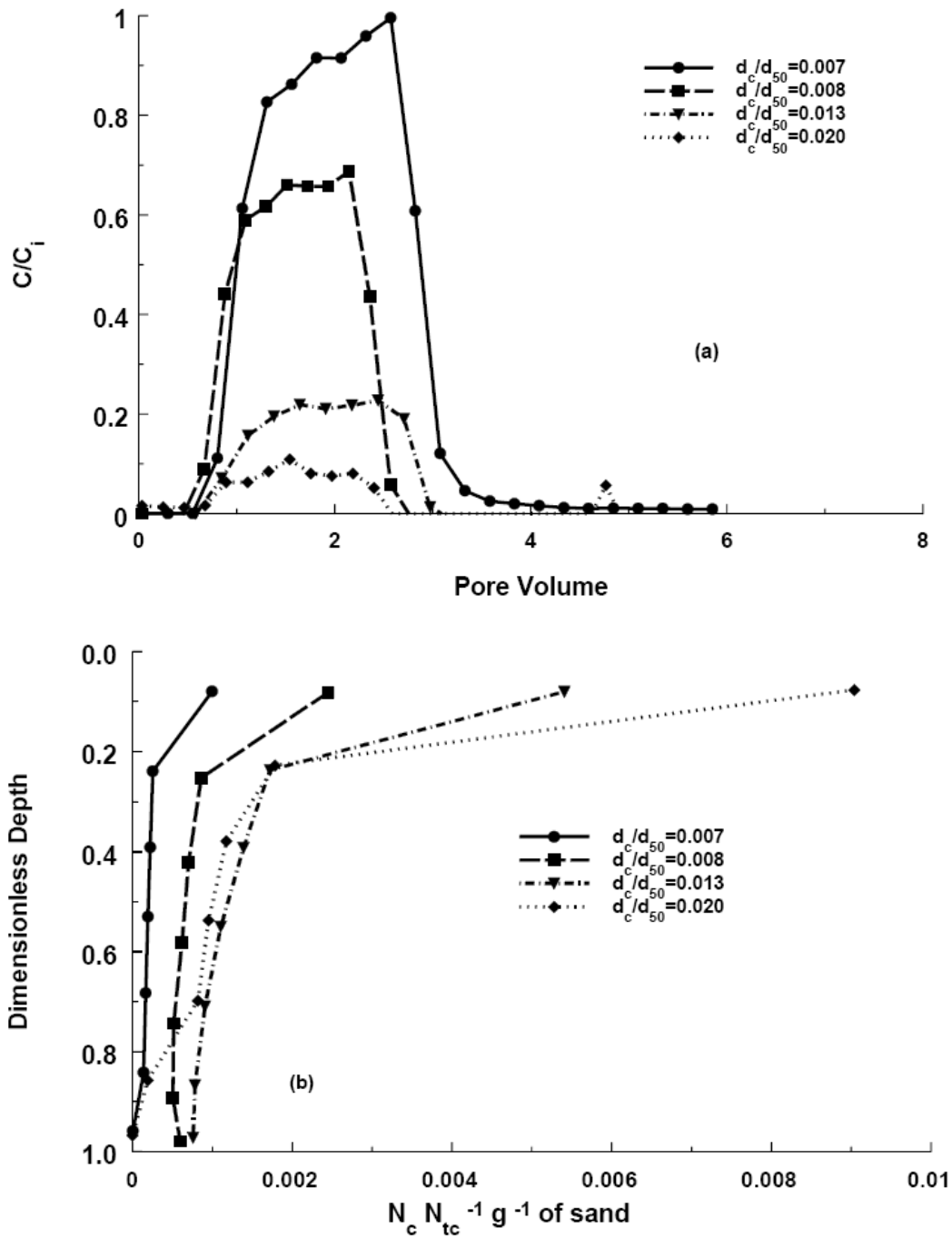
Figure 1. Breakthrough curves (Fig. 1a) and deposition profiles (Fig. 1b) when the IS was 6 mM, the pH was 10, the ratio of the colloid diameter (d_c=1.1 or 3 µm) to the median grain size (d_{50}=360, 240, or 150 µm) was varied from 0.007 to 0.02, and the Darcy velocity was approximately 0.1 cm min^{-1}.

(a)

(b)
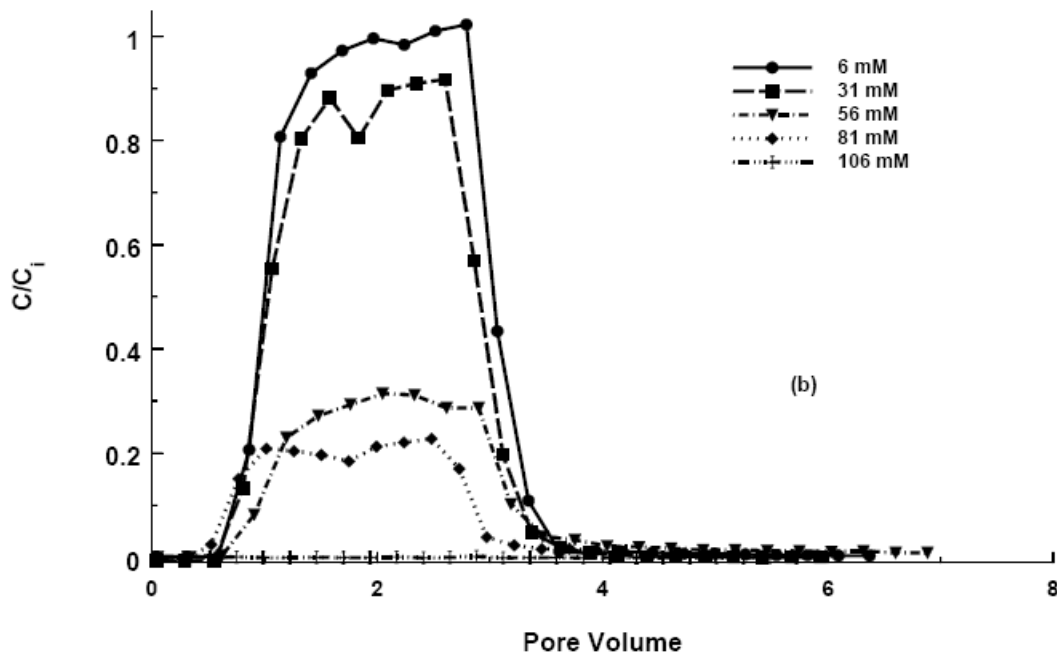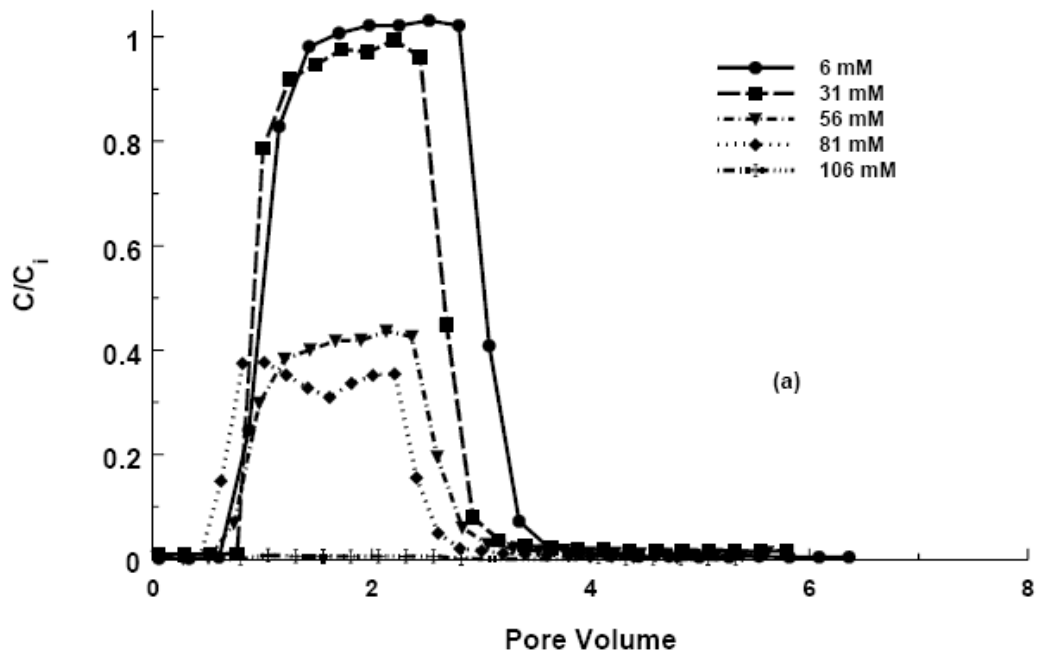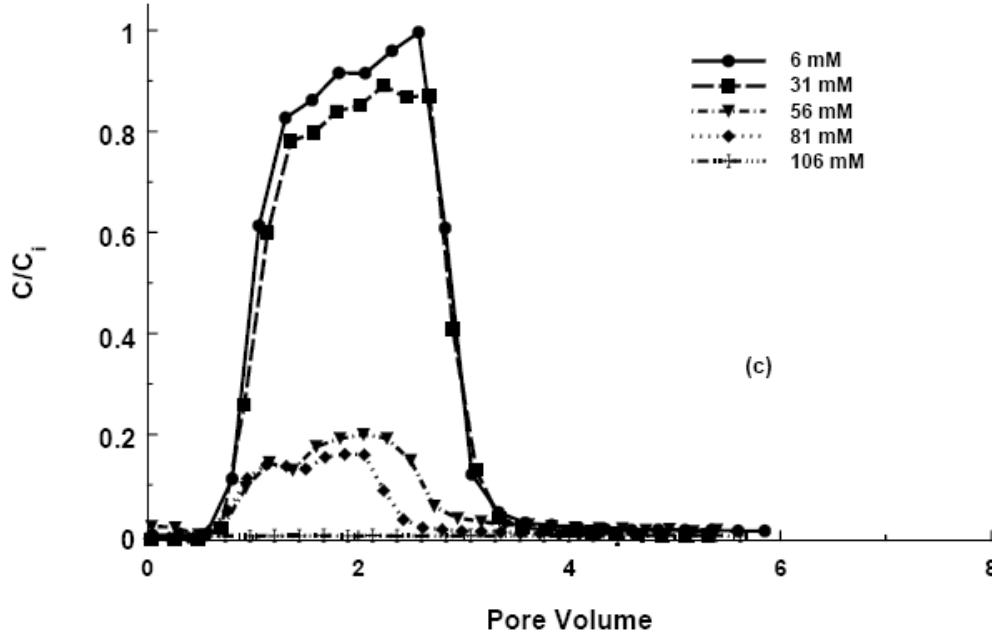
Figure 2. Breakthrough curves for 1.1 μm modified carboxyl latex microspheres in 360 (Fig. 2a; d_c/d_{50}=0.003), 240 (Fig. 2b; d_c/d_{50}=0.005), and 150 (Fig. 2c; d_c/d_{50}=0.007) μm Ottawa sand when the IS ranged from 6 to 106 mM and the Darcy velocity was approximately 0.1 cm min^{-1}.

shown in Fig. 5a only 39, 12, and 11% of the injected colloids were recovered in the effluent for the 360, 240, and 150 μm sand, respectively. In contrast, effluent recovery for transport experiment conducted using only 6 mM solution and 150 μm sand was greater than 83% of the injected colloids (Table 1). Hence, adjustments in solution IS were observed to significantly increase the total deposition in these sands, with enhanced deposition occurring in finer textured sand and for higher initial IS conditions.

Mass balance information further indicates that the amount of colloids recovered in the second "release" peak (PV>8) shown in Figs. 4a and 5a accounted for only a small percentage of the injected colloids. For the 56/6 mM conditions shown in Fig. 4a only 5, 6, and 7% of the injected colloid mass was released in the second peak for the 360, 240, and 150 μm sands, respectively. For the 106/6 mM experiments shown in Fig. 5a only 19, 11, and 10% of the injected colloid mass was released in the second peak for the 360, 240, and 150 μm sands,

respectively.

All of the above observations strongly indicate that the solution chemistry played an important role in colloid deposition and that this process was interrelated with pore structure. We postulate that straining and solution chemistry are coupled in the following ways. First, we believe that colloids may collide with grain surfaces via sedimentation, interception, and diffusion as assumed in traditional filtration theory. In the presence of an energy barrier to deposition in the primary minima, colloids that are weakly associated with the grain surface via the secondary minima can be translated along grain surfaces by hydrodynamic shear to regions of the pore space that are more favorable for deposition such as small pore spaces that are formed adjacent to grain-to-grain contacts. Deposition of colloids in these straining locations is expected to be greater than on other regions of the solid-water surface due to chemical and physical considerations.

DLVO forces holding colloids in the smallest region of the pore space are greater than on a single solid-water interface due to the presence of multiple solid-water interfaces (Hoek and Agarwal, 2006). The fluid drag force is also decreased in the smallest region of the pore space because of lower fluid velocities (see Table 3). Finally, physical limitations that are imposed by the size of the colloid and pore, and/or by changes in pore surface topology are also expected to play a role in colloid retention.

Increasing the IS results in a greater depth of the secondary minima (Table 2). Therefore, under unfavorable attachment conditions, increasing the solution IS may lead to greater numbers of colloids that are directed to small pore spaces where straining occurs. Once colloids are retained in the smallest region of the pore space, reduction of DLVO forces does not necessarily release these colloids because of physical limitations (size of colloid and pore) and reduced fluid drag in these locations.

(a)

(b)
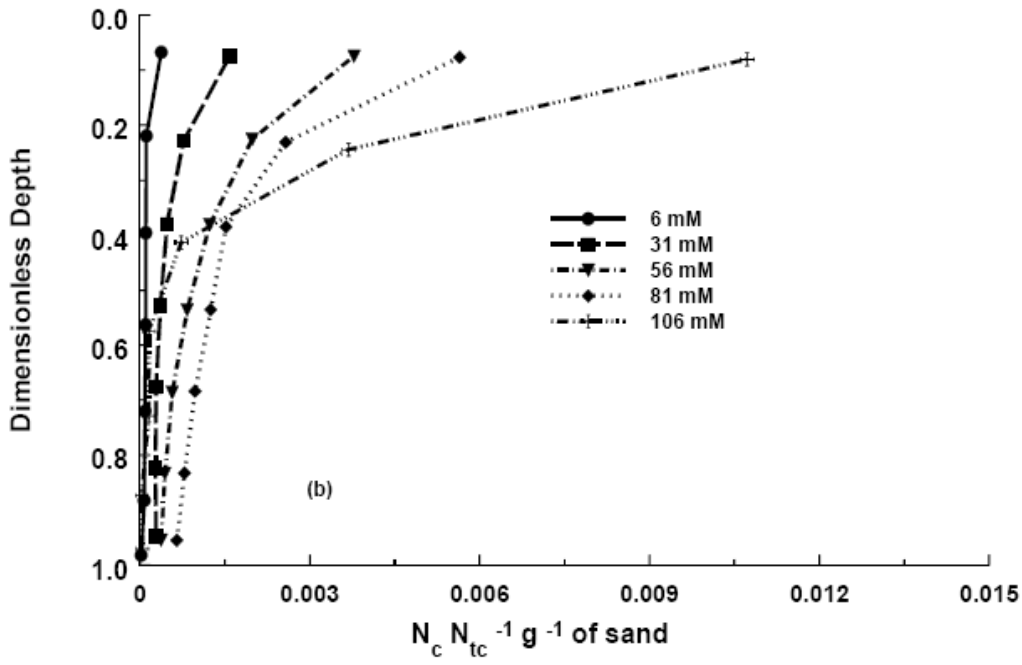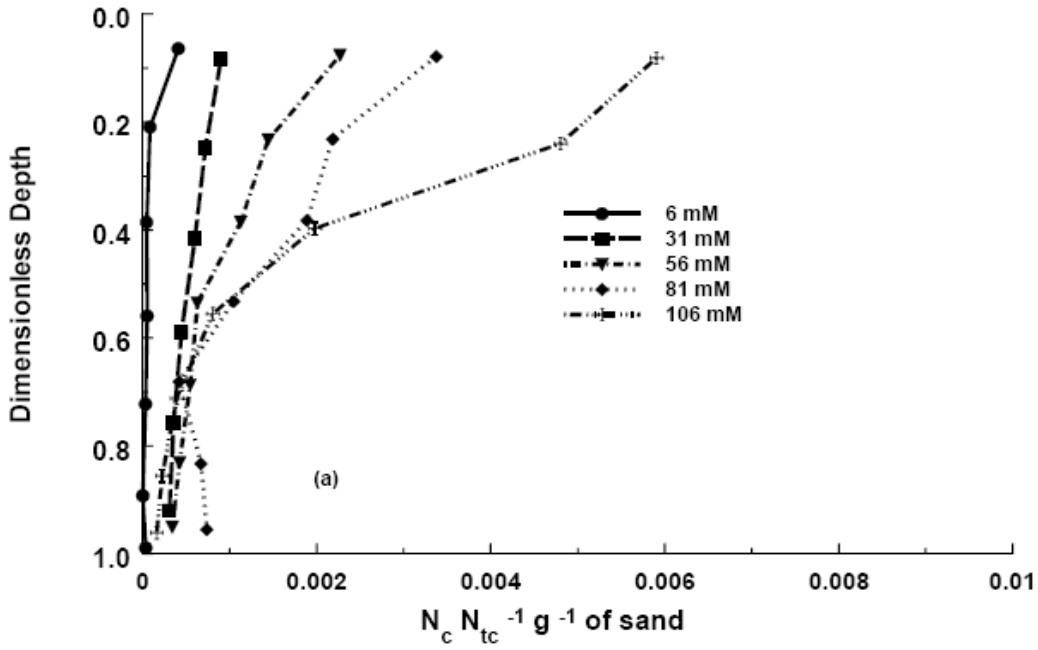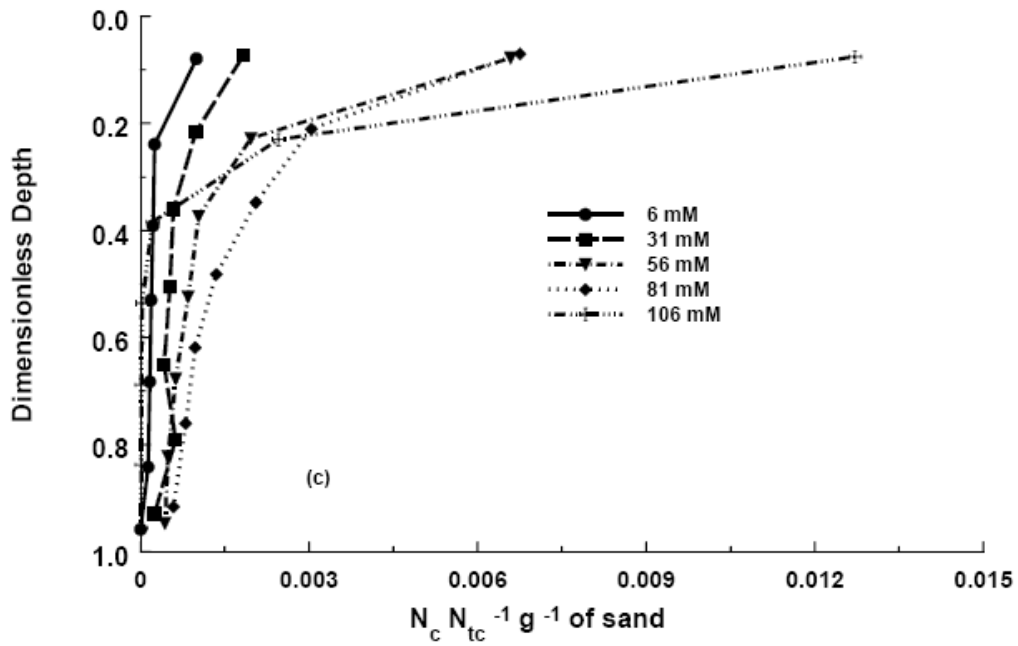
Figure 3. Deposition profiles for 1.1 μm modified carboxyl latex microspheres in 360 (Fig. 3a; d_c/d_{50}=0.003), 240 (Fig. 3b; d_c/d_{50}=0.005), and 150 (Fig. 3c; d_c/d_{50}=0.007) μm Ottawa sand when the IS ranged from 6 to 106 mM and the Darcy water velocity was approximately 0.1 cm min^{-1}.
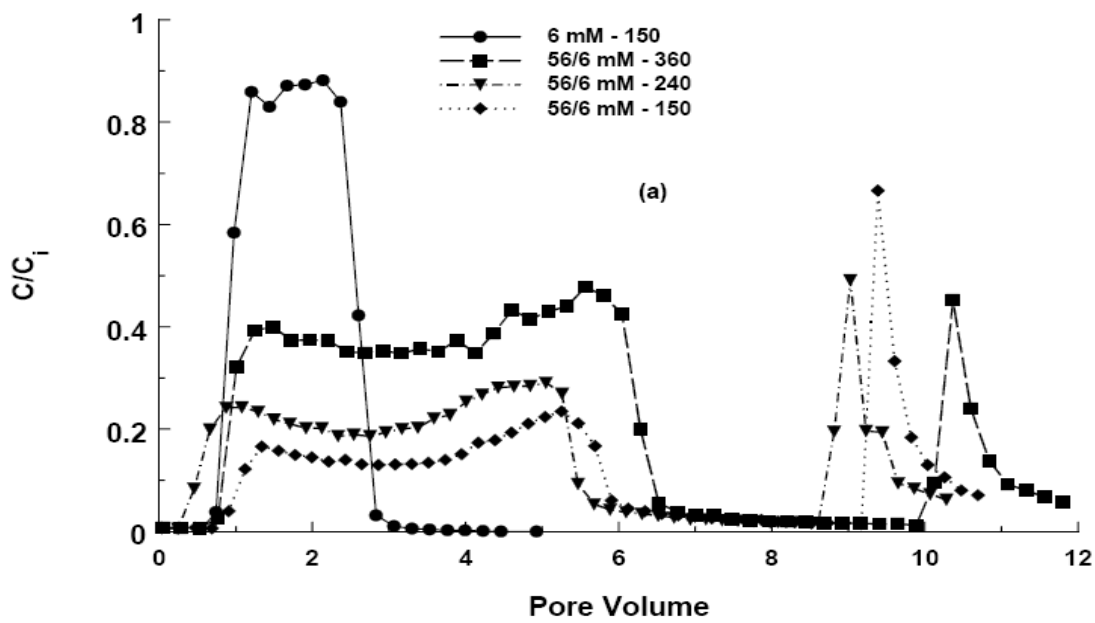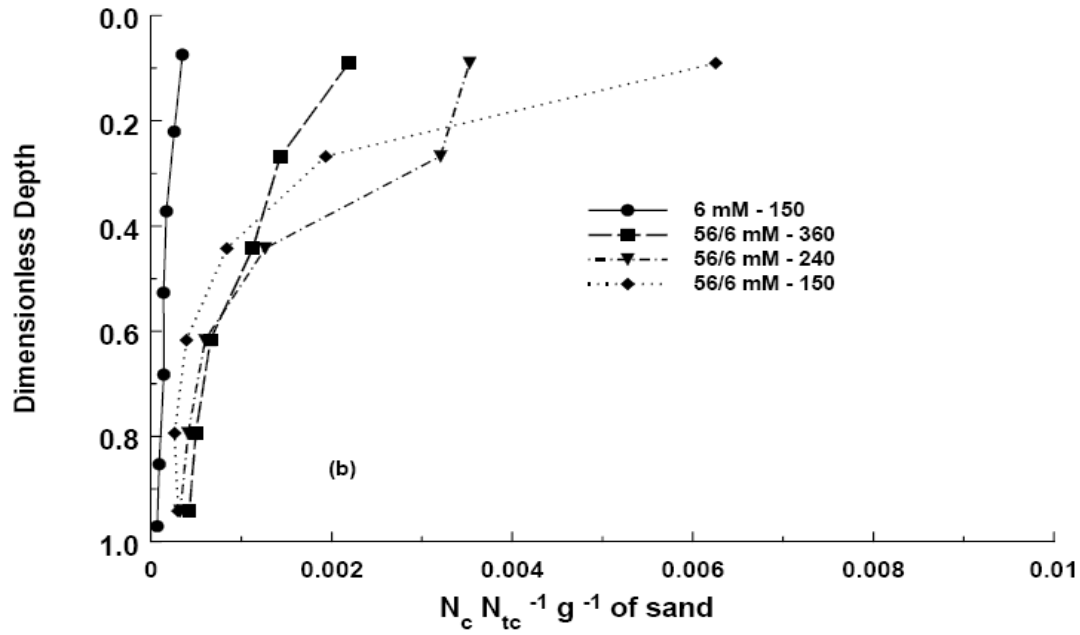
Figure 4. Breakthrough curves (Fig. 4a) and deposition profiles (Fig. 4b) for 1.1 μm modified carboxyl latex microspheres in 150, 240, and 360 μm Ottawa sand when the Darcy water velocity was approximately 0.2 cm min^{-1}. In these experiments the column was flushed with colloid suspension and eluant at an IS of 56 mM for around the first 8-10 pore volumes and then switched to low IS solution of 6 mM for the final 2-3 pore volumes.
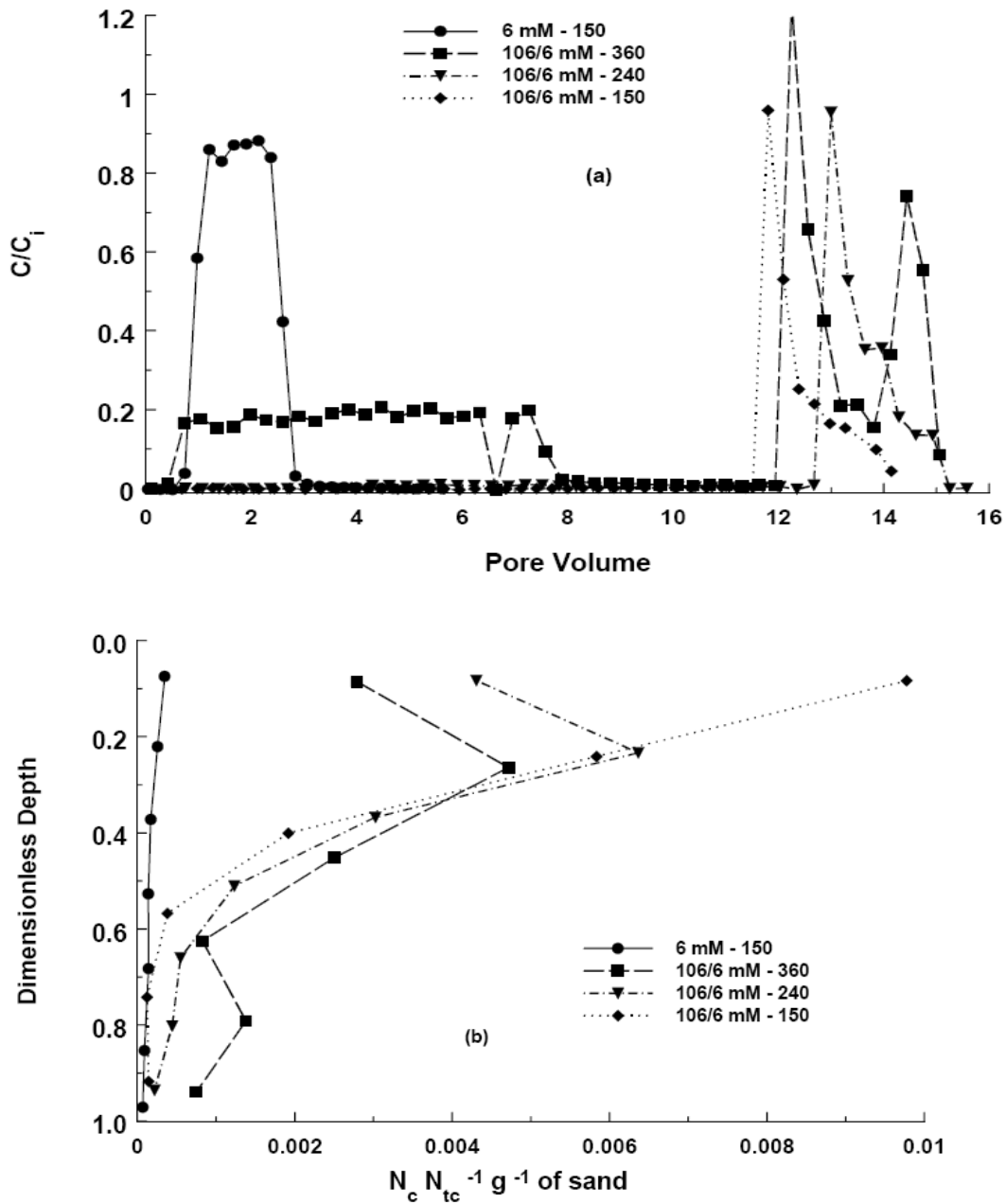
Figure 5. Breakthrough curves (Fig. 5a) and deposition profiles (Fig. 5b) for 1.1 μm modified carboxyl latex microspheres in 150, 240, and 360 μm Ottawa sand when the Darcy water velocity was approximately 0.2 cm min⁻¹. In these experiments the column was flushed with colloid suspension and eluant at an IS of 106 mM for around the first 8-10 pore volumes and then switched to low IS solution of 6 mM for the final 2-3 pore volumes.

(a)

(b)

111
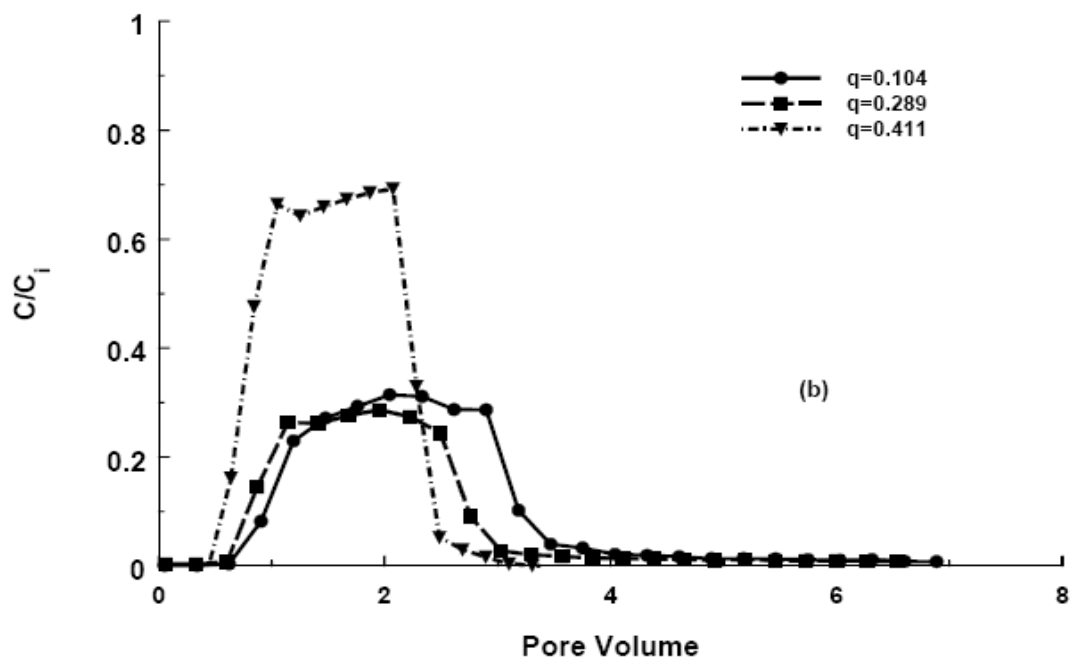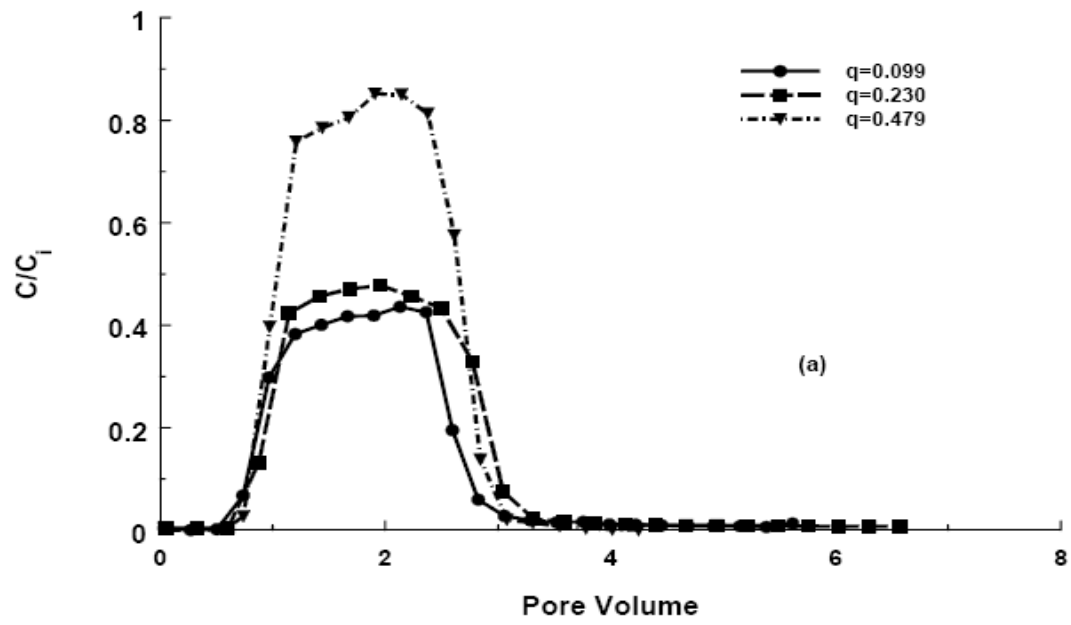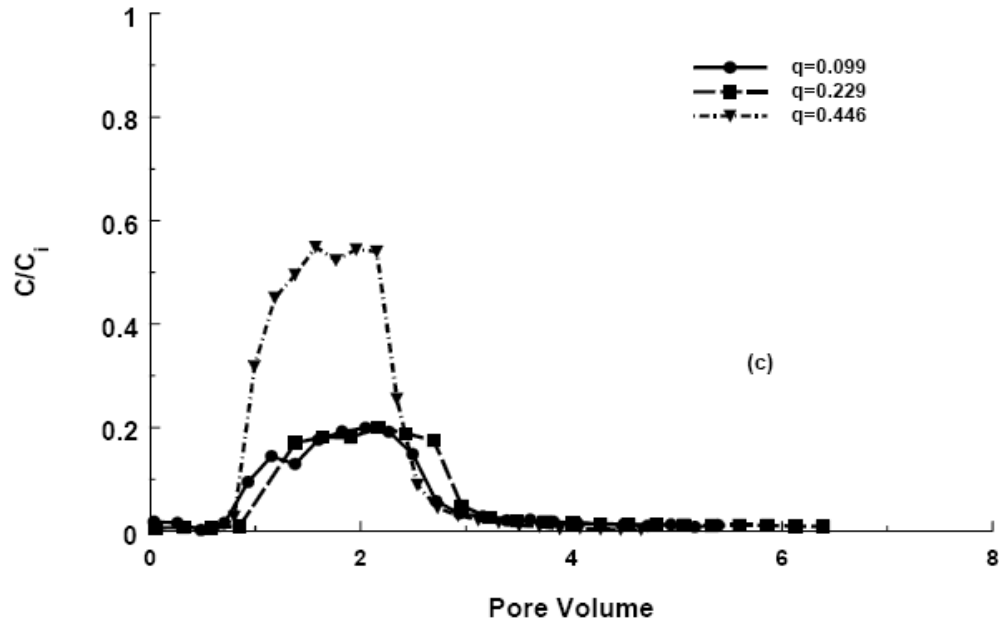
Figure 6. Breakthrough curves for 1.1 μm colloids in 360 (Fig. 6a), 240 (Fig. 6b), and 150 (Fig. 6c) μm sand when the IS was 56 mM and the Darcy velocity was approximately 0.1, 0.2, and 0.45 cm min^{-1}.
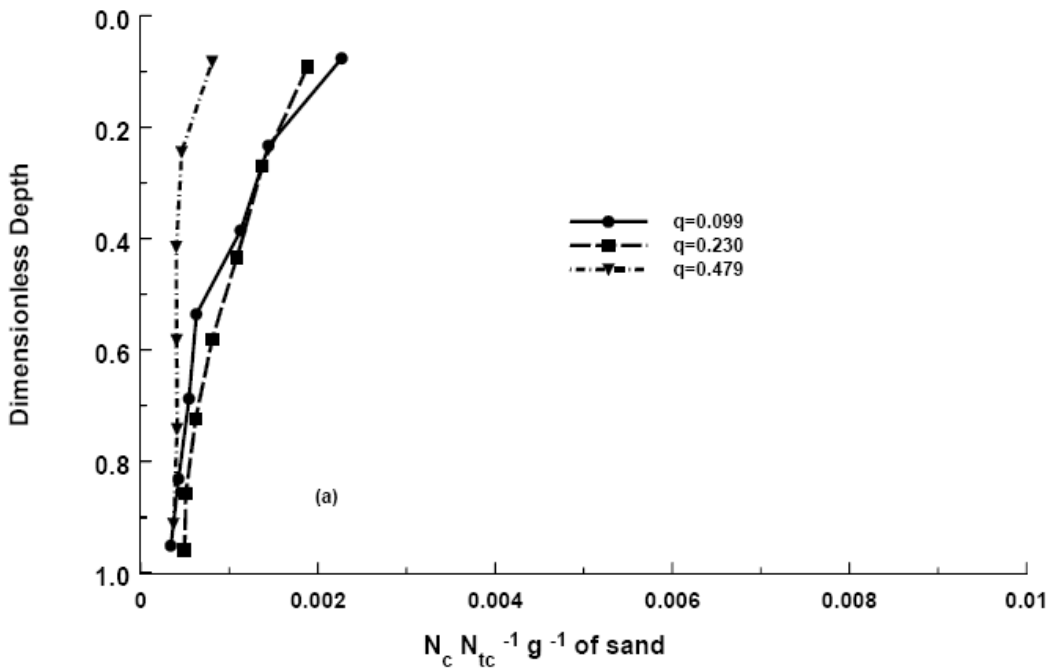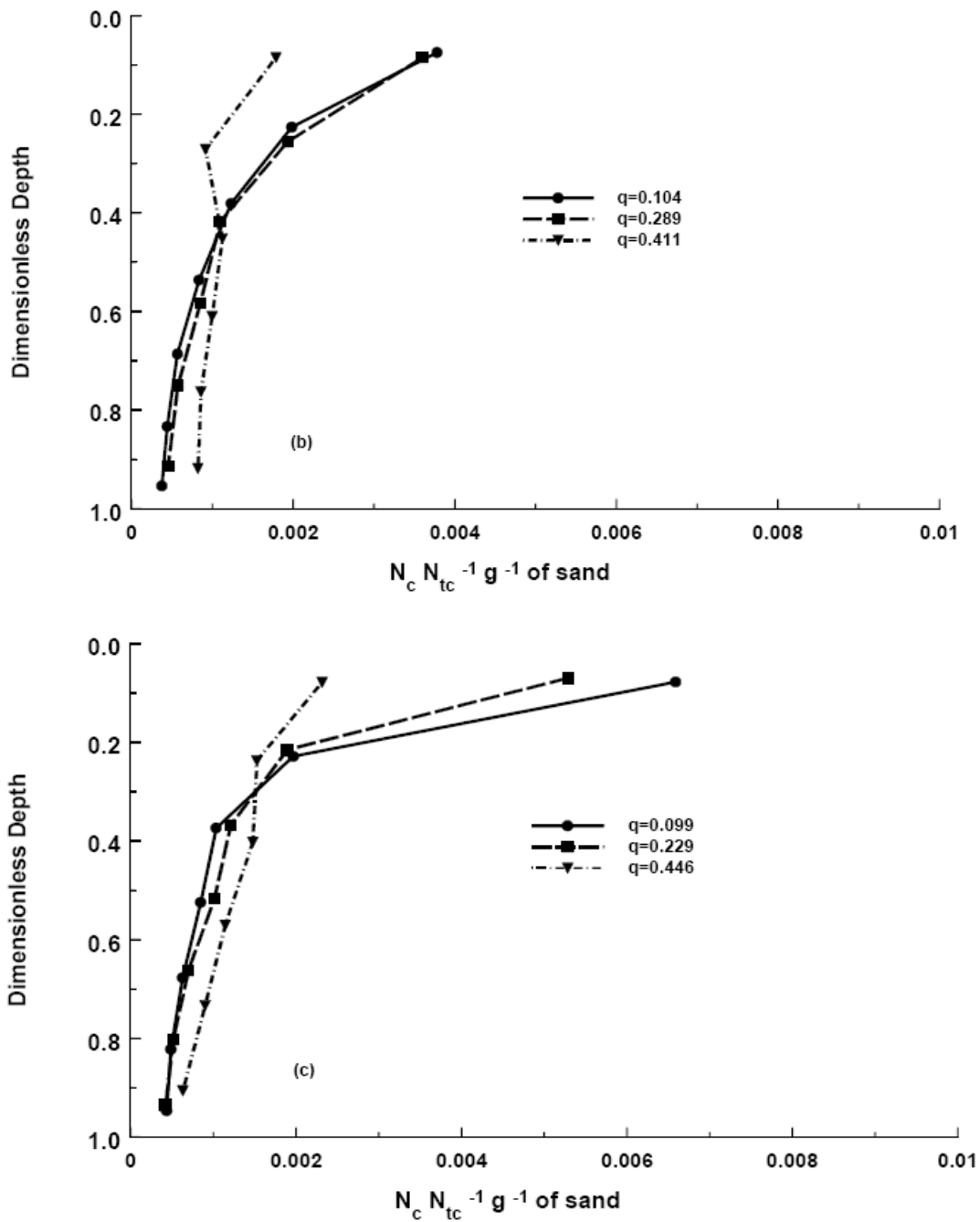
Figure 7. Deposition profiles for 1.1 μm colloids in 360 (Fig. 7a), 240 (Fig. 7b), and 150 (Fig. 7c) μm sand when the IS was 56 mM and the Darcy velocity was approximately 0.1, 0.2, and 0.45 cm min^{-1}.
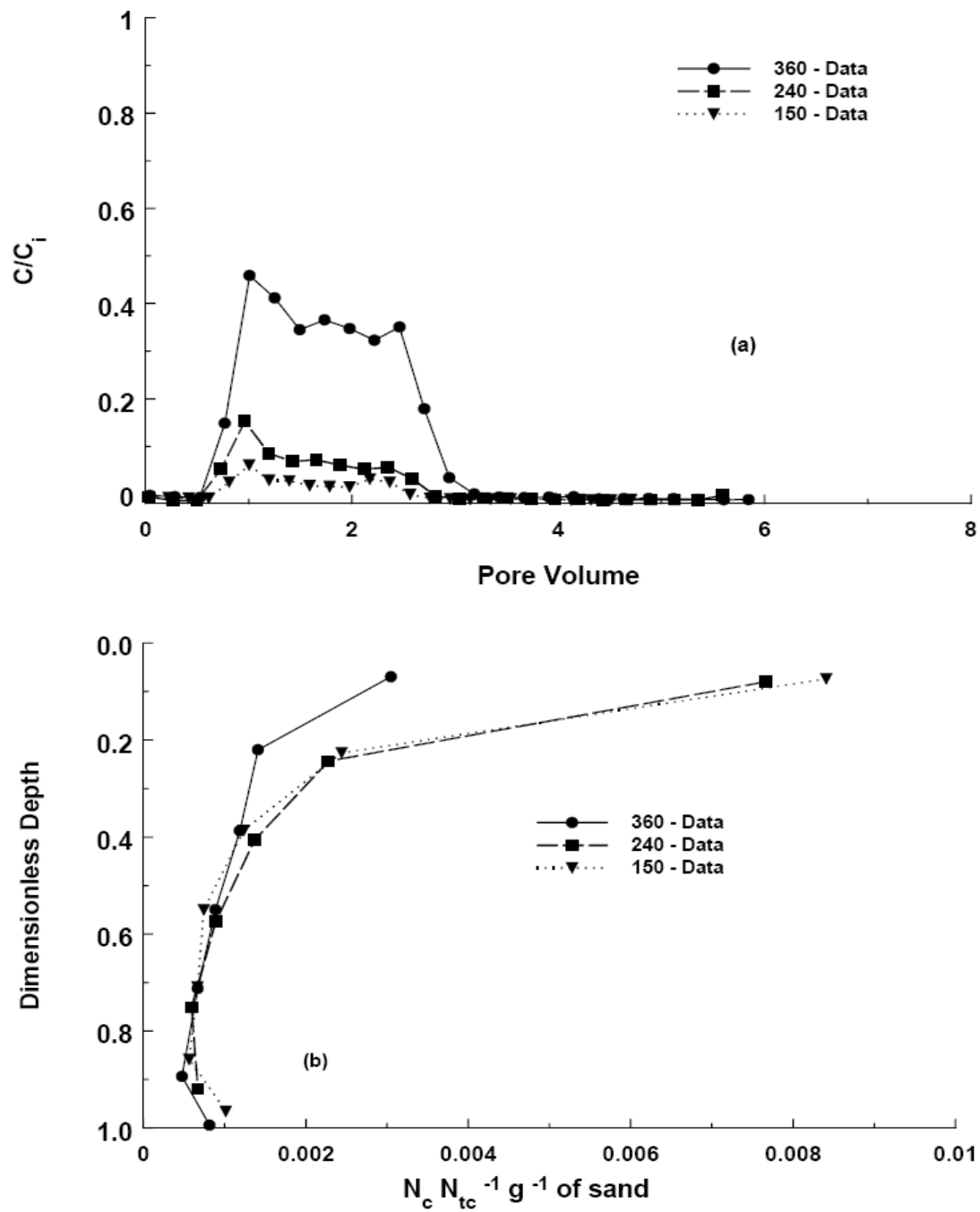
Figure 8. Breakthrough curves (Fig. 8a) and deposition profiles (Fig. 8b) for 3 μm colloids in 360, 240, and 150 μm sand when the IS was 6 mM and the Darcy velocity was approximately 0.45 cm min^{-1}.

Influence of Hydrodynamics on Colloid Retention

As the water velocity increases the magnitudes of the lift and drag forces that act on colloids near solid surfaces will increase (Cushing and Lawler, 1998; Bergendahl and Grasso, 1998; Li et al., 2005), and the volume of low velocity (stagnant) regions is expected to decrease. All of these factors may inhibit straining of colloids in small pore spaces. It is therefore likely that the shape and magnitude of the deposition profiles for strained colloids will be very sensitive to flow rate. Figure 6 presents effluent concentration curves for 1.1 µm colloids in 360 (Fig. 6a; d_c/d_{50}=0.003), 240 (Fig. 6b; d_c/d_{50}=0.005), and 150 (Fig. 6c; d_c/d_{50}=0.007) µm sand when the IS was 56 mM and the Darcy velocity was approximately 0.1, 0.2, and 0.45 cm min^{-1}. Corresponding deposition profiles for these same systems are presented in Figs. 7a, 7b, and 7c. For a given sand and IS=56 mM the effluent concentration curves and deposition profiles were very similar when the velocity was 0.1 and 0.2 cm min^{-1}. The influence of water velocity on the effluent concentration curves and deposition profiles was much more pronounced when the velocity was more than doubled to a value approaching 0.45 cm min^{-1}. In this case, the higher Darcy velocity produced an increase in the effluent concentration that was approximately 35% regardless of sand size. The highest Darcy velocity (q=0.45 cm min^{-1}) also produced a much more gradual change in the deposition profiles with depth; i.e, the profiles were less hyper-exponential. In this case, we hypothesize that the fluid drag forces were sufficient to inhibit colloid retention in regions of the pore space that would otherwise retained colloids at the lower Darcy velocities (0.1 and 0.2 cm min^{-1}).

In order to further compare the role of hydrodynamics on colloid straining, additional transport experiments were conducted with 3 µm colloids in 360 (d_c/d_{50}=0.008), 240 (d_c/d_{50}=0.013), and 150 (d_c/d_{50}=0.02) µm sand when the IS was 6 mM and the Darcy velocity was about 0.1 (Fig. 1) and 0.45 (Fig. 8) cm min^{-1}. Comparison of Figures 1 (0.1 cm min^{-1}) and 8 (0.45 cm min^{-1}) indicate that increasing the flow rate produced greater deposition, especially for the coarser textured 360 µm sand. The effluent concentration after around one pore volume at the higher flow rate (0.45 cm min^{-1}) also tended to decrease as injection of colloids continued. This time-dependent deposition behavior has typically been ascribed to ripening; i.e, favorable colloid-colloid interactions during attachment. Recall that the experimental conditions were designed to

minimize colloid attachment in this instance, so as to better deduce mechanisms of colloid straining. Hence, the data in Fig. 8 suggests that increasing the flow rate may lead not only to colloid retention in pores and at grain-grain junctions, but that the deposition morphology may also influence subsequent retention in these locations. One potential explanation is that retained colloids in a pore constriction reduce the effective size of the pore and therefore increase subsequent straining at this location. A second hypothesis is that colloid-colloid interactions are enhanced in pores because the number of collisions in small pores has the potential to drastically increase relative to that in bulk solution. Additional research is needed to further test these hypotheses, but is beyond the scope of this work.

Comparison of Figs. 1, 6, 7, and 8 indicates that increasing the Darcy velocity from 0.1 to 0.45 cm min^{-1} had an opposite effect on colloid deposition for the 3 μm colloids in 6 mM solution (increasing extent of deposition) than the 1.1 μm colloids in 56 mM solution (decreasing deposition). Differences in the influence of velocity on the deposition behavior for these two colloids are likely a result of the deposition morphology in the small pore spaces and the fluid drag forces. Size limitations in small pores are also expected to more pronounced for the 3 than 1.1 μm colloids, and release of these colloids by fluid drag forces is therefore believed to be more difficult. Conversely, for the 1.1 μm colloids in 56 mM solution we hypothesized that increasing the water velocity and associated fluid drag were sufficient to inhibit colloid retention in small pores.

Conclusions

Experimental and theoretical studies were undertaken to determine the role of solution chemistry and hydrodynamics on straining under unfavorable attachment conditions. To better isolate the effects of straining on colloid retention, the experimental conditions were selected to minimize the potential for colloid attachment (solution pH of 10, simple aqueous chemistries, quartz sands, and highly negatively charged colloids that were hydrophilic). DLVO calculations, analysis of torques, and mass balance information confirm our assumption that attachment did not play a dominant role in colloid deposition. Experimental data and analysis of torques indicate a

116

complex interaction of hydrodynamics, solution chemistry, colloid size, and pore structure (grain size) on colloid transport and straining. Specific findings are highlighted below.

- Straining increases in magnitude with increasing IS due to an increased force and number of colloids that are funneled to and retained in small pores formed adjacent to grain-grain junctions.

- Straining can play a very significant role in colloid deposition when d_c/d_{50} is as low as 0.003.

- Reduction in solution IS will not release colloids that are retained in straining locations.

- The shape of the colloid deposition profile is highly sensitive to the physical (colloid and grain size, and system hydrodynamics) and chemical (solution IS and pH) properties of a system due to the interrelation of these parameters on straining.

- Increasing the flow rate of a system tends to decrease the amount of straining as a result of the increased fluid drag force that acts on colloids in pores, but the magnitude of this effect is expected to be highly dependent on the solution chemistry and the size of the colloid and sand.

This information is believed to be essential for predicting colloid transport and fate in many natural environments.

Chapter 6

Summary, Conclusions and Recommendations

Scope and Objectives

Groundwater can be protected against contamination with pathogenic microorganisms by applying adequate setback distances between sources of contamination and production wells using the soil as a barrier. Generally, the pathogenic contaminations reach the groundwater by passing through the unsaturated zone (vadose zone). The unsaturated zone, therefore, plays an important role in protecting drinking water supplies from pathogen contamination. Viruses, and more recently, protozoa have been recognized as pathogens of major health concern. Due to their persistence in the environment and their infectivity, they may be considered as the most critical water borne pathogens for drinking water production. Because of their environmental persistence, their retention in the soil is vital during soil passage so that their removal can occur by the natural inactivation. Therefore, an accurate understanding of the processes that control the fate and transport of pathogenic microorganisms in saturated and unsaturated porous media is needed to estimate the adequate setback distances.

The research presented in this thesis was mainly aimed to explore the fundamental mechanisms involved in the transport and fate of viruses and colloids in saturated and unsaturated porous media. The overall objectives were as follows:

1- To examine the effect of water content on the fate and transport of bacteriophages in porous media, in particular the effect of water content on virus attachment onto the solid-water interface (SWI).   .

2- To investigate the extent of attachment of bactriophages to the AWI and the factors controlling it.

3- To explore the effects of water content and solution ionic strength on colloid transport and deposition under various saturation levels.

4- To investigate the role of solution chemistry and hydrodynamics on colloid attachment and removal by straining.

This research comprised extensive laboratory experiments and modeling. Bacteriophages were used as surrogates for pathogenic viruses and latex microsphere particles as representatives of fecal bacteria.

Summary and Conclusions

As discussed in chapter 2, the transport of bacteriophages MS2 and ϕX174 were studied at various water contents and solution chemistries in terms of pH and ionic strength (IS). The objective was to explore the effect of water content on the SWI attachment. Our results showed that the retention of viruses in the soil column increased as water saturation decreased only when the chemical conditions were favorable for attachment to the SWI (pH 7 and higher IS). Our analysis of results indicated that the enhanced retention of ϕX174 viruses at lower water content was caused by increased attachment to the SWI and that retention by the AWI was not significant. The trend of breakthrough data of MS2, however, was less straight forward for being able to separate out the role of the AWI. Although attachment of MS2 viruses to the AWI could not be ruled out in our experiments, we suspected that the increased retention of this phage under unsaturated condition was also due to enhanced attachment to the SWI.

Increased attachment to the SWI under unsaturated conditions was attributed to increased mass transfer of viruses to the SWI due to a reduced diffusion length at lower water content. Our results clearly demonstrated that if there is any attachment to the AWI, it is reversible. When unfavorable conditions occur for attachment to the SWI, the attached viruses may be detached by moving solid-water-air contact lines.

In chapter 3, the importance of virus attachment to the AWI and the factors controlling it was investigated. The water saturation ranged from 1 to 0.5. Bacteriophages MS2 and ϕX174 were used as surrogates for pathogenic viruses in this study. Phosphate buffered solutions with different pH values (7.5, 6.2, 5.5, and 5) were utilized. Under saturated conditions, virus retention increased as pH decreased and a one-site kinetic model produced a good fit to the breakthrough curves. Under unsaturated conditions, a two-site kinetic model was needed to fit the breakthrough curves satisfactorily. The second site was attributed to the adsorption of phages to the AWI. According to our results, ϕX174 exhibited a high affinity to the AWI at pH values below 6.6 (the isoelectric point of ϕX174). Although it is believed that MS2 is more hydrophobic than ϕX174, MS2 had a lower affinity to the AWI than (X174, presumably due to the lower isoelectric point of MS2, which is equal to 3.9. Our results suggest that electrostatic forces between viruses and the AWI are the key factors causing virus attachment to the

AWI.

Under unsaturated conditions, viruses captured within the column could be recovered in the column outflow by re-saturating and immediately draining the column. Draining of columns under saturated conditions, however, did not result in any recovery of viruses. Therefore, the recovery could be attributed to the release of viruses adsorbed to the AWI. In contrast with chapter 2 which little virus attachment to the AWI was found, chapter 3 demonstrates a significant virus attachment to the AWI when water pH is below the isoelectric point of the virus.

Chapter 4 describes experiments and mathematical modeling conducted to quantitatively evaluate the role of water saturation, pore-water ionic strength, and grain size on the transport of latex microspheres in porous media. Experiments were carried out under chemically unfavorable conditions for colloid attachment to both solid-water interfaces (SWI) and air-water interfaces (AWI) using negatively charged and hydrophilic colloids and modifying the solution chemistry with a bicarbonate buffer to pH 10. DLVO calculations and complementary batch experiments demonstrated that partitioning of colloids to the SWI and AWI was insignificant across the range of the ionic strengths considered. The breakthrough curve and final deposition profile were measured in each experiment, indicating colloid retention was highly dependent on the suspension ionic strength, water content, and sand grain size. It was observed that colloid retention increased with increasing ionic strength, decreasing water content, and smaller grain size. In contrast to conventional filtration theory, most colloids were found deposited close to the column inlet, and hyper-exponential deposition profiles were observed. A mathematical model, accounting for time and depth dependent straining, produced a reasonably good fit for both the breakthrough curves and final deposition profiles.

As described extensively in this chapter, experimental and modeling results suggest that straining – the retention of colloids in low velocity regions of porous media such as grain junctions – is the primary mechanism of colloid retention under both saturated and unsaturated conditions for the experimental conditions tested. The extent of low- velocity regions of flow within the pore structure is enhanced with decreasing water content, leading to a greater amount of retention. Higher ionic strength also contributes to

straining; due to the fact that the number of colloids being held in secondary energy minimum increases with ionic strength. These weakly associated colloids are prone to translate to low-velocity regions formed at grain-grain junctions and dead-end pores and become trapped.

To compliment the previous work on the effect of straining in colloid retention and demonstrate the role of solution chemistry and system hydrodynamic on colloid straining, experimental and theoretical studies were undertaken as described in chapter 5. Negatively charged latex microspheres (1.1, 6 and 3 μm) and quartz sands (360, 240, and 150 μm) were used in packed column studies that encompassed a range in suspension ionic strengths (6-106 mM) and Darcy water velocities (0.1-8 0.45 cm min-1). DLVO calculations and batch experiments suggested that attachment of colloids to the solid-water interface was not a significant mechanism of deposition for the selected experimental conditions. Breakthrough curves and hyperexponential deposition profiles were strongly dependent on the solution chemistry, the system hydrodynamics, and the colloid and collector grain size, with increasing deposition occurring for increasing ionic strength, lower flow rates, and larger ratios of the colloid to the median grain diameter.

For selected systems, the ionic strength of the effluent solution was decreased to 6 mM following obtaining the complete breakthrough curves. In this case, only a small portion of the deposited colloids was recovered in the effluent and the majority was still retained in the sand. These observations suggest that the extent of colloid removal by straining is strongly coupled to solution chemistry as it was also seen in previous study. Increasing the solution ionic strength is believed to increase the force and number of colloids in the secondary minimum of the DLVO interaction energy distribution. Theoretical calculations implies that weakly associated colloids via secondary energy minimum can be funneled to small pores formed adjacent to grain-grain junctions by hydrodynamic forces. Colloid-colloid interactions may be enhanced by hydrodynamic forces and a higher frequency of colloid-colloid collisions in these locations.

Concluding remarks and Recommendations

Previous studies on unsaturated colloid transport have mainly focused on the determination of the colloid concentration in the effluent. Breakthrough concentrations

are typically simulated by using a variety of parameters to best fit the data that consider SWI and/or AWI adsorption rate coefficients, and/or straining coefficients. Few studies have reported the shape of the colloid deposition profiles for unsaturated conditions. However, our results demonstrate that consideration of both breakthrough curves and deposition profiles in model fitting is vital to gain insight on the controlling deposition mechanisms.

Extensive laboratory and modeling studies have provided ample evidence that viruses and colloidal particles can be significantly retained in subsurface porous media under certain physicochemical and hydrodynamic conditions. It was demonstrated that unsaturated conditions can play an important role in retention of viruses either due to enhanced attachment to the SWI or attachment to the AWI if the chemical conditions are favorable for attachment to either interfaces. However, retention of larger colloids such as bacteria and protozoa under unsaturated and unfavorable conditions can be attributed to straining in small regions of pores such as grain-grain contacts and dead-end pores. The major obstacle to quantitatively predicting the fate and transport of colloidal particles in a real-word situation is our incomplete understanding of the mutual effect of the mentioned processes where attachment to the AWI and SWI and also straining can occur.

Further advancement in understanding of colloidal transport processes in subsurface porous media under various saturations will require extensive research efforts, both at the fundamental and applied levels. On one hand, little information is yet available about the relative importance of attachment to the AWI versus SWI and straining under real-world field situations. Progress in this respect can only be made by additional studies from laboratory experiments conducted under carefully controlled chemical and physical conditions. On the other hand, additional information is needed on key processes such as the kinetics of colloid attachment and detachment to/from the AWI and SWI and on the mechanisms controlling straining.

In our view, the most important research needs include the following areas:

- Influence of chemical and physical heterogeneity on colloid transport and deposition in natural porous media, including the characterization and quantification of heterogeneities in natural porous media.

- Colloid transport in unsaturated porous media, including the influence of the water saturation on colloid transport as well as the effect of wetting-drying cycles on colloid mobilization in soils.

- Quantitative prediction of colloid (e.g. viruses, bacteria, and protozoa) mobilization and deposition in natural porous media as a function of solution composition and flow conditions.

- Importance of various mechanisms in colloid retention (i.e. attachment and detachment to/from the AWI and SAW and staining) in real-world field situations.

The above list is not meant to be complete; it only lists selected aspects that we currently consider to be important. Ultimately, combined research at the field, column, and pore scales, both fundamental and applied, will improve our ability to predict the adequate setback distances between the sources of contamination and production wells for drinking water. This we consider to be a great challenge and at the same time a key to protecting our natural soil and water resources.

References

Ackerman, H. W., and M. S. Dubow, Viruses of Prokaryotes, vol. 2, Natural Groups of Bacteriophages, pp. 190–191, CRC Press, Boca Raton, Fla., 1987.

Adamczyk, Z., Siwek, B., Zembala, M., Belouschek, P., Kinetics of localized adsorption of colloid particles. Adv. Colloid Int. Sci. 48, 151–280, 1994.

Albinger, O., Biesemeyer, B.K., Arnold, R.G. Logan, B.E., Effect of bacterial heterogeneity on adhesion to uniform collectors by monoclonal populations. FEMS Microbiol. Lett. 124 (3), 321–326, 1994.

Auset, M. and Keller, A. A., Pore-scale processes that control dispersion of colloids in saturated porous media. Water Resources Research, 40 (3): W03503, 10.1029/2003WR002800, 2004.

Bales, R.C., S.R. Hinkle, T.W. Kroeger, K. Stocking, and C.P. Gerba, Bacteriophage adsorption during transport through porous media: chemical perturbation and reversibility. Environ. Sci. Technol. 25, 2088–2095, 1991.

Bales, R.C., S. Li, K.M. Maguire, M.T. Yahya, and C.P. Gerba, MS2 and poliovirus transport in porous media: hydrophobic effects and chemical perturbations. Water Resources Res. 29, 957–963, 1993.

Baumann T. and C. J. Werth, Visualization and modeling of polystyrol colloid transport in a silicon micromodel, Vadose Zone Journal, 3: 434-443, 2004.

Bergendahl, J., Grasso, D., Colloid generation during batch leaching tests: Mechanics of disaggregation. Colloids and Surfaces A: Physicochem. Eng. Aspects 135, 193–205, 1998.

Bergendahl, J., Grasso, D., Prediction of colloid detachment in a model porous media: Thermodynamics. AIChE J. 45(3), 475-484, 1999.

Bergendahl, J., Grasso, D., Prediction of colloid detachment in a model porous media: Hydrodynamics. Chem. Eng. Sci. 55, 1523–1532, 2000.

Bitton, G., Adsorption of viruses onto surfaces in soil and water. Wat. Res., 9, 473-484, 1975.

Bitton, G., O.C. Pancorbo, and S.R. Farrah, Virus transport and survival after land application of sewage sludges. Appl. Environ. Microbiol. 47, 905–909, 1984.

Bolster, C.H., Mills, A.L., Hornberger, G.M., Herman, J.S., Spatial distribution of bacteria following Ž . miscible displacement experiments in intact cores. Water Resour. Res. 35 6 , 1797–1807, 1999.

Bradford, S.A., S.R. Yates, M. Bettahar, and J. Simunek, Physical factors affecting the transport and fate of colloids in saturated porous media. Water Resour. Res. 38(12):1327 DOI: 10.1029/2002WR001340, 2002.

Bradford, S.A., J. Simunek, M. Bettahar, M.Th. van Genuchten, and S.R. Yates, Modeling colloid attachment, straining, and exclusion in saturated porous media. Environ. Sci. Technol. 37:2242–2250, 2003.

Bradford, S.A., Abriola, L.M., Dissolution of residual tetrachloroethylene in fractional wettability porous media: Incorporation of interfacial area estimates, Water Resour. Res. 37, 1183– 1195, 2001.

Bradford, S.A., Simunek, J., Bettahar, M., Tadassa, Y.F., van Genuchten, M.Th., Yates, S.R., Straining of colloids at textural interfaces, Water Resour. Res., 41, Art. No. W10404, doi:10.1029/2004WR003675, 2005.

Bradford, S. A., Simunek, J., Bettahar, M., van Genuchten, M. Th., Yates, S. R., Significance of straining in colloid deposition: Evidence and implications. Water Resour. Res., 42, Art. No. W12S15, doi:10.1029/2005WR004791, 2006a.

Bradford, S.A., Simunek, J., Walker, S.L., Transport and straining of E. coliO157:H7 in saturated porous media. Water Resour. Res. 42, Art. No. W12S12, doi:10.1029/2005WR4805, 2006b.

Bradford, S. A., Torkzaban, S., Walker, S. L., Coupling of physical and chemical mechanisms of colloid straining in saturated porous media. Water Res., 2007.

Bradford, S.A., Bettahar, M., Simunek, J., van Genuchten, M.T., Straining and attachment of colloids in physically heterogeneous porous media. Vadose Zone J. 3, 384–394, 2004.

Bradford, S.A., Bettahar, M., Straining, attachment, and detachment, of *Cryptosporidium* oocysts in saturated porous media. J. Environ. Qual. 34, 469–478, 2005.

Bradford, S.A., Simunek, J., Bettahar, M., Tadassa, Y.F., van Genuchten, M.T., Yates, S.R., Straining of colloids at textural interfaces. Water Resour. Res. 41, Art. No. W10404, doi:10.1029/2004WR003675, 2005.

Bradford, S.A., Bettahar, M., Concentration dependent colloid transport in saturated porous media. J. Contam. Hydrol. 82, 99–117, 2006.

Bradford, S.A., Tadassa, Y.F., Pachepsky, Y.A., Transport of *Giardia* and manure suspensions in saturated porous media. J. Environ. Qual. 35, 749–757, 2006a.

Bradford, S.A., Tadassa, Y.F., Jin, Y., Transport of coliphage in the presence and absence of manure suspension. J. Environ. Qual. 35, 1692–1701, 2006c.

Bradford, S.A., Simunek, J., Bettahar, M., van Genuchten, M.T., Yates, S.R., Significance of straining in colloid deposition: Evidence and implications. Water Resour. Res., 42, W12S15, doi:10.1029/2005WR004791, 2006d.

Brow, C.N., Li, X., Ricka, J., Johnson, W.P., Comparison of microsphere deposition in porous media versus simple shear systems. Colloids and Surfaces. A: Physicochem. Eng. Aspects 252, 125–136, 2005.

Camesano, T.A., Logan. B.E., Influence of fluid velocity and cell concentration on the transport of motile and nonmotile bacteria in porous media. Environ. Sci. Technol. 32 (11), 1699–1708, 1998.

Cherrey, K.D., Flury, M., Harsh, J.B., Nitrate and colloid transport through coarse Hanford sediments under steady state, variably saturated flow.

Water Resour. Res. 39, 1165. doi: 10.1029/ 2002WR001944, 2003.

Chi, F. H., G. L. Amy, Kinetic study on the sorption of dissolved natural organic matter onto different aquifer materials: the effects of hydrophobicity and functional groups, J. Colloid Interface Sci. 274 (2) 380–391, , 2004.

Chu, Y., Y. Jin, M. Flury, and M.V. Yates, Mechanisms of virus removal during transport in unsaturated porous media. Water Resources Res. 37, 253–263, 2001.

Chu, Y., Y. Jin, T. Baumann, and M. V. Yates. Effect of soil properties on saturated and unsaturated virus transport through columns. J. Environ. Qual. 32: 2017-2025, 2003.

Compere, F., Porel, G., Delay, F., Transport and retention of clay particles in saturated porous media: Influence of ionic strength and pore velocity. J. Contam. Hydrol.

49, 1–21, 2001.

Corapcioglu, M.Y., and H. Choi, Modeling colloid transport in unsaturated porous media and validation with laboratory column data, Water Resour. Res., 32:3437–3449, 1996.

Costanza-Robinson, M., and M. L. Brusseau, Air-water interfacial areas in unsaturated soils: Evaluation of interfacial domains, Water Resour. Res., 38(10), 1195, doi:10.1029/2001WR000738, 2002.

Craun G.F. and R. Calderon. Microbial riskes in groundwater systems, epidemiology of waterborne outbreaks. Proceedings of the Ground Water Foundation's 12th Annual Fall Symposium 1996, Boston, MA. American Water Works Association, Denver, CO, pp.9-15, 1996.

Crist, J.T., McCarthy, J.F., Zevi, Y., Baveye, P., Throop, J.A., Steenhuis, T.S., Pore-scale visualization of colloid transport and retention in partly saturated porous media. Vadose Zone J. 3 (2), 444-450, 2004.

Crist, J.T., Zevi, Y., McCarthy, J.F., Throop, J.A., Steenhuis, T.S., Transport and retention mechanisms of colloids in partially saturated porous media. Vadose Zone J. 4, 184-195, 2005.

Cushing, R. S., Lawler, D. F., Depth filtration: Fundamental investigation through three-dimensional trajectory analysis. Environ. Sci. Technol. 32, 3793-3801, 1998.

de Jonge, H., Jacobsen, O.H., de Jonge, L.W., Moldrup, P., Particle-facilitated transport of prochloraz in undisturbed sandy loam soil columns. Soil Sci. Soc. Am. J. 27, 1495–1503, 1998.

de Jonge, L. W., Kjaergaard, C., Moldrup, P., Colloids and colloid-facilitated transport of contaminants in soils: An introduction. Vadose Zone J. 3, 321-325.

De Marsily, G. 1986.Quantitative hydrogeology. Academic Press, San Diego, CA, USA 440 p, 2004.

DeNovio N.M., Saiers, J.E., Ryan, J.N., Colloid movement in unsaturated porous media. Recent advances and future directions. Vadose Zone Journal 3, 338-351, 2004.

Derjaguin B.V., Landau, L.D., Theory of the stability of strongly charged lyophobic sols and of the adhesion of strongly charged particles in solutions of electrolytes. Acta Physicochim. USSR 14, 733–762, 1941.

Derjaguin B.V., Theory of the stability of strongly charged lyophobic sols and of the adhesion of strongly charged particles in solutions of electrolytes, Acta Physicochim. USSR, 14, 733-762, 1954.

Dowd, S.E., S.D. Pillai, S. Wang, and M.Y. Corapcioglu, Delineating the specific influence of virus isoelectric point and size on virus adsorption and transport through sandy soils. Appl. Environ. Microbiol. 64:405–410, 1998.

Ducker, W. A., Z. Xu, and J. N. Israelachvili, Measurements of hydrophobic and DLVO forces in bubble-surface interactions in aqueous solutions, Langmuir, 10(9), 3279– 3289, 1994.

Elimelech, M., and C.R. O'Melia. Kinetics of deposition of colloidal particles in porous-media. Environ. Sci. Technol. 24:1528-1536, 1990.

Elimelech, M., Nagai, M., Ko, C.H., Ryan, J.N., Relative insignificance of mineral grain zeta potential to colloid transport in geochemically heterogeneous porous media. Environ. Sci. Technol. 34, 2143-2148, 2000.

El-Farhan, Y.H., N.M. DeNovio, J.S. Herman, and G.M. Hornberger, Mobilization and transport of soil particles during infiltration experiments in and agricultural field, Shenandoah Valley, Virginia. Environ. Sci. Technol. 34, 3555–3559, 2000.

Foppen, J.W.A., Mporokoso, A., Schijven, J.F., Determining straining of *Escherichia coli* from breakthrough curves. J. Contam. Hydrol. 76, 191–210, 2005.

Franchi, A., O'Melia, C.R., Effects of natural organic matter and solution chemistry on the deposition and reentrainment of colloids in porous media. Environ. Sci. Technol. 37(6), 1122–1129, 2003.

Gargiulo, G., Bradford, S. A., Simunek, J., Ustohal, P., Vereecken, H., Klumpp, E., Bacteria transport and deposition under unsaturated conditions: the role of the matrix grain size and the bacteria surface protein. J. Contam. Hydrol., 2007, in press.

Gerba, C.P., Applied and theoretical aspect of virus adsorption to surfaces. Adv. Appl. Microbial. 30. 133-168, 1984.

Gerba, C.P., JE.Jr. Smith. Sources of pathogenic microorganisms and their fate during land application of wastes. J. Environ. Qual. 34(1):42-8. Review.

Gerba, C.P., and J.B. Rose. 1990. Viruses in source and drinking water. In:

Drinking Water Microbiology. (G.A. McFeters, ed.) Science Tech., Inc., Madison, WI, pp. 380-396, 2005.

Gerba, C.P., Y. Marzouk, Y. Manor, E. Idelovitch, and J.M. Vaughn, Virus removal during land application of wastewater: a comparison of three projects. In: AWWA Research Foundation, Future of water reuse 3 AWWA Res. Found., Denver, CO, pp. 1518–1529, 1984.

Gracia, A., Morel, G., Saulner, P., Lachaise, J., Schechter, R.S., The z-potential of gas bubbles. J. Coll. Interf. Sci. 172, 131–136, 1995.

Gregory, J., Approximate expression for retarded van der Waals interaction. J. Coll. Interf. Sci. 83, 138-145, 1981.

Ginn, T.R., Wood, B.D., Nelson, K.E., et al., Processes in microbial transport in the natural subsurface. Advances in Water Resources, 25 (8/12), 1017-1042, 2002.

Gomez-Suarez, C., H.J. Busscher, and H.C. van der Mei, Analysis of bacterial detachment from substratum surfaces by the passage of air-liquid interfaces. Appl. Environ. Microbiol. 67, 2531–2537, 2001.

Gordon, C; Toze, S, Influence of groundwater characteristics on the survival of enteric viruses. J. Appl. Microbiol., 95(3):536-544, 2003.

Goyal S.M., B.H. Keswick, and C.P. Gerba. Viruses in groundwater beneath sewage irrigated cropland. Water Res. 18:299-302, 1984.

Harvey R. W., and H. Harms, Use of Microorganisms and Microspheres as Tracers in groundwater. In: G. Britton (ed.) Encyclopedia of Environmental Microbiology, John Wiley & Sons. New York. pp. 3194-3202, 2002.

Herzig, J.P., Leclerc, D.M., LeGoff, P., Flow of suspension through porous media: Application to deep filtration. Ind. Eng. Chem. Res., 62, 129– 157, 1970.

Hoek, E. M. V., and G. K. Agarwal, Extended DLVO interactions between spherical particles and rough surfaces. J. Coll. Interf. Sci. 298, 50-58, 2006.

Hogg, R., Healy, T.W., Fuerstenau, D.W., Mutual coagulation of colloidal dispersions. Trans. Faraday Soc. 62, 1638-1651, 1966.

Hurst, C.J, Survival of enteroviruses in rapid-infiltration basins during the land application of waste-water. Appl. Environ. Microbiol. 40, 192–200, 1980.

Hahn, M.W., Abadzic, D., O'Melia, C.R., Aquasols: On the role of secondary minima.

Environ. Sci. Technol. 38, 5915–5924, v.

Hahn M.W., O'Melia. C.R., Deposition and reentrainment of brownian particles in porous media under unfavorable chemical conditions: some concepts and applications. Environ. Sci. Technol. 38(1), 210–220, 2004.

ISO (International organization for Standardization), Water quality – Detection and enumeration of bacteriophages – part 1: Enumeration of F-specific RNA-bacteriophages, ISO 10705-2, Geneva, 2000.

ISO (International organozation for Standardization), Water quality – Detection and enumeration of bacteriophages – part 2: Enumeration of somatic coliphages, ISO 10705-2, Geneva, 2000.

Israelachvili, J. N., *Intermolecular and surface forces*, 2nd ed.; Academic Press: London, 1992.

Jin, Y., Y. Chu, and Y. Li, Virus removal and transport in saturated and unsaturated sand columns, J. Contam. Hydrol., 43, 111–128, 2000.

Jin, Y., Flury, M., Fate and transport of viruses in porous media. Adv. Agr. 77, 39–102, 2002.

Johnson, K.L., Kendall, K., Roberts, A.D., Surface energy and the contact of elastic solids. Proceedings of the Royal Soc. of London A 324, 301–313, 1971.

Johnson, P. R., and M. Elimelech, Dynamics of colloid deposition in porous media: Blocking based on random sequential adsorption, Langmuir, 11, 801– 812, 1995.

Johnson, W. P., Li, X. Q., Yal, G., Colloid retention in porous media: Mechanistic confirmation of wedging and retention in zones of flow stagnation. Environ. Sci. Technol. 41, 1279-1287, 2007.

Jorgensen, P. H., Examination of the penetration of enteric viruses in soils under simulated conditions in the laboratory, Water Sci. Technol., 17, 197–199, 1985.

Kalogerakis, N; Alvarez, P; Psillakis, E, Special issue: recent advances in bioremediation. Environment International, 31(2):147, 2005.

Keller, A.A., and S. Sirivithayapakorn, Transport of colloids in unsaturated porous media: Explaining large-scale behavior based on pore-scale mechanisms, Water Resour. Res. 40:W12403, doi:10.1029/2004WR003315, 2004.

Keswick, B.H. and C.P. Gerba, Viruses in groundwater. Environ. Sci. Technol. 14:1290–

1297, 1980.

Kretzschmar, R., Barmettler, K., Grolimun, D., Yan, Y.D., Borkovec, M., Sticher. H., Experimental determination of colloid deposition rates and collision efficiencies in natural porous media. Water Resour. Res. *33* (5), 1129–1137, 1997.

Kung, K.-J. S., Preferential flow in a sandy vadose zone: 1. Field observation, Geoderma, 46, 51– 58, 1990a.

Kung, K.-J. S., Preferential flow in sandy vadose zone: 2. Mechanism and implications, Geoderma, 46, 59–71, 1990b.

Kuznar, Z.A., Elimelech, M., Direct microscopic observation of particle deposition in porous media: Role of the secondary energy minimum, Coll. Surf. A: Physicochem. Eng. Aspects 294, 156–162, 2007.

Lance, J.C., and C.P. Gerba, Virus movement in soil during saturated and unsaturated flow. Appl. Environ. Microbiol. 47:335–341, 1984.

Lenhart, J.J., and J.E. Saiers. Transport of silica colloids through unsaturated porous media: Experimental results and model com parisons. Environ. Sci. Technol. 36:769–777, 2002.

Li, C., Somasundaran, P., Reversal of bubble charge in multivalent inorganic salt solutions—Effect of magnesium. J. Coll.Interf. Sci.146, 216–218, 1991.

Li, X., Scheibe, T.D., Johnson, W.P., Apparent decreases in colloid deposition rate coefficient with distance of transport under unfavorable deposition conditions: A general phenomenon. Environ. Sci. Technol. 38 (21), 5616-5625, 2004.

Li, X., Lin, C.-L., Miller, J. D., Johnson, W. P., Pore-scale observation of microsphere deposition at grain-to-grain contacts over assemblage-scale porous media domains using X-ray microtomography. Environ. Sci. Technol. 40, 3762-3768, 2006.

Li, C., and P. Somasundaran, Reversal of bubble charge in multivalent inorganic salt solutions—Effect of magnesium. J. Colloid and Interface Sci.146, 216–218, 1991.

Li, X., Johnson, W.P., Nonmonotonic variations in deposition rate coefficients of microspheres in porous media under unfavorable deposition conditions. Environ. Sci. Technol. 39, 1658–1665, 2005.

Li, X., Lin, C.L., Miller, J.D., Johnson, W.P., Role of grain-to-grain contacts on profiles of retained colloids in porous media in the presence of an energy barrier to deposition. Environ. Sci. Technol. 40, 3769–3774, 2006b.

Li, X., Zhang, P., Lin, C.L., Johnson, W.P., Role of hydrodynamic drag on microsphere deposition and re-entrainment in porous media under unfavorable conditions. Environ. Sci. Technol. 39, 4012–4020, 2005.

Logan, B.E., D.G. Jewett, R.G. Arnold, E.J. Bouwer, and C.R. O'Melia. Clarification of clean-bed filtration models. J. Eron. Eng. 121:869–873, 1995.

Marinova. K.G., R.G. Alargova, N.D. Denkov, O.D. Velev, D.N. Petsev, I.B. Ivanov, and R.P. Borwankar, Charging of oil-water interfaces due to spontaneous adsorption of hydroxyl ions. Langmuir. 12: 2045-2051, 1996.

Marquardt, D.W., An algorithm for least-squares estimation of non-linear parameters. J. Soc. Ind. Appl. Math. 11:431-441, 1963.

McDowell-Boyer, L. M., J. R. Hunt, and N. Sitar, Particle transport through porous media, *Water Resour. Res.*, *22*, 1901–1921, 1986.

McGechan, M.B., and D.R. Lewis, Transport of particulate and colloid-sorbed contaminants through soil. Part 1: General principles. Biosyst. Eng. 83:255–273, 2002.

Mehra, O. P., and M. L. Jackson, Iron oxide removal from soils and clays by a dithionite-citrate system buffered with sodium bicarbonate, in Clays and Clay Minerals, Proceedings of 7th National Congress, pp. 317–327, Pergamon, Tarrytown, N. Y., 1960.

Nasser, A.M.; Adin, A.; Fattal, B, Adsorption of poliovirus 1 and F+ bacteriophages onto sand. Water Science and Technology, 27(7–8), 331–338, 1993.

Parfitt R.L., J.D. Russell, and V.C. Farmer, Confirmation of the surface structure of goethite and phosphated goethite. J. Chem. Soc. Faraday Trans. I, 72, 1082-1087, 1976.

Patzek, T. W., Silin, D. B., Shape factor and hydraulic conductance in noncircular capillaries I. One-phase creeping flow. J. Coll. Interf. Sci., 236, 295-304, 2001.

Patzek, T. W., Kristensen, J. G., Shape factor and hydraulic conductance in noncircular capillaries II. Two-phase creeping flow. J. Coll. Interf. Sci., 236, 305-317, 2001.

Penrod, S.L., T.M. Olson, and S.B. Grant. Deposition kinetics of two viruses in packed beds of quartz granular media. Langmuir. 12:5576–5587, 1996.

Poletika, N.N., W.A. Jury, and M.V. Yates, Transport of bromide, simazine, and MS-2 coliphage in a lysimeter containing undisturbed, unsaturated soil. Water Resour. Res. 31:801–810, 1995.

Powelson, D.K., Gerba, C. P., Yahya, M.T., Virus transport and removal in wastewater during aquifer recharge. Water Res. 27, 583– 590, 1993.

Powelson, D.K., J.R. Simpson, and C.P. Gerba, Virus transport and survival in saturated and unsaturated flow through soil columns. J. Environ. Qual. 19, 396–401, 1990.

Powelson, D.K., and C.P. Gerba, Viral removal from sewage effluents during saturated and unsaturated flow through soil columns. Water Research. 28: 2175–2181, 1994.

Powelson, D.K, and A.L. Mills, Transport of Escherichia coli in sand columns with constant and changing water content water saturations. J. Environ. Qual. 30(1), 238-245, 2001.

Ramachandran, V., Fogler, H. S., Plugging by hydrodynamic bridging during flow of stable colloidal particles within cylindrical pores. J. Fluid Mech. 385, 129-156, 1999.

Redman, J.A., Grant, S.B., Olson, T.M., Estes, M.K., Pathogen filtration, heterogeneity, and potable reuse of wastewater. Environ. Sci. Technol. 35, 1798–1805, 2001.

Redman, J.A., Walker, S.L., Elimelech, M., Bacterial adhesion and transport in porous media: Role of the secondary energy minimum. Environ. Sci. Technol. 38, 1777-1785, 2004.

Rittmann, BE; Valocchi, AJ; Seagren, E; Ray, C; Wrenn, B, Critical review of in situ bioremediation. Topical report GRI-92/0322. Gas Research Inst., Chicago, IL., and Department of Energy, Morgantown, WV. Morgantown Energy Technology Center. 185 pp, 1992.

Robinson, D.A., and S.P. Friedman, The effect of particle size distribution on the effective dielectric permittivity of saturated granular media. Water Resour. Res. 37:33–40, 2001.

Ryan, J.N., Elimelech, M., Colloid mobilization and transport in groundwater. Coll. Surf. A 107, 1–56, 1996.

Ryan, J.N., T.H. Illangasekare, M.I. Litaor, and R. Shannon, Particle and plutonium mobilization in macroporous soils during rainfall simulations. Environ. Sci. Technol. 32:476–482, 1998.

Saiers, J.E., G.M. Hornberger, D.B. Gower, and J.S. Herman, The role of moving air-water interfaces in colloid mobilization within the vadose zone. Geophys. Res. Lett. 30:2083, doi:10.1029/2003GL018418, 2003.

Saiers, J.E., and J.J. Lenhart, Ionic-strength effects on colloid transport and interfacial reactions in partially saturated porous media. Water Resour. Res. 39:1256. doi:10.1029/2002WR001887, 2003a.

Sakoda, A., Y. Sakai, K. Hayakawa, and M. Suzuki. Adsorption of viruses in water environment onto solid surfaces. Water Sci. Tech. 35, 107-114, 1997.

Sakthivadivel, R., Theory and mechanism of filtration of non-colloidal fines through a porous medium. Rep. HEL 15-5. Hydraul. Eng. Lab., Univ. of Calif., Berkeley, CA, 1966.

Schafer, A., P. Ustohal, H. Harms, F. Stauffer, T. Dracos, and A.J.B. Zehnder. Transport of bacteria in unsaturated porous media. J. Contam. Hydrol. 33:149–169, 1998.

Schijven, J.F., Rietveld, L.C., How do field observations compare with models of microbial removal Proceedings of the Groundwater Foundation's 12th Annual Fall Symposium. AWWA Research Foundation, Denver, pp. 105–114, 1996.

Schijven, J. F. and S.M Hassanizadeh, Removal of viruses by soil passage: overview of modelling, processes, and parameters. Crit. Rev. Env. Sci. and Tech. 30, 49-127, 2000.

Schijven J.F. and J. Simunek, Kinetic modeling of virus transport at the field scale. J. Contam. Hydrol. 55, 113-135, 2002.

Schwarzenbach R. P., Gschwend P.M., Imboden D.M., Environmental organic chemistry, Wiley-Interscience: New York, 1993.

Seyfried, M. S., and P. S. C. Rao, Solute transport in undisturbed columns of an aggregated tropical soil: Preferential flow effects, Soil Sci. Soc. Am. J., 51, 1434–1444, 1987.

Shields, P.A. and S.R. Farrah, Determination of the electrostatic and hydrophobic character of enteroviruses and bacteriophages. Abstr. Q-82. Program Abstr. 87th

Annu. Meet. Am. Soc. Microbiol. American Society for Microbiology, Washington, D.C, 1987.

Sigg, L., W., Stumm. The interaction of anions and weak acids with the hydrous goethite (a- FeOOH) surface. Colloids Surf., 2, 101-117, 1981.

Simunek, J., van Genuchten, M.Th., Sejna, M., *The HYDRUS-1D software package for simulating the one-dimensional movement of water, heat, and multiple solutes in variably-saturated media -Version 3.0*, HYDRUS software series 1, Department of Environmental Sciences, University of California Riverside, Riverside, CA, 240pp, 2005.

Sirivithayapakorn, S., and A.A. Keller, Transport of colloids in unsaturated porous media: A pore scale observation of processes during the dissolution of air-water interface. Water Resour. Res. 39(12), 1346, doi:10.1029/2003WR002487, 2003.Saiers, J.E., and J.J. Lenhart, Ionic-strength effects on colloid transport and interfacial reactions in partially saturated porous media. Water Resour. Res. 39:1256. doi:10.1029/2002WR001887, 2003a.

Tan, Y., Cannon, J.T., Baveye, P., Alexander, M., Transport of bacteria in an aquifer sand - experiments and model simulations. Water Resour. Res. 30, 3243–3252, 1994.

Taylor, D. H., Influence of pH and electrolyte composition on adsorption of poliovirus by soils and minerals. Appl. Environ. Microbiol. 42:976-984, 1981.

Thompson, S.S., and M.V. Yates, Bacteriophage inactivation at the air–water–solid interface in dynamic batch systems. Appl. Environ. Microbiol., 65(3):1186–1190, 1999.

Tipping, E., The adsorption of aquatic humic substances by iron oxides. Geochimica et Cosmochimica Acta 45, 191–199, 1981.

Tong, M., Li, X., Brow, C.N., Johnson, W.P., Detachment-Influenced transport of an adhension-deficient bacterial strain within water-reactive porous media. Environ. Sci. Technol. 39, 2500–2508, 2005.

Toride, N., Inoue, M., Leij, F.J., Hydrodynamic dispersion in an unsaturated dune sand. Soil Sci. Soc. Am. J. 67, 703–712, 2003.

Torkzaban, S., Hassanizadeh, S.M., Schijven, J.F., de Bruin, H.A.M., de Roda Husman,

A.M., Virus transport in saturated and unsaturated sand columns, Vadose Zone J. 5, 877-885, 2006a.

Torkzaban, S., Hassanizadeh, S.M., Schijven, J.F., van den Berg, H.H.J.L., Role of air-water interfaces on retention of viruses under unsaturated conditions. Water Resour. Res. 42, W12S14, doi:10.1029/2006WR004904, 2006b.

Torkzaban, S., Bradford, S.A., van Genuchten, M.T., Walker, S.L., Colloid transport in unsaturated porous media: the role of water content and ionic strength on particle straining. J. Contam. Hydrol., 2006, submitted.

Trouwborst, T., S. Kuyper, J. C. de Jong, and A. D. Plantinga, Inactivation of some bacterial and animal viruses by exposure to liquid-air interfaces, J. Gen. Virol., 24, 155–165, 1974.

Tufenkji, N., Elimelech, M., Spatial distributions of Cryptosporidium oocysts in porous media: Evidence for dual mode deposition. Environ. Sci. Technol. 39, 3620-3629, 2005b.

Tufenkji, N., Redman, J.A., Elimelech, M., Interpreting deposition patterns of microbial particles in laboratory-scale column experiments. Environ. Sci. Technol. 37 (3), 616–623, 2003.

Tufenkji, N., Miller, G.F., Ryan, J.N., Harvey, R.W., Elimelech, M., Transport of *Cryptosporidium* oocysts in porous media: role of straining and physicochemical filtration. Environ. Sci. Technol. 38, 5932–5938, 2004.

Tufenkji, N., Elimelech, M., Deviation from the classical colloid filtration theory in the presence of repulsive DLVO interactions. Langmuir 20, 10818–10828, 2004.

Tufenkji, N., Elimelech, M., Breakdown of colloid filtration theory: role of the secondary energy minimum and surface charge heterogeneities. Langmuir 21, 841–852, 2005a.

Verwey E.J.W., Overbeek, J.T.G., 1948. Theory of the stability of lyophobic colloids. Elsevier, Amsterdam.

Walker, S.L., Redman, J.A., Elimelech, M., Role of cell surface lipopolysaccharides in *Escherichia coli* K12 adhesion and transport. Langmuir 20, 7736–7746, 2004.

Wang, D.S., Gerba, C.P., Lance, J.C., Effect of soil permeability on virus removal through soil. Appl. Environ. Microbiol. 42, 83–88, 1981.

Wan, J., Wilson, J.L., Visualization of the role of the gas–water interface on the fate and transport of colloids in porous media. Water Resour. Res. 30, 11–23, 1994a.

Wan, J., Tokunaga, T.K., Film straining of colloids in unsaturated porous media: Conceptual model and experimental testing. Environ. Sci. Technol., 31, 2413–2420, 1997.

Wan, J.M., Tokunaga, T.K., Partitioning of clay colloids at air–water interfaces. J. Coll. Interf. Sci. 247, 54–61, 2002.

Wan, J., and J.L. Wilson, Colloid transport in unsaturated porous media, Water Resour. Res., 30:857–864, 1994b.

Wan, J., J. L. Wilson, and T. L. Kieft, Influence of the gas-water interface on transport of microorganisms through unsaturated porous media, Appl. Environ. Microbiol., 60(2), 509–516, 1994.

Wilson, SC; Jones, KC, Bioremediation of soil contaminated with polynuclear aromatic hydrocarbons (PAHs): A review. Environmental Pollution, 81(3):229-249, 1993.

Yao, K.M.,M.T. Habibian, and C.R. O'Melia. Water and waste water filtration: Concepts and applications. Environ. Sci. Tech nol. 5:1105–1112, 1971.

Yates D. E. and T. W. Healy, The structure of the silica/ electrolyte interface. J. Colloid Interface Sci. 55, 9- 19, 1975.

Yates, M.V, S.R. Yates, J. Wagner, and C.P. Gerba. Modelling virus survival and transport in the subsurface. J. Contam. Hydrol. 1:329–345, 1987.

Yoon, J. S., Germaine, J. T., Culligan, P. J., Visualization of particle behavior with a porous medium: Mechanisms for particle filtration and retardation during downward transport. Water Resour. Res. 42, W06417, doi:10.1029/2004WR003660, 2006.

Xu, S., Gao, B., Saiers, J. E., Straining of colloidal particles in saturated porous media. Water Resour. Res. 42, W12S16, doi:10.1029/2006WR004948, 2006.

Zerda, K. S., Adsorption of viruses to charge-modified silica, Ph.D. dissertation, Dep. of Virol. and Epidemiol., Baylor Coll. of Medicine, Houston, Tex., 1982.

Zevi, Y., Dathe, A., McCarthy, J. F., Richards, B. K., Steenhuis, T. S., Distribution of colloid particles onto interfaces in partially saturated sand. Environ. Sci. Technol. 39, 7055-7064, 2005.